C-X Bond Activation by Low-Valent First-Row Transition Metal Centers

A DISSERTATION
SUBMITTED TO THE FACULTY OF THE GRADUATE SCHOOL
OF THE UNIVERSITY OF MINNESOTA BY

Elodie Eléonore Julie Marlier

IN PARTIAL FUFILLMENT OF THE REQUIREMENTS
FOR THE DEGREE OF
DOCTOR OF PHILOSOPHY

Connie C. Lu, Co-advisor
Kristopher McNeill, Co-advisor

October, 2011

Acknowledgements

First, I would like to thank my two advisors, Kris McNeill and Connie Lu, who have been great scientific mentors. While my path through graduate school was not a traditional one, I am so thankful and feel incredibly lucky that I have had the chance to work with both of you and be part of your research groups. The transition between research projects could have not been as easy if it had not been for your support and encouragement.

Numerous thanks go to my amazing coworkers. It has been a pleasure working with and getting to know each of you. I especially would like to thank the inorganic girls of the McNeill group who I am indebted to. Each of you has taught me so much in the lab, in the classroom and in life. I also would like to thank my undergraduate mentee Bridget Ulrich for her dedication to work and overall fun attitude. A very special thanks goes to my Lu group members who welcomed me with open arms and made my last year a productive and pleasant one.

During my many lab moves, I came to rely on the wonderful staff in the chemistry department. All of you have been a great help, especially Jason Radde and Ben Geisbauer who helped numerous times when it came to moving the glovebox.

To the instrument facility staff: thank you for your continuous willingness to help, it has been greatly appreciated. I would especially like to thank Dr. Letitia Yao for sharing with me some great conversations, fantastic Asian food, plenty of candy and a place to hide when I needed it.

I also would like to thank the members of the volleyball crew for some epic Wednesday nights. It has been great playing with all of you.

I would also like to thank the people outside of the department that have supported me through my five years. To Emma and Daniel, thank you for listening and being a source to the outside world and to Jean and Darrel who have never failed to ask me how school was going and always showed great interest in my research.

I would like to thank my parents who have always been there to help me and have shown me great support, especially during the past five years. Thank you for wanting to understand what I was working on, for motivating me and for believing in me.

Finally, I would like to thank Andy for being there every day. I can’t imagine having accomplished this goal without you. Thank you.

Table of Contents

List of Tables

Chapter One

Chapter Two

Chapter Three

Chapter Five

Chapter Six

List of Figures

Chapter One

Chapter Two

Chapter Three

Chapter Four

Chapter Five

Chapter Six

List of Schemes

Chapter Three

Chapter Four

Chapter Five

Chapter Five

List of Charts

Chapter Five

Chapter Five

List of Symbols and Abbreviations

1,1-DCE	1,2-dichloroethylene
Å	Ångström
A	hyperfine coupling constant
$AgNO_3$	silver nitrate
atm	atmosphere
BDI	β-diketiminate
$(BDI^{QQ})H$	1,3-bis(quinolyl)propenediimine or Zatka ligand
$(BDI^{Q(SO3H)Q(SO3H)})H$	1,3-bis(quinolyl-5-sulfonic acid) propenediimine
BISBI	2,2'-bis(diphenylphosphinomethyl)biphenyl
br	broad
C	Celsius
cDCE	*cis*-dichloroethylene
CE	chlorinated ethylene
$CDCl_3$	chloroform
CH_2Cl_2	methylene chloride
CD_2Cl_2	deuterated methylene chloride
CH_3CN	acetonitrile
CD_3CN	deuterated acetonitrile
CD_3I	deuterated methyl iodide
cm^{-1}	wavenumber
COD	cycloocta-1-5-diene
COSY	correlation spectroscopy
CV	cyclic voltammetry
d	doublet
D_2O	deuterated water
DBFphos	4,6-bis(diphenylphopshino)dibenzofuran
Dc	calculated density
DCE	dichloroethylene
dd	doublet of doublets
deg	degree
DFT	density functional theory
d_6-DMSO	deuterated dimethylsulfoxide
DMSO	dimethylsulfoxide
dppe	1,2-bis(diphenylphosphino)ethane
dppf	1,1'-bis(diphenylphosphino)ferrocene
dt	doublet of triplets
dtbpe	1,2-bis(di-*tert*-butylphosphino)ethane
δ	chemical shift in ppm
EDTA	ethylenediaminetetraacetic acid
EPA	Environmental Protection Agency
EPR	electron paramagnetic resonance
ESI-TOF MS	electrospray ionization time of flight mass spectrometry
Et_2O	diethyl ether

eV	electron volt
ε	molar absorptivity
Fc	ferrocene
g	g factor
g	gram
G	Gauss
GC	gas chromatograph
GC-EI-MS	gas chromatography-electron impact-mass spectrometry
GC-MS	gas chromatography-mass spectrometry
GHz	gigahertz
GOOF	goodness of fit
HCl	hydrochloric acid
H_3PO_4	phosphoric acid
HMBC	heteronuclear multiple bond correlation
HMQC	heteronuclear multiple quantum correlation
HRMS	high-resolution mass spectrometry
Hz	hertz
^{iPr}DPDBFphos	4,6-bis(3-diisopropylphosphinophenyl)dibenzofuran
IR	infrared
J	coupling constant
K	Kelvin
KC_8	potassium graphite
kcal	kilocalorie
L	liter
λ_{ex}	excitation wavelength
λ_{max}	wavelength absorbance maximum
LDE	ligand distortion energy
M	metal
M	molar
m	multiplet
MCL	maximum contaminant level
Me	methyl
MeOH	methanol
Mg	milligram
MHz	megahertz
mL	milliliter
MLCT	metal to ligand charge transfer
mM	millimolar
mmol	millimole
MN-GFM	minnesota gaussian functional module
mol	mole
MO	molecular orbital
mV	millivolt
mW	milliwatt
m/z	mass-to-charge ratio
μ_B	Bohr magneton

μ_{eff}	effective magnetic moment
$\mu_{S.O.}$	spin-only magnetic moment
μ	bridging
μL	microliter
NaOH	sodium hydroxide
$[^{n}Bu_4N]PF_6$	tetrabutylammonium hexafluorophophate
nm	nanometer
NMR	nuclear magnetic resonance
ORTEP	Oak Ridge thermal ellipsoid plot
PCE	perchloroethylne
PEG	polyethylene glycol
PFK	perfluorokerosene
PPG	polypropylene glycol
ppm	parts per million
θ	degrees of data collection
π	pi bonding orbital
r	radius
reflns	reflections
s	singlet
S	spin
sh	shoulder
SHE	standard hydrogen electode
SOMO	singly occupied molecular orbital
SPANphos	8,8’-bis(diphenylphosphino)-4,4,4’,4’,6,6’-hexamethylspiro-2,2’-bichroman
σ	sigma bonding orbital
t	triplet
TCE	trichloroethylene
tDCE	trans-dichloroethylene
d_8-THF	deuterated tetrahydrofuran
THF	tetrahydrofuran
Tol	toluene
(Tol-BDI$^{(2\text{-}pp)2}$)H	2-(4-tolyl)-1,3-bis(2-isopropylpyridyl)propenediimine
TRANSphos	2,11-bis(diphenylphosphinomethyl) benzophenanthrene
UV	ultraviolet
UV-vis	ultraviolet-visible
V	volt
V	volume
VC	vinyl chloride
VOC	volatile organic compound
W	line width
Xantphos	9,9-dimethyl-4,6-bis(diphenylphosphino)xanthene
Z	number of independent structures in unit cell

-PART I-

Development of Cobalamin Model Complexes for the Study of Reductive Dehalogenation

-Chapter One-

Introduction

1.1 Chlorinated solvents in the environment

Since the introduction of the Clean Water Act in 1977, the Environmental Protection Agency (EPA) has been committed to ensuring the quality of our water supply. Now, three decades later, this commitment has been renewed with aims to clean up the water supply of contaminants. In January 2011, a new strategic goal was implemented where contaminants were to be addressed as a group rather than individual compounds. The first compounds to be targeted under this new initiative are carcinogenic volatile organic compounds (VOCs). This came as no surprise, considering VOCs have plagued our groundwater supply in abundance, due to their presence in such household products as paints, adhesives, cleaning supplies, and plastics.[1] In 2007, Squillace and co-workers tested for the presence of 55 VOCs in groundwater from more than 5000 wells across the country and found that two VOCs stood out in terms of their occurrences at concentrations greater than or near their Maximum Contaminant Levels (MCLs). Perchloroethylene (PCE) and trichloroethylene (TCE) were not only detected in 11% and 5% of the wells, respectively, but more importantly, they were ranked 1 and 3 in terms of the frequency of concentration greater than MCLs (Figure 1.1).[2]

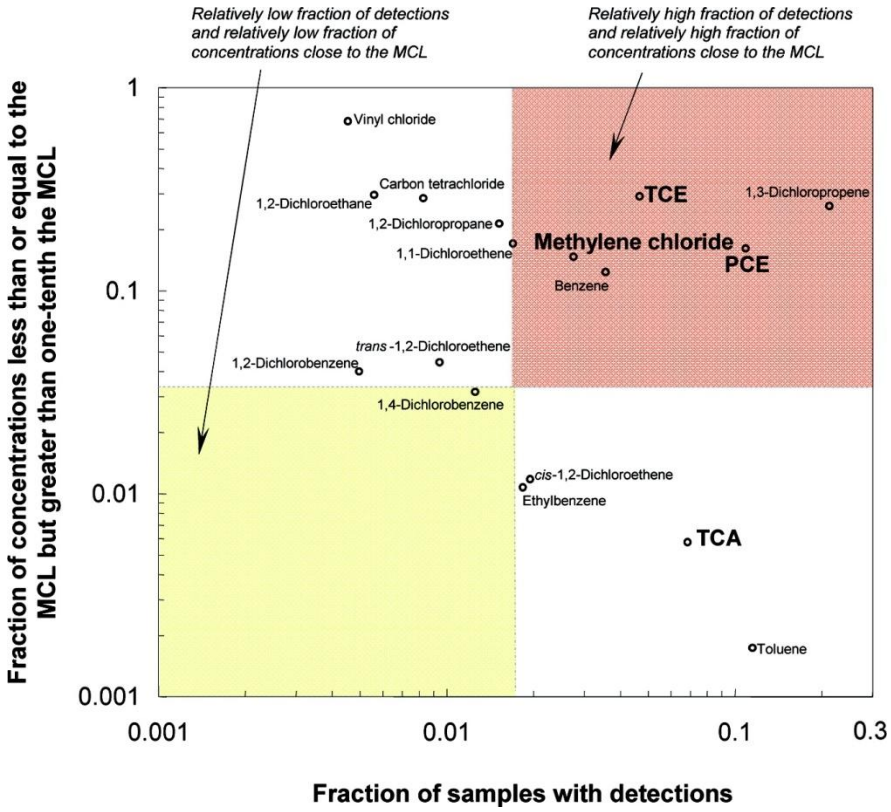

Figure 1.1. Occurrence of VOC in drinking water wells, relative to their MCLs. Figure is taken from reference 2.

Although PCE and TCE were identified as priority pollutants by the EPA in 1977, they have been an environmental nuisance for nearly a century, with records showing cattle poisoning dating back to the early 1920s.[3-4] While both chemicals have had a wide range of uses, PCE was mainly used as a cleaning fluid in the dry-cleaning and textile processing industries, and TCE's most prominent uses were as a vapor degreasing solvent in the metal industry and as an extraction solvent for natural fats and oils.[3-4] Both chemicals are still in use today as chemical precursors for the production of fluorocarbons and hydrofluorocarbons, but their production and use have dramatically declined.[5] At their peak, PCE and TCE production reached 763 and 600 million pounds

respectively.[3-4] In 2002, the annual production of PCE was down to 430 million pounds while TCE has seen a larger decline to 330 million pounds in 2005.[5]

While the production and use of PCE and TCE have decreased, the damage caused by chlorinated ethylenes (CEs) will take decades to repair. Both PCE and TCE are anticipated to be human carcinogens.[5-8] Human studies are showing incidences of liver and kidney cancers and non-Hodgkin's lymphoma from occupational exposure to TCE.[5-8] For PCE there is limited data due to the exposure of dry-cleaning workers to a multitude of solvents; however there is some evidence connecting esophageal cancer, cervical cancer, and non-Hodgkin's lymphoma to PCE exposure.[5-7] Additionally, cancer studies in animals show that PCE exposure causes benign and malignant liver and kidney tumors, as well as mononuclear-cell leukemia.[5] Further health concerns over PCE and TCE water contamination are directed toward their less-chlorinated daughter products, such as the known carcinogen vinyl chloride (VC).[5, 9] While partial reductive dechlorination of PCE and TCE can lead to carcinogenic species, complete removal of the chlorine atoms results in the production of the benign compound ethylene (Figure 1.2).

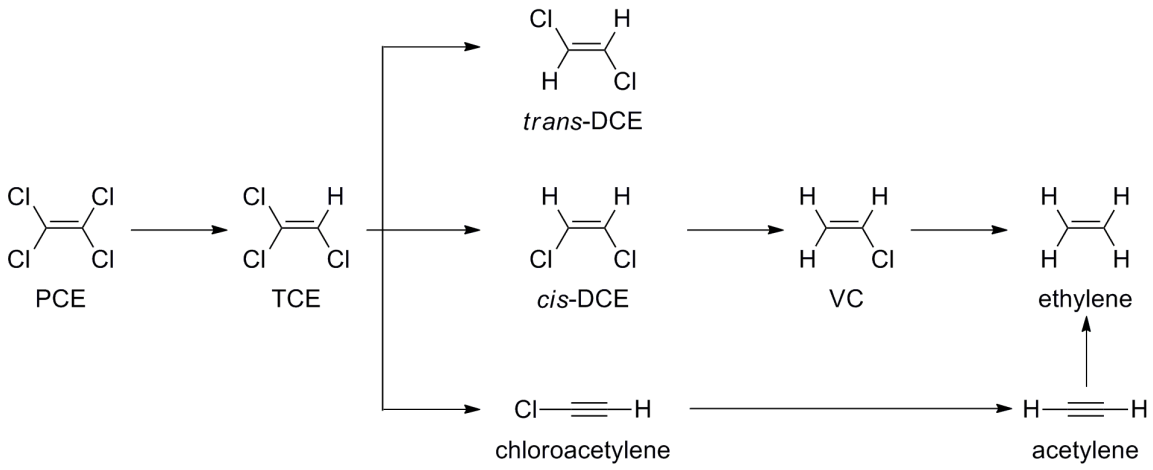

Figure 1.2. Sequential removal of chlorine atoms from PCE to ethylene.

1.2 Remediation of chlorinated ethylenes by cobalamin

As a result of their considerable health concerns and widespread contamination, remediation strategies for water affected by CEs have been implemented. One remediation strategy has focused on natural attenuation using microorganisms.[10] Early studies of microorganisms revealed the participation of metallocofactors, specifically corrinoids, in the reductive dehalogenation of a variety of substrates.[10-11] In 1991, Gantzer and Wackett examined the dechlorination of CEs with an array of metallocofactors including cobalamin (Vitamin B_{12}), coenzyme F_{430}, and hematin (Figure 1.3). In the presence of a reducing agent, cobalamin and coenzyme F_{430} were found to dechlorinate PCE completely to ethylene, while hematin was able to degrade PCE to VC.[12]

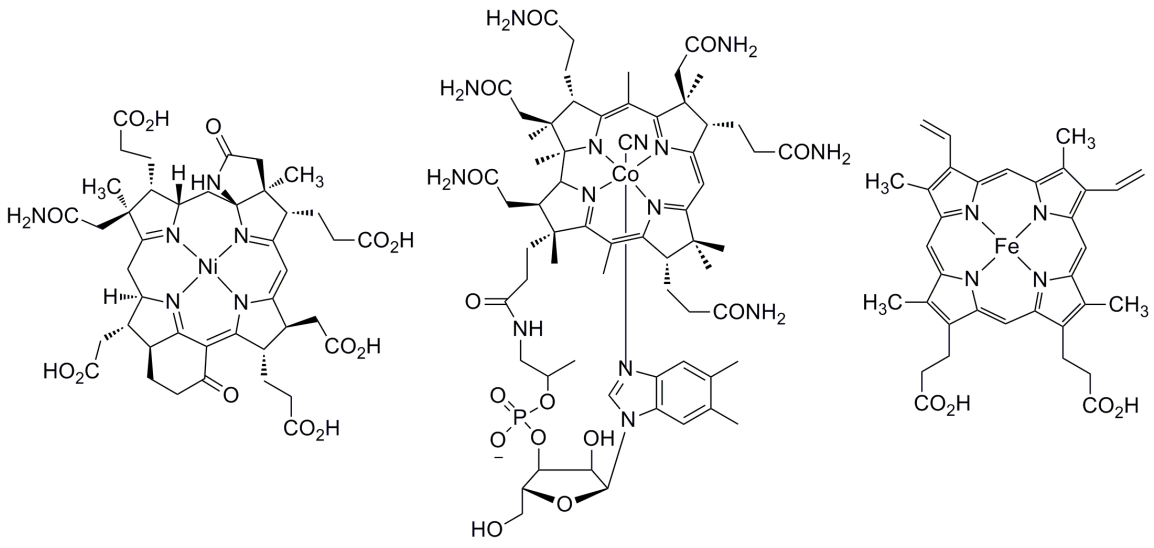

Coenzyme F_{430} **Cobalamin** **Hematin**

Figure 1.3. Cofactors used in reductive dechlorination.

The study also reported the relative rates of dechlorination by the three cofactors showing that dechlorination mediated by cobalamin was faster than coenzyme F_{430} and much

faster than hematin.[12] Recently it was revealed that all reductive dehalogenases, the enzymes responsible for reductive dehalogenation, contain a corrinoid with the exception of one that employs a heme.[13] This observation further affirmed the role of cobalamin in the process of reductive dehalogenation.

Subsequent studies have examined the kinetics of reductive dechlorination by cobalamin and found discrepancies in the rates of dechlorination and distribution of products. The rates of dechlorination seem highly dependent on the experimental conditions such as pH, temperature, and the concentrations of bulk reagents and cobalamin, resulting in a difficulty in comparing the various studies.[14-20] While the rates of dechlorination may vary between studies, the trends of dechlorination appear the same. Higher chlorinated substrates react fastest, and rates slow down as the chlorine content decreases, with the exception of the fast conversion of vinyl chloride to ethylene.[12, 14-18] The slowest reaction is the dechlorination of *cis*-DCE to VC, resulting in a build-up of *cis*-DCE in the environment.[12, 14-18]

In addition to rates of degradation, the products of dechlorination mediated by cobalamin have also been highly debated, with the detection of acetylene products in some studies and the different distributions of DCE products observed for the dechlorination of TCE.[18] These conflicting rates and products have led to an interest in the mechanism of reductive dehalogenation mediated by cobalamin and have contributed to vastly different proposed mechanisms, including inner vs. outer-sphere electron transfer, the presence of radicals, and the formation of organocobalt intermediates.[21-33] A recent review by Kliegman and McNeill evaluated the mechanistic studies on cobalamin-mediated dehalogenation using both cobalamin and its model complexes.[18] Seeing that

the review highlighted the importance of the cobalt-vinyl intermediate and the lack of understanding on the involvement of radicals, it prompted a study on the role of free radicals investigated by radical traps.[18] Interestingly, the study showed that the reaction did not solely proceed by an inner or outer-sphere mechanism and hypothesized the formation of a cage from which radical intermediates could escape and react to form organocobalt complexes and organic products (Figure 1.4).[34]

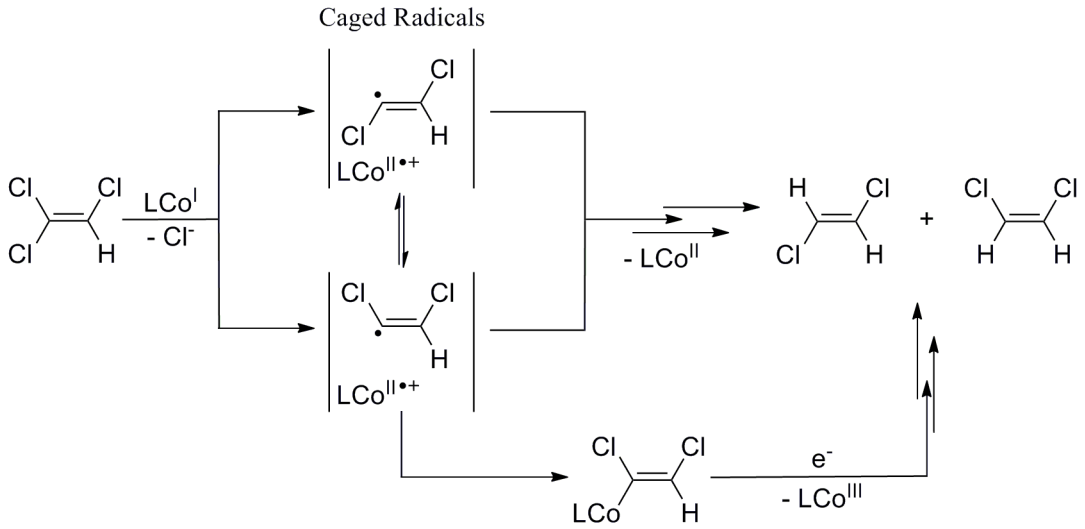

Figure 1.4. Mechanism of cobalamin-mediated dechlorination of TCE and PCE via caged radical intermediates. PCE follows the same mechanism as TCE.
Figure is adapted from reference 34.

Although the mechanism is yet to be completely elucidated, it is widely accepted that the Co(I) oxidation state of vitamin B_{12}, cob(I)alamin, is known to be crucial to the dechlorination process.[26]

1.3 Important characteristics of cob(I)alamin

Reductive dehalogenation of halogenated substrates depends on the reducing capacity of the transition metal complex. The potential intermediates formed and the distribution of products are all influenced by this parameter. Furthermore, it has been shown that the reduction potential, when correlated with product ratio in the reduction of TCE, can be used as a probe for the mechanism.[22]

As previously mentioned, cob(I)alamin has been found to play a central role in the process of reductive dehalogenation. The $Co^{I/II}$ couple observed for cobalamin is -0.59 V (vs. SHE), making cob(I)alamin a strong reductant.[35-39] This is one characteristic that allows cobalamin to reduce CEs, which have high reduction potentials (Table 1.1).

Table 1.1. Calculated reduction potentials (vs. SHE) for chlorinated ethylenes.[40]

CE	E° (mV)
PCE	-598
TCE	-674
cis-DCE	-955
trans-DCE	-1012
1,1-DCE	-802
VC	-1141

The calculated potentials for CE have more negative reduction potentials with decreasing chlorine content, corresponding with substrates that are more difficult to reduce. Furthermore, the calculated potentials for the chlorinated ethylenes are greater than the cobalamin $Co^{I/II}$ couple, suggesting an obstacle to the reaction. Since a substrate is more likely to be reduced if it has a less negative reduction potential, this suggests that cobalamin must be utilizing an additional chemical property when reducing chlorinated ethylenes.[18] This property has been hypothesized to be the nucleophilicity of Co(I).

Due to its high nucleophilicity, the cobalt center in cob(I)amin has been referred to as a "supernucleophile."[41-42] Nucleophilicity has been quantified by Pearson *et al*. and is defined as the log of the second order rate constant for the attack of the substrate by a specific nucleophile divided by the second order rate constant for the attack of MeOH by the nucleophile (Figure 1.5).[41-43] In the case of Pearson, methyl iodide was used as the substrate.[41-43]

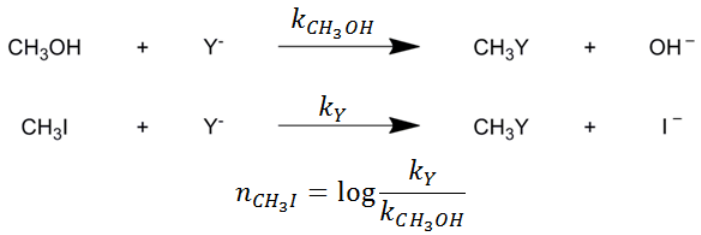

Figure 1.5. Definition of the nucleophilicity constant n_{CH3I}.
Figure is adapted from reference 42.

Using Pearson's method, Schrauzer and co-workers were able to determine the nucleophilicity reactivity constant for cobalamin to be 14.4.[41-42] The chloride ion had a nucleophilicity reactivity constant of 4.37, making it a weaker nucleophile compared to cobalamin.[41-42] Interestingly, Schrauzer found that leaving groups effects were 10 times greater in Co(I) complexes than typical S_N2 reactions.[41]

Schrauzer has hypothesized that the increased nucleophilic effects of Co(I) complexes are due to directional abilities and high charge density of the d_{z2} orbital, its highest occupied molecular orbital.[41] This hypothesis was tested by looking at the effect of axial bases on the nucleophilicity of Co(I) complexes.[41] As expected, when the base was a strong electron donor, increased nucleophilic character was observed.[41] The

nucleophilic character of cob(I)alamin is believed to work in tandem with its electrochemical properties to allow for the reduction of chlorinated ethylenes.

1.4 Current models for cobalamin

As previously mentioned, the insight into the mechanism of reductive dehalogenation has been strongly advanced by the use of model complexes that mimic cobalamin but are not as structurally complicated. The most common model complexes for cobalamin are cobaloxime [bis(dimethylglyoximato)cobalt] and porphyrin-containing complexes such as 5, 10, 15, 20-tetrakis-(4-carboxyphenyl)-porphyrin cobalt ((TCPP)Co) (Figure 1.6).[21-23, 25-26, 31, 38, 44-46]

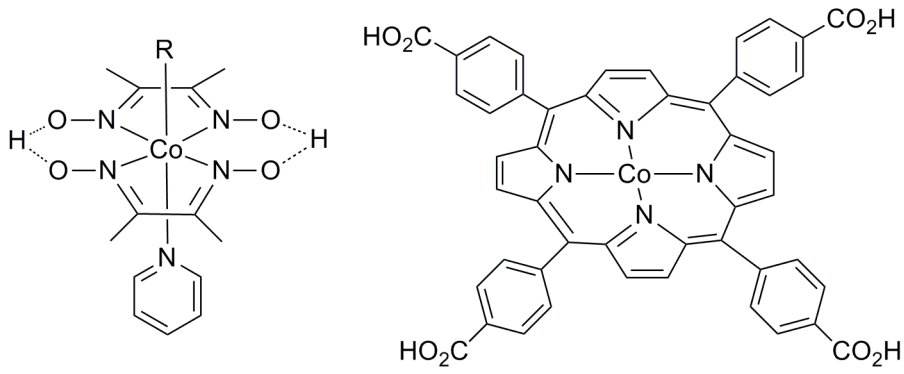

Cobaloxime
R = CH_3, Cl, Br

(TCPP)Co

Figure 1.6. Cobalamin model complexes.

Cobaloxime has been extensively used to understand the mechanism of dechlorination by allowing for the isolation of chlorovinyl cobalt complexes which are key intermediates in the mechanism of reductive dehalogenation.[25-27, 31, 47] Current cobaloxime studies aim to further understand the formation of the cobalt-vinyl complex by determining the carbon isotope fractionation during the reaction of cobaloxime and TCE by isotope ratio mass spectrometry (IRMS).[48]

Cobalt porphyrins have been explored as potential catalysts for reductive dehalogenation of CE since the discovery of the catalytic activity of porphyrin complexes

toward the dechlorination of chloromethanes.[49] Dror and Schlautmann followed with the dechlorination of PCE using water-soluble cobalt, iron and nickel porphyrins.[44, 50] This prompted a more detailed kinetic and mechanistic study by Fritsch and McNeill, investigating the dechlorination of PCE, TCE, cDCE, and tDCE by a survey of cobalt porphyrins complexes, including (TCPP)Co.[45-46] Remarkably, (TCPP)Co was found to have dechlorination rates superior to those of cobalamin.[45]

While cobaloxime and cobalt porphyrin complexes have been crucial to understanding the mechanism of reductive dehalogenation and developing better catalysts, both systems mimic the tetraaza coordination environment of the corrin but do not match its monoanionic charge. This leaves room for improvement in the development of a cobalamin model complex.

1.5 Scope of thesis

The objective of the first part of this dissertation is to synthesize a cobalamin model complex that can mimic both the monoanionic charge and the tetraaza coordination environment of the cobalamin corrin while demonstrating reactivity toward C-X bonds. In the second chapter, the monoanionic tetradentate β-diketiminate ligand ($BDI^{QQ}H$) is evaluated as a possible corrin model. Through the preparation of a series of first row transition metal complexes and DFT calculations, it is shown that the ligand is poorly suited to be model for the corrin due to its inflexibility, preventing it from accommodating different ionic radii and thus stabilizing the different oxidation states of cobalt. The third chapter is dedicated to the synthesis and characterization of an improved, more flexible β-diketiminate ligand, Tolyl-$BDI^{(2\text{-}pp)2}H$. An isolable Co(I) complex is prepared in this chapter and is shown to be comparable to cobalamin(I) both in terms of its electrochemistry and reactivity toward C-X bonds.

-Chapter Two-

Metal Ion Size and Coordination Mode in Complexes of a β-Diketiminate Ligand with Pendant Quinoline Arms

In part from:

Marlier, E. E.; Sadowsky, D.; Cramer, C.; McNeill, K. *Inorg. Chim. Acta*, **2011**, 369, 173-179.

2.1 Overview

A suite of late first row transition metal complexes has been synthesized using a monoanionic nitrogen donor β-diketiminate ligand with quinolyl pendant arms, $BDI^{QQ}H$ (**1**). $BDI^{QQ}NiOTf$ (**2**), $BDI^{QQ}CuCl$ (**4**), $BDI^{QQ}ZnCl$ (**5**) were prepared from the reaction of **1** with $Ni(OTf)_2$, $CuCl_2 \cdot 2H_2O$ and $ZnCl_2$ respectively. $BDI^{QQ}NiCl$ (**3**) was synthesized from an anion exchange of **2** with $^{n}Bu_4NCl$. Reaction of **1** and CoI_2 afforded the unexpected $[(BDI^{QQ})_2Co]^{+}I^{-}$ (**6**). To increase the water solubility of these complexes, a derivative of the $BDI^{QQ}H$ ligand, $BDI^{Q'Q'}H$ (**1a**) was synthesized by substituting a hydrogen on each quinolyl pendant arm with a sulfonic acid group. The derivative ligand was used to synthesize $BDI^{Q'Q'}ZnCl$ (**5a**) from **1a** and zinc chloride. Through density functional theory (DFT) calculations, ligand geometries in BDI^{QQ} complexes were investigated and it was found that smaller ionic radius and higher charge destabilize 1:1 metal-ligand complexes relative to alternative 1:2 complexes like **6** owing to significant conformational strain in 1:1 complexes involving metals with small ionic radii. Synthesis and characterization of these complexes, including crystal structures of **4** and **5**, are reported, in addition to the results of DFT calculations.

2.2 Introduction

In recent years, reports of β-diketiminate (BDI) complexes have increased dramatically, spanning the entire periodic table from main group elements to lanthanides.[1] While most BDI examples are monoanionic bidentate ligands, there are only a handful of examples of monoanionic tridentate and tetradenate BDIs. For example, nitrogen and mixed atom donor monoanionic tridentate BDIs have been employed in applications involving polymer synthesis, such as the ring opening polymerization of lactide.[2-3] The current repertoire of monoanionic tetradentate nitrogen donor BDI ligands is far less expansive.[4] The first example of which we are aware appeared in 1971 when Zatka and co-workers prepared a ligand with quinolyl groups as pendant arms on a simple β-diketiminate backbone.[5] Roesky and co-workers also used a β-diketiminato derivative with substituted ethylene diamine pendant arms to prepare a variety of lanthanides and early transition metal complexes.[6-9] We previously reported a group of divalent metal complexes using a similar ligand to Zatka, differing by the presence of a tolyl group on the central carbon of the BDI backbone.[10]

Our prolonged interest in monoanionic tetradentate nitrogen donor BDI ligands stems from their potential as models for the corrin in vitamin B_{12} and the corphin in cofactor F_{430}. BDI ligands with pendant arms are potentially well suited for this task due to their ability to mimic and simplify the coordination environment of these two macrocycles as well as offer flexibility via facile modification of their pendant arms. In an effort to understand their utility as models, we have investigated the metal binding properties of the previously mentioned Zatka ligand, $BDI^{QQ}H$, by preparing a suite of metal complexes.

In this work, we report the synthesis of a series of late, first row transition metal complexes using $BDI^{QQ}H$, **1** and its derivative $BDI^{Q'Q'}H$, **1a**. Two nickel(II) complexes, $BDI^{QQ}NiOTf$ (**2**) and $BDI^{QQ}NiCl$ (**3**), are reported in addition to a copper(II) complex, $BDI^{QQ}CuCl$ (**4**) and two zinc(II) complexes, $BDI^{QQ}ZnCl$ (**5**) and $BDI^{Q'Q'}ZnCl$ (**5a**). The fluorescence properties of complex **5** are evaluated in the presence and absence of other divalent metals. The last member of the series is an unexpected bis-ligand cobalt(III) iodide complex, $[(BDI^{QQ})_2Co]^+I^-$ (**6**). The surprising binding mode observed in **6** led us to investigate this ligand system using a computational chemistry approach. DFT calculations were carried out on various $BDI^{QQ}M^{n+}$ complexes, where M is a d^0 ion, in order to investigate the effect of the ionic size and formal charge of M on the geometries and conformational energies of the coordinating BDI^{QQ} ligand. In addition, a set of calculations was carried out on the analogous neutral $BDI^{QQ}MCl_x$ complexes.

2.3 Results & discussion

Synthesis and Characterization of Metal Complexes

Compound **1**, BDI^{QQ}H was synthesized according to a literature procedure by Zatka *et al.* in 99% yield.[5] Compound **1** was fully characterized using ^{1}H NMR, ^{13}C NMR, UV-vis spectroscopy and high resolution mass spectrometry (HRMS). The ^{1}H NMR spectrum contains a doublet at 12.65 ppm, indicative of the amine proton and eight distinct resonances in the aromatic region. The elemental composition of **1** was confirmed by HRMS using a polyethylene glycol (PEG) exact mass internal standard. Compound **1** was reacted with late first row metals to give a suite of metal complexes.

Compound **2**, BDI^{QQ}NiOTf was synthesized by reacting compound **1** with potassium bis(trimethylsilyl)amide, followed by addition of nickel triflate under inert atmosphere. The complex was isolated in 25% yield (Figure 2.1).

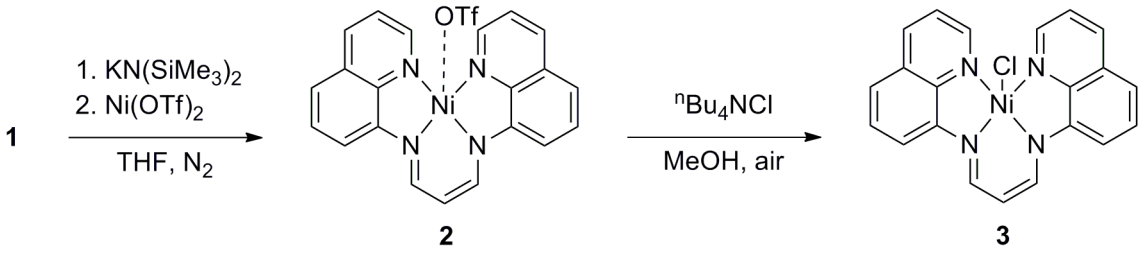

Figure 2.1. Synthetic route to complexes **2** and **3**.

An anion exchange with tetrabutylammonium chloride was carried out to give compound **3**, BDI^{QQ}NiCl, in 98% yield. Both nickel complexes were characterized by HRMS and ^{1}H NMR, ^{13}C NMR, IR and UV-vis spectroscopy. The elemental composition for **2** and **3** was verified by HRMS using a PEG exact mass internal standard. Both ^{1}H NMR spectra showed the disappearance of the amine peak and an upfield shift (from 7.13 ppm to 5.70 ppm) of the resonance corresponding to the proton on the central carbon of the BDI

backbone. The IR spectrum of **2** revealed four bands associated with a triflate, specifically 1267cm^{-1} (SO_3 asym. stretch), 1219 cm^{-1} (CF_3 sym. stretch), 1141 cm^{-1} (CF_3 asym. stretch) and 1027 cm^{-1} (SO_3 sym. stretch). The strong asymmetric stretch for the sulfonyl group at 1267 cm^{-1} indicates the presence of an ionic triflate, as it falls within the expected ionic triflate range of 1235 cm^{-1} to 1288 cm^{-1}.[11-12] Conductivity measurements of **2** and **3** revealed that both complexes were weak electrolytes, leading us to hypothesize that the triflate ion is weakly coordinated. Considering the similarity between the UV-vis absorbance and ^{1}H NMR spectra of **3** and those of an analogous zinc complex **5** (described below), we believe the chlorine is bound in the case of **3**.

The syntheses of **4**, BDI^{QQ}CuCl, and **5**, BDI^{QQ}ZnCl, were carried out in identical manner. Ligand **1** was reacted with either copper chloride or zinc chloride in the presence of three equivalents of 1.0 M sodium hydroxide (Figure 2.2).

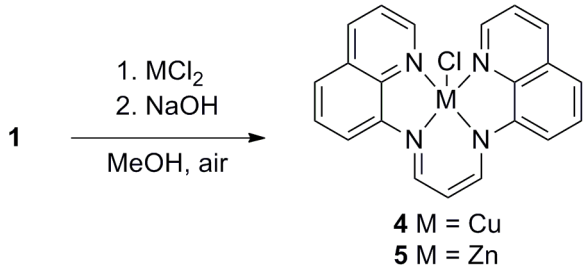

Figure 2.2. Synthetic route to complexes **4** and **5**.

Compound **4** was isolated in 40% yield and was characterized by HRMS, UV-vis spectroscopy and X-ray crystallography. The elemental composition of **4** was confirmed by HRMS using a PEG exact mass internal standard. X-ray quality crystals of **4** were grown from layering a methanol solution of **4** with diethyl ether. The geometry around copper was found to be distorted square pyramidal with a tau value of 0.39.[13] Compound **5** was isolated in 73% yield and was characterized by the same techniques as **4** as well as

^{1}H NMR and ^{13}C NMR spectroscopy. The elemental composition of **5** was verified by HRMS using a PEG exact mass internal standard. Crystals of **5** suitable for X-ray crystallography were grown using the same method as **4** and also showed a similar geometry where **5** can be described as a distorted square pyramid with a tau value of 0.36.[13] In the ^{1}H NMR spectrum of **5**, the disappearance of the resonance for the amine proton and a nearly 2 ppm upfield shift of the resonance belonging to the proton of the central carbon of the BDI backbone can be observed.

To complete the series of metal complexes, we attempted to synthesize a cobalt(II) chloride complex. Although HRMS indicated the presence of this complex using the same method as **4** and **5**, we were unable to isolate it in pure form. When cobalt(II) iodide was used as the metal precursor in a one to one ratio in the presence of three equivalents of 1.0 M NaOH, the unexpected synthesis of **6**, a cationic cobalt(III) complex was observed (Figure 2.3).

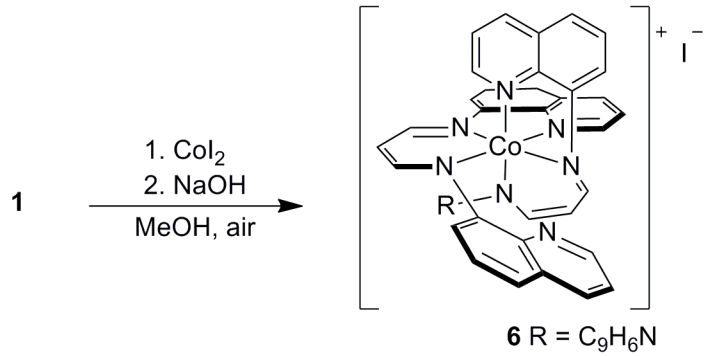

Figure 2.3. Synthetic route to complex **6**.

The cobalt metal is bound in a tridentate manner to two ligands in an octahedral geometry with an outer-sphere iodide counterion. Compound **6** can be synthesized in 83% yield when using two equivalents of ligand for one equivalent of cobalt iodide. Compound **6** was characterized by HRMS, ^{1}H NMR and ^{13}C NMR spectroscopy. Using HRMS and a

PEG exact mass internal standard, the elemental composition of **6** was verified. In the ^{1}H NMR spectrum, a total of 13 distinct and two overlapping peaks were present caused by the break of symmetry due to the bound and unbound quinolines. An upfield triplet at 5.21 ppm was observed for the proton on the central carbon of the BDI backbone. Considering the spectroscopic similarity between bound and unbound quinolines, 2D correlation spectroscopy (COSY) was used to further verify the assignment of each shift to a specific proton. These assignments are presented in the experimental procedure section. An X-ray diffraction experiment was conducted with crystals of **6** that were obtained from a concentrated THF solution. While the data set was of insufficient quality for publication (R = 0.11), the connectivity was rigorously established.

In an effort to increase the water solubility of the metal complexes, a modification on the BDI^{QQ}H ligand was introduced. A sulfonic acid group was substituted on each pendant quinolyl groups to create the ligand derivative BDI$^{Q'Q'}$H (**1a**) (Figure 2.4). Compound **1a** was synthesized in quantitative yield by reacting 8-aminoquinoline-5-sulfonic acid with 1,1,3,3-tetramethoxypropane in a 1:1 mixture of MeOH and HCl. It was characterized by ^{1}H NMR spectroscopy and HRMS. In the ^{1}H spectrum, a total eight resonances are observed including a doublet at 12.64 ppm, belonging to the amine proton. The elemental composition of **1a** was verified by HRMS using a polyethylene glycol (PEG) exact mass internal standard. Compound **1a** was reacted with zinc chloride to give BDI$^{Q'Q'}$ZnCl (**5a**) at near quantitative yield, which was characterized by HRMS, ^{1}H NMR and UV-vis spectroscopy (Figure 2.4).

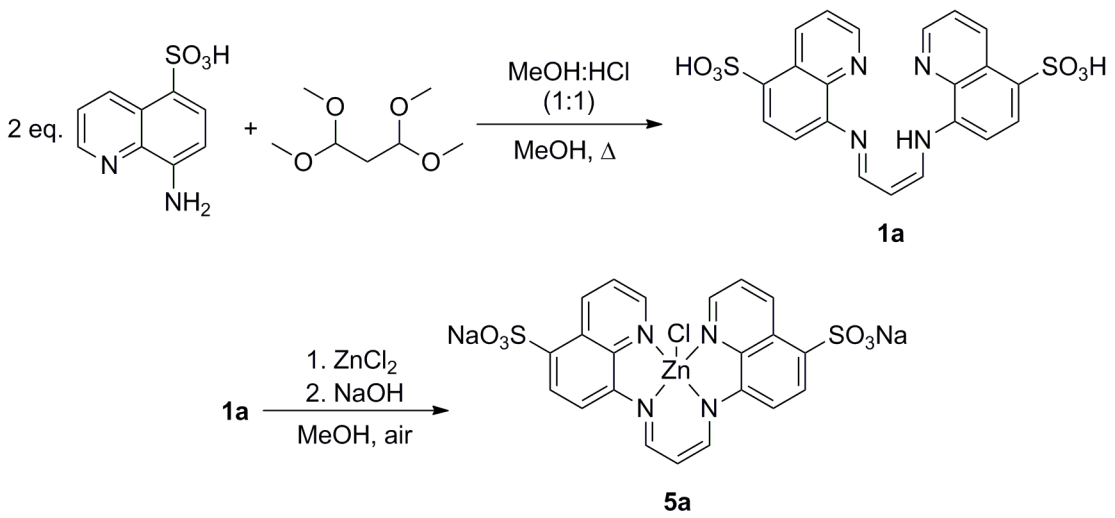

Figure 2.4. Synthetic route to compounds **1a** and **5a**.

When comparing the ^{1}H spectrum of **5a** to **1a**, a loss of the amine proton resonance is observed as well as a nearly 2 ppm upfield shift of the resonance belonging to the proton of the central carbon of the BDI backbone. This same shift is observed upon metallation of **1** with zinc chloride to make complex **5**.

*UV-vis Spectroscopy of complexes **2 - 5***

The UV-vis absorbance spectra of complexes **2-5** have three essentially identical features that are also observed in the spectrum of **1** (Figure 2.5). The two intense bands below 250 nm and a single band at 419 nm correspond to ligand based π-π* and n-π* transitions respectively. These assignments are similar to those found for 5-aminoquinoline where π-π* and n-π* transitions have been associated with two bands at 286 nm, 296 nm and one band at 361 nm respectively.[14] Upon metallation of **1**, the band at 419 nm is red-shifted to 525 nm.

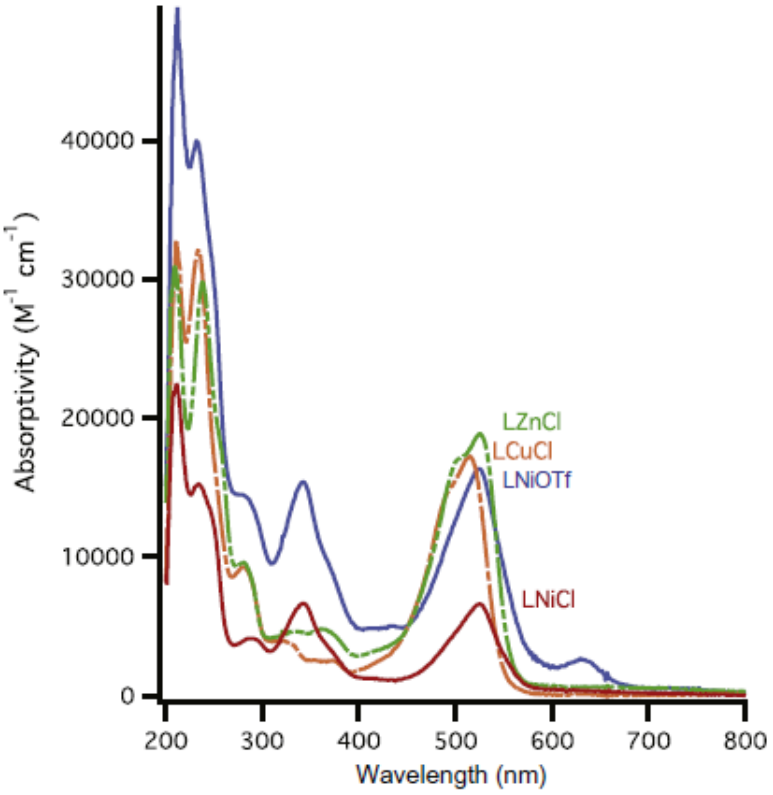

Figure 2.5. UV-vis spectrum of complexes **2-5**.

In the case of 8-aminoquinoline and derivatives complexes, a similar red shift has been observed between free ligand and metal complex however the shift was of much smaller magnitude (~ 10 nm).[15-16] We previously observed a similar magnitude (ca. 100 nm) shift in the tolyl-BDI^{QQ}H system.[10]

The UV-vis spectra for **4** and **5** are very similar. In addition to three ligand-based bands, they both contain a weak band at 280 nm. The spectra for **2** and **3** are more complex. Both contain an additional strong band at 343 nm, correlated with a molar absorptivity value of the same magnitude as the ligand based transitions, assigned as a MLCT band. Complex **2** possesses a unique feature at 631 nm with a low molar absorptivity of 2200 M^{-1} cm^{-1}. We hypothesize that this is a d-d transition. This feature could be due to the difference in geometry between **2** and **3** where **2** is a four-coordinate

cation with a weakly coordinating anion and **3** is hypothesized to be a neutral five-coordinate complex similar to **4** and **5**. Lastly, the molar absorptivity values for the visible absorbances of these complexes are in the range of 10^4 M^{-1} cm^{-1}. Although these are intense, these values are expected for aminoquinoline complexes.[10, 15, 17]

*Fluorescence properties of BDI^{QQ}ZnCl, **5***

Fluorescent sensors for biologically relevant metals have been of growing interest.[18] Zinc has been at the focus of this interest considering it is the second most abundant transition metal in the human body.[19-21] Quinoline derivatives have long been used as fluorescent sensors for zinc.[17, 22-24] For example, Zhou and co-workers recently synthesized a fluorescent sensor for Zn^{2+} based on a Schiff base ligand containing a quinoline.[25] These prior studies led us to investigate the luminescence of complex **5** and determine its quantum yield using fluorescein as a standard. The quantum yield of the fluorescein dianion in methanol has been reported by Magde and coworkers to be 0.91 ± 0.015.[26] The emission spectra for these studies resulted from excitation at 485 nm and were recorded from 495 nm to 800 nm. The fluorescence spectrum of **5** exhibits a maximum at 560 nm and its quantum yield in methanol was determined to be 0.15 ± 0.014 (Figure 2.6).

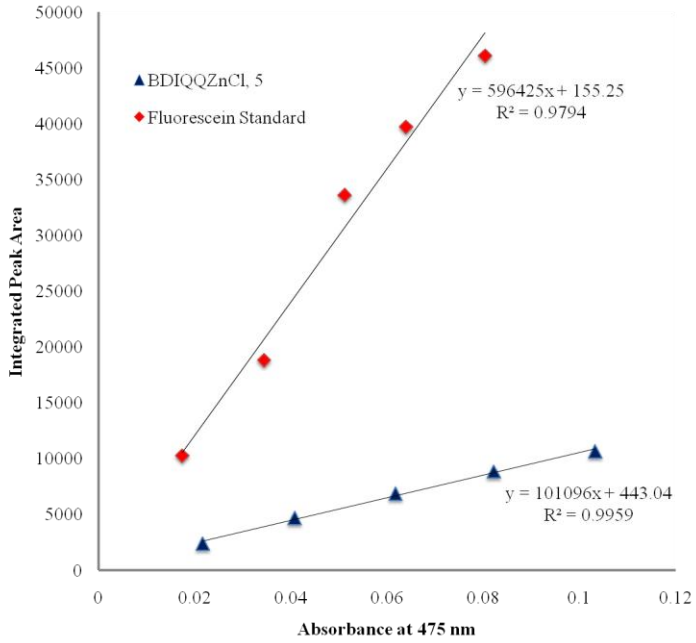

Figure 2.6. Quantum yield determination plot. The fluorescein dianion (red) was used as a standard to measure the quantum yield of $BDI^{QQ}ZnCl$, **5** (blue).

In competition studies, the fluorescence of complex **5** was monitored as a divalent cation was added in a 20 fold excess (Figure 2.7). Addition of Mg^{2+}, Ca^{2+}, Ba^{2+}, Fe^{2+} and Ni^{2+} did not change the fluorescence of **5** while Co^{2+} had a slight quenching effect and Cu^{2+} completely quenched its fluorescence. Zhou and co-workers saw similar results with Cu^{2+} and Co^{2+} and concluded the Zn^{2+} metal was displaced from the zinc complex by Cu^{2+} and Co^{2+}.[25]

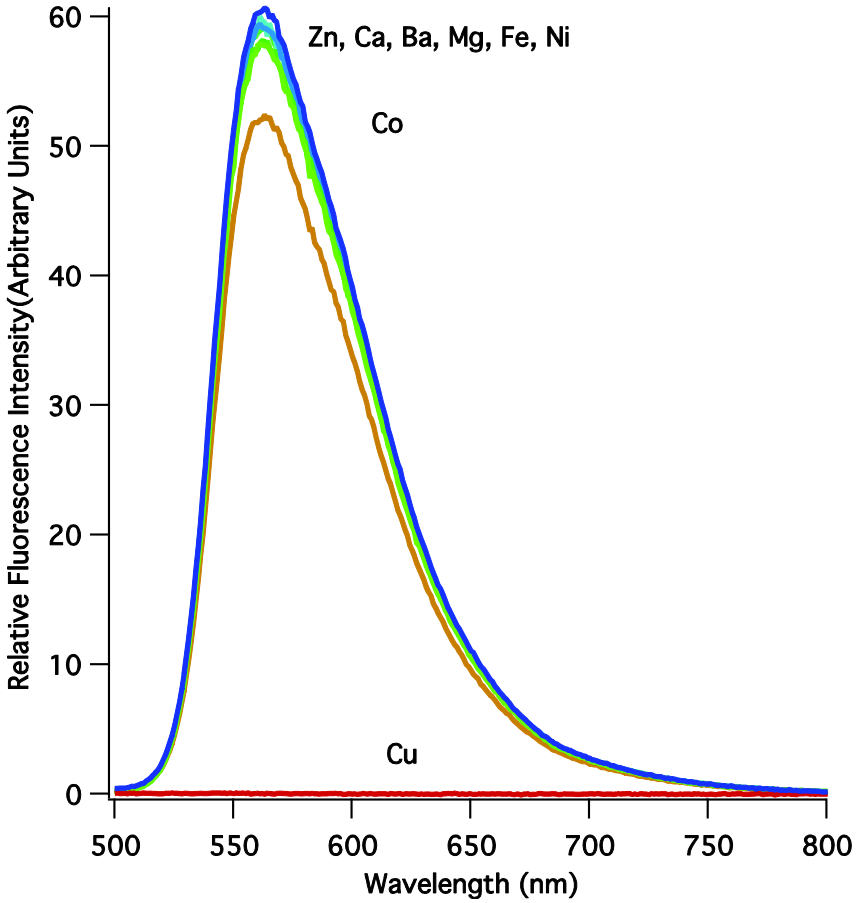

Figure 2.7. Fluorescence emission spectra (λ_{ex} = 485 nm) of complex **5** (6.9 x 10^{-6} M) upon addition of divalent metals Mg^{2+}, Ca^{2+}, Ba^{2+}, Fe^{2+}, Co^{2+}, Ni^{2+}, Cu^{2+} and Zn^{2+}(1.56 x 10^{-4} M) in methanol.

A similar behavior was observed when the same divalent cations were added to ligand **1** in the presence of excess base. Reaction of **1** and Zn^{2+} led to strong fluorescence where as Cu^{2+} led to weak fluorescence (Figure 2.8). The free ligand **1** demonstrates fluorescence due to the complexation of adventitious trace metals. Addition of EDTA gives complete quenching of the luminescence of **1**.

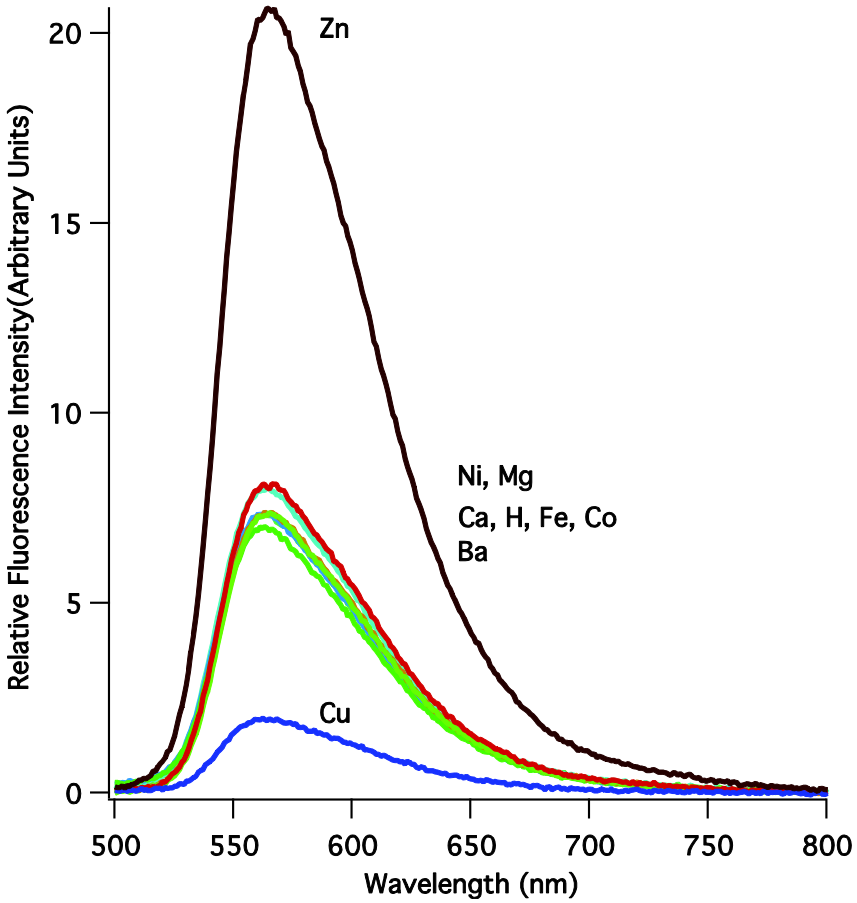

Figure 2.8. Fluorescence emission spectra (λ_{ex} = 485 nm) of complex **1** (5.9 x 10^{-6} M) upon addition of divalent metals Mg^{2+}, Ca^{2+}, Ba^{2+}, Fe^{2+}, Co^{2+}, Ni^{2+}, Cu^{2+} and Zn^{2+}(6.0 x 10^{-6} M) in methanol in the presence of NaOH (2.5 x 10^{-4} M).

*Solid-State Structures of complexes **4** - **5***

As previously mentioned, the geometry of complexes **4** and **5** can be described as distorted square pyramidal with similar tau values of 0.39 and 0.36 respectively. A closer comparison of the two complexes reveals analogous structures (Figure 2.9).

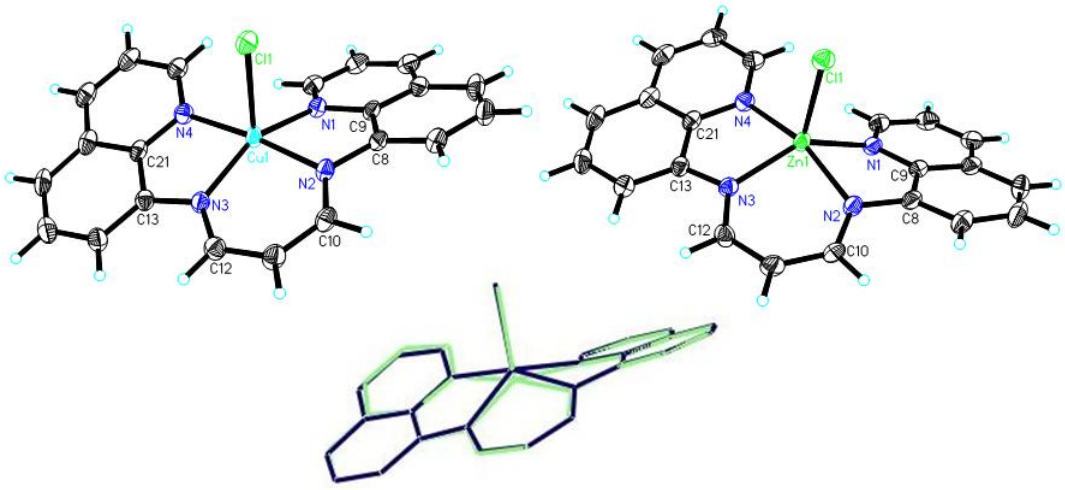

Figure 2.9. ORTEP diagram of **4** (top left) and **5** (top right), with thermal ellipsoids drawn at the 50% probability level. Overlay of structures **4** (green) and **5** (blue) is also shown.

The unit cell dimensions of the two structures are within 0.15 Å and 3.0º of each other for the axis length and angles (Table 2.1). Both structures show the same distortion from square pyramidal geometry with elongated M-N1 bond distances as well as a torsion angle between the quinolyl pendant arm and the BDI backbone that deviates from 180º (Table 2.2).

Table 2.1. Crystallographic data for $BDI^{QQ}CuCl$ (**4**) & $BDI^{QQ}ZnCl$ (**5**).

	$BDI^{QQ}CuCl$, 4	**$BDI^{QQ}ZnCl$, 5**
Formula	$C_{21}H_{15}ClN_4Cu$	$C_{21}H_{15}ClN_4Zn$
formula wt, g mol^{-1}	422.36	424.19
Morphology	Needle	Plate
Color	Green-Red	Red
Lattice Type	Triclinic	Triclinic
Space Group	P-1	P-1
a, Å	8.782(5)	8.931(5)
b, Å	8.975(5)	8.954(3)
c, Å	11.280(6)	11.330(7)
α, deg	97.160(5)	100.21(2)
β, deg	97.00(1)	96.58(3)
γ, deg	103.01(1)	102.59(1)
V, Å	849.1(9)	859.1(8)
Z	2	2
Dc,g cm^{-3}	1.652	1.640
μ, mm^{-1}	1.457	1.599
F(000)	430	432
θ range, deg	1.84 to 26.40	1.85 to 26.37
reflns collected	3442	7177
unique reflns	3442	3471
data/restraint/parameters	3442 / 0 / 245	3471 / 0 / 244
R1, wR2 [$I>2\sigma(I)$]	0.0396, 0.0933	0.0317, 0.0724
R1, wR2 [all data]	0.0560, 0.1013	0.0423, 0.0779
GOOF	1.075	1.011
largest diff peak, hole, e $Å^{-3}$	0.413, -0.462	0.322, -0.306

Table 2.2. Experimental bond distances and angles $BDI^{QQ}CuCl$ (**4**) & $BDI^{QQ}ZnCl$ (**5**).

	$BDI^{QQ}CuCl$, 4	**$BDI^{QQ}ZnCl$, 5**
Bond Lengths (Å)		
$M\text{-}N_1$	2.078(3)	2.168(2)
$M\text{-}N_2$	1.958(3)	2.062(2)
$M\text{-}N_3$	1.972(3)	2.045(2)
$M\text{-}N_4$	1.999(3)	2.125(2)
$N_1\text{-}N_3$	3.920(4)	3.958(3)
$N_2\text{-}N_4$	3.9516(4)	4.135(3)
Bond Angles (deg)		
$N_2\text{-}M\text{-}N_3$	92.9(1)	90.38(8)
$C_{10}\text{-}N_2\text{-}C_8\text{-}C_9$	156.4(3)	152.8(2)
$C_{12}\text{-}N_3\text{-}C_{13}\text{-}C_{21}$	179.0(3)	175.9(2)
Q,Q Twist[a]	18.4	25.0

[a] Twist angle defined as the angle between the two least-squares planes of the quinolyl groups

Torsion angle C12-N3-C13-C21 is close to 180º (179.0º (**4**) and 175.9º (**5**)) while torsion angle C10-N2-C8-C9 is 156.4º and 152.8º for **4** and **5** respectively. This indicates that although the ligand is fully conjugated, it is not planar. One of the pendant arms appears to deviate from planarity in order to accommodate the size of the metal. Zinc has an ionic radius of 0.68 Å when five-coordinate while similar coordinated copper(II) is slightly smaller with an ionic radius of 0.65 Å.[27]

The binding mode observed in **6** can be considered the result of poor binding of Co(III) to all four nitrogens, explaining its preference for binding to two ligands in tridentate fashion (Figure 2.10).

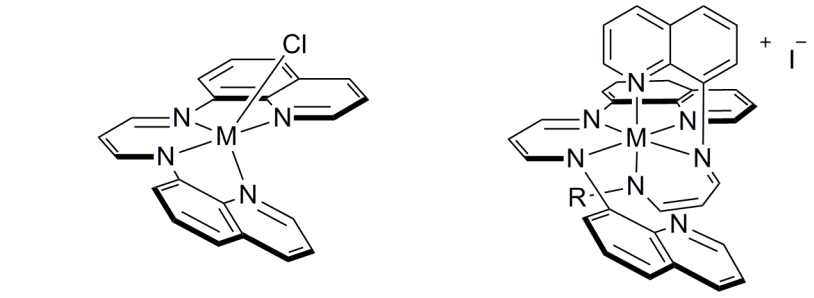

Mono-ligand Distorted Square Pyramid
$BDI^{QQ}MCl$
M = Cu (**4**), Zn (**5**)

Bis-ligand Octahedron
$[(BDI^{QQ})_2M]^+I^-$
M = Co (**6**)

Figure 2.10. Different binding modes observed in the metal complexes series using **1** as a ligand. In the case of the bis-ligand octahedron, the second unbound quinoline has been replaced by R for clarity.

Considering the ionic radius of low-spin cobalt(III) is 0.55 Å, we have hypothesized that metals with small ionic radius are not well supported by this rigid ligand.[27] In an effort to test our hypothesis and understand the binding mode of **1**, we turned to DFT calculations to analyze the effect of ionic radius and charge on the conformational energy of the ligand.

Computational Studies

Using DFT, ligand distortion energy calculations were performed on $BDI^{QQ}M^{n+}$ complexes with different d^0 metal ions, M, coordinated. The functional chosen for the DFT calculations was the M06-L functional, which has been shown to be particularly useful for computations of compounds involving transition metal compounds.[28-29] We define the ligand distortion energy as the gas-phase cost associated with distorting the *bare* anionic ligand from its optimal gas-phase geometry to the geometry that it adopts in the ligand-metal complex (i.e., a single-point energy calculation is performed after having

removed the metal from the optimized geometry of the complex). Ligand distortion energy calculations were correlated with Shannon effective ionic radii in order to facilitate quantitative comparison across a broad spectrum of metals not limited to transition metals.[27] Six-coordinate radii were used in all cases for consistent comparisons as they are available for all ions examined. By selecting metals from four columns of the periodic table, we anticipate that differences in electrostatics will be minimized beyond second-order effects coupled to conformational strain associated with changing ionic radii.

The results for the Group 1 $BDI^{QQ}M$, the Group 2 $BDI^{QQ}M^{+}$ and $BDI^{QQ}MCl$ complexes show an identical trend of decreasing BDI^{QQ} distortion energy with increasing effective ionic radius (Table 2.3 and Figure 2.11).

Table 2.3. Ligand distortion energy (LDE) values from DFT calculations and their Shannon ionic radii for Group 1, 2, 3 and 4 metals. The ionic radii values used are those reported by Shannon for hexavalent complexes.[27]

M	r(M) [Å]	LDE($BDI^{QQ}M^{n+}$) [kcal/mol]	LDE($BDI^{QQ}MCl$) [kcal/mol]
Group 1 - n = 0			
Li	0.76	8.2	
Na	1.02	5.6	
K	1.38	3.2	
Rb	1.52	2.5	
Cs	1.67	1.9	
Group 2 - n = 1			
Be	0.45	31.3	19.7
Mg	0.72	11.5	10.6
Ca	1.00	7.8	5.8
Sr	1.18	6.5	4.1
Ba	1.35	5.3	3.7
Group 3 - n = 2			
Sc	0.75	15.5	
Group 4 - n = 3			
Ti	0.61	25.2	

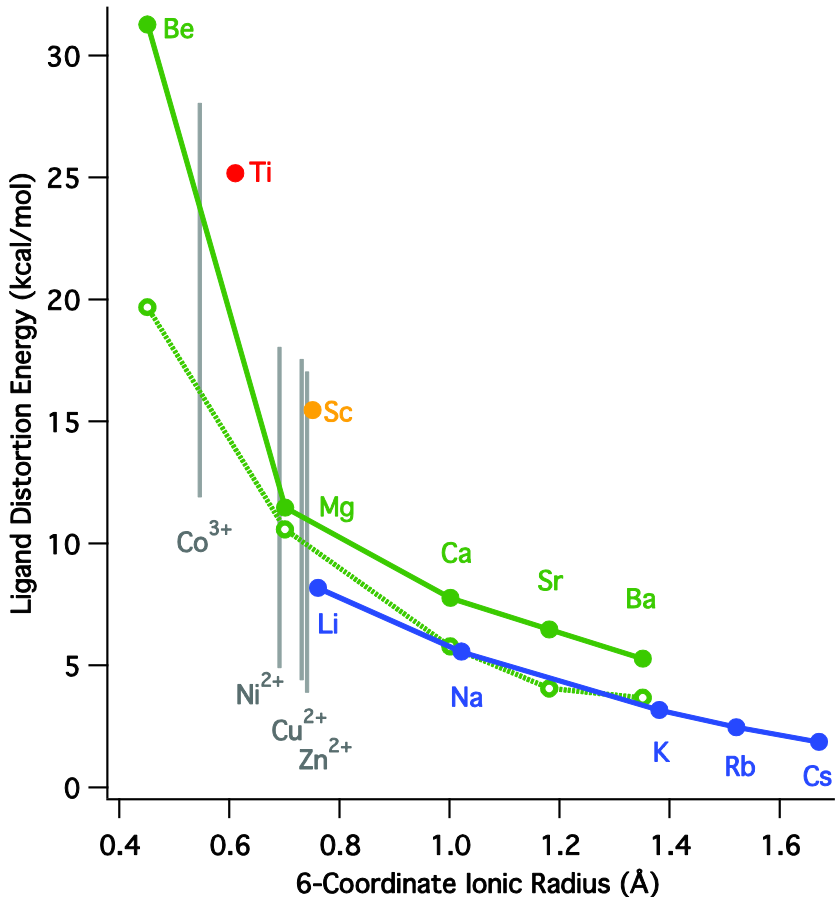

Figure 2.11. Ligand distortion energy (kcal/mol) versus Shannon effective 6-coordinate ionic radii of various d^0 metal ions.[27] Ligand distortion energies were calculated by comparing the gas phase energy of the conformations adopted by the free and tetradentate-bound ligand. Filled symbols correspond to $BDI^{QQ}M^{n+}$ ($0 \leq n \leq 3$) and open symbols to $BDI^{QQ}MCl$ complexes. The ionic radii (low spin for Co and Ni) of the transition metals examined in this study are denoted with vertical lines.

For Group 1 metals, the 9. 1 Å difference in ionic radii between Li (0.76 Å) and Cs (1.67 Å) corresponds to a 6.3 kcal/mol ligand distortion energy change. This trend is more prominent when looking at both cationic $BDI^{QQ}M^{+}$ and neutral $BDI^{QQ}MCl$ complexes formed from Group 2 metals. In the case of Group 2 metals, a distortion energy difference of 26.0 kcal/mol and 23.4 kcal/mol for the cationic and neutral BDI^{QQ} complexes can be observed over a similar ionic radii range of 0.90 Å. The increased

BDI^{QQ} distortion energies of the alkali earth series can be largely explained by the smaller effective ionic radii of Group 2 compared to Group 1, although coordination of Cl^- reduces distortion to some extent by reducing the electrophilicity of the metal cations. Consideration of BDI^{QQ} distortion energies for metal cation complexes where the metal cations are of similar size but differing in formal charge suggests that additional destabilization is associated with large charge. Thus, comparing Li, Mg and Sc, we observe an increase in ligand distortion energy with a higher formal charge. Scandium with a radius of 0.75 Å has the highest energy, 15.5 kcal/mol while Mg (0.72 Å) and Li (0.76 Å) have distortion energies of 11.5 kcal/mol and 8.2 kcal/mol respectively.

2.4 Conclusions

A series of first row transition metal complexes have been prepared using a monoanionic tetradentate β-diketiminate with pendant quinoline ligand arms. While the nickel, copper and zinc 2+ ions were shown to bind to the ligand in a tetradentate manner, this was not the case for cobalt(III), which bound two ligands, each in a tridentate manner. Through the use of crystallography and DFT calculations, it was shown that the ligand is poorly suited to metals with smaller ionic size due to its inflexibility. Although BDI ligands with pendant arms have the potential to serve as models for vitamin B_{12} and other cofactors, this specific ligand is not well suited to the task due to its inability to adjust to varying metal radii. This is especially important in view of the difference in size among the +1, +2, and +3 oxidation states of cobalt in vitamin B_{12}. Our current efforts are thus focused on a more flexible BDI ligand. The BDI^{QQ} ligand does show promise as a fluorescent sensor for Zn. Similarly, the dramatic decrease in the fluorescence intensity of the zinc complex in the presence of Cu^{2+} could provide the basis for detection or imaging of cupric ions.

2.5 Experimental procedures

General Considerations. Experiments were conducted in air under ambient conditions unless otherwise stated. Reagents and solvents were purchased commercially and used without further purification at the exception of 8-amino-5-quinoline sulfonic acid, which was synthesized according to a literature procedure.[30] UV-vis absorbance data was collected with an OceanOptics CHEMUSB2 spectrophotometer using a quartz cuvette. Infrared (IR) spectra were collected with a Midac M series spectrometer. ^{1}H NMR and 2D NMR spectra were acquired on a Varian Inova instrument at 500 MHz equipped with an inverse probe at the exception of **3** whose spectra were acquired on a Varian Inova instrument at 800 MHz with a HCN cold probe. ^{13}C shifts were established from 2D HMQC (Heteronuclear Multiple Quantum Correlation) and HMBC (Heteronuclear Multiple Bond Correlation) NMR experiments. ^{1}H and ^{13}C shifts were assigned based on 2D NMR (Tables 2.4 and 2.5). ^{19}F NMR spectra were acquired on a Varian Inova instrument at 292 MHz. ^{1}H and 2D spectra were referenced to the residual solvent peak while ^{19}F spectra were referenced to internal fluorobenzene at -113.15 ppm. All chemical shifts are reported in ppm. Mass spectrometry (MS) data was acquired on a Bruker BioTOF ESI-MS under positive mode. Polyethylene glycol (PEG) standard was used for High Resolution Mass Spectrometry (HRMS). Conductivity measurements were taken using a Vernier conductivity probe. Fluorescence measurements were acquired on a Varian Cary Eclipse Fluorescence Spectrophotometer using a quartz cell with a path length of 10 mm. For the fluorescence study, UV-vis measurements were acquired on Cary 100 Bio UV-Visible Spectrophotometer using disposable CVD-UV plastic cuvettes (220 - 900 nm) from Ocean Optics.

Table 2.4. ^{1}H shift assignment from COSY experiments. Spectra of compounds **1**, **5** & **6** were acquired in d_6-DMSO. Shifts for compound **6** are reported for both bound and unbound side respectively. Spectra of **2** & **3** were performed in d_3-CD_3CN.

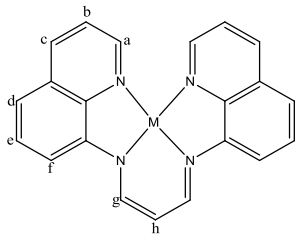

Complex	1	2	3	5	6
HN	12.65	-	-	-	-
a	9.06	8.58	8.85	9.24	8.35, 7.56
b	7.74	7.68	7.80	7.87	7.50, 7.04
c	8.53	8.58	8.63	8.69	8.07, 8.09
d	7.94	7.89	7.94	7.92	7.22, 7.80
e	7.76	7.68	7.76	7.74	7.22, 7.76
f	7.96	7.68	7.76	7.73	7.07, 7.51
g	9.23	7.85	8.61	8.52	7.45, 6.57
h	7.13	5.70	5.68	5.32	5.21

Table 2.5. ^{13}C shift assignment from HMQC and HMBC experiments. Spectra of compounds **1**, **5** & **6** were acquired in d_6-DMSO. Shifts for compound **6** are reported for both bound and unbound side respectively. Spectra of **2** & **3** were performed in d_3-CD_3CN.

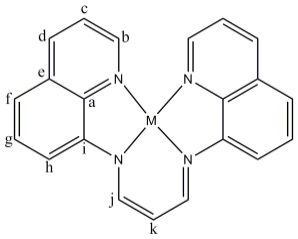

Complex	1	2	3	5	6
a	138.3	unknown	145.0	139.1	144.0, 127.9
b	149.9	141.4	155.0	148.7	137.9, 148.7
c	123.0	130.2	125.4	122.7	125.7, 120.8
d	137.1	153.3	142.8	139.8	151.3, 135.1
e	128.9	143.5	131.6	138.4	146.0, 143.0
f	125.8	116.4	118.0	112.4	120.7, 125.8
g	126.8	124.1	126.8	128.5	113.5, 125.3
h	116.7	130.4	131.8	121.1	128.2, 125.2
i	135.0	147.4	149.8	142.7	147.8, 149.8
j	161.0	148.4	150.2	153.1	143.9, 161.3
k	101.8	100.4	102.2	97.4	93.5

BDI^{QQ}H (1). Compound **1** was prepared according to a published method by Zakta *et al*. [5]. The resulting solid was isolated and dried under vacuum to yield a bright yellow solid (5.59 g, 99%). UV (DMSO) λ_{max}, nm (ε/dm^3 mol^{-1} cm^{-1}): 262, 419 (35600 ± 300). ^{1}H NMR (500 MHz, d_6-DMSO): δ 12.65 (1 H, d, *J* = 14.5 Hz, HN); 9.23 (2 H, t, *J* = 11.5 Hz, CH); 9.06 (2 H, dd, *J* = 1.5 and 4.0 Hz, ar. CH); 8.53 (2 H, dd, *J* = 1.5 and 8.0 Hz, ar.

CH); 7.96 (2 H, d, *J* = 8.0 Hz, ar. CH); 7.94 (2 H, d, *J* = 8.0 Hz, ar. CH); 7.76 (2 H, dd, *J* = 8.0 and 8.0 Hz, ar. CH); 7.74 (2 H, dd, *J* = 4.0 and 8.5 Hz, ar. CH); 7.13 (1 H, t, *J* = 11.5 Hz, CH). ^{13}C NMR (125 MHz, d_6-DMSO): δ 161.0, 149.9, 138.3, 137.1, 135.0, 128.9, 126.8, 125.8, 123.0, 116.7, 101.8. ESI-HRMS-TOF *m/z*: $[M + H]^+$ calc. for $C_{21}H_{17}N_4$, 325.1448; found, 325.1456.

BDI$^{Q'Q'}$H (1a). In a 50 mL reaction flask, 8-amino-5-quinoline sulfonic acid (0.71 g, 3.1 mmol) was dissolved in 20 mL of MeOH, which was heated to 65º C. Once all of the solid had dissolved completely, 1,1,3,3-tetramethoxypropane (0.26 mL, 1.6 mmol) was added dropwise via syringe. The solution was stirred for 20 minutes and then acidified with 10 mL of a 1:1 mixture of 3.5 M HCl and MeOH, added dropwise. Within minutes, a bright orange solid began to precipitate. The solution was heated to reflux for an additional hour, then allowed to cool to room temperature. The resulting solid was collected by filtration, washed with a 1:1 mixture of MeOH and ether, and dried under vacuum to yield a bright orange solid (0.76 g, 92%). UV (MeOH) λ_{max}, nm (ε/dm^3 mol^{-1} cm^{-1}): 250, 424 (29000). ^{1}H NMR (500 MHz, d_6-DMSO): δ 12.64 (d, J = 13.0 Hz, 1H); 9.26 (dd, J = 1.5, 8.5 Hz, 2H); 9.08 (t, J = 12.5 Hz, 2H); 9.04 (dd, J = 1.5, 4.0 Hz, 2H); 8.07 (d, J = 8.0 Hz, 2H); 7.83 (d, J = 8.0 Hz, 2H); 7.76 (dd, J = 4.5, 8.5 Hz, 2H); 7.15 (t, J = 11.5 Hz, 1H). ESI-HRMS-TOF *m/z*: $[M - H]^-$ calc. for $C_{21}H_{15}N_4O_6S_2$, 483.0438; found, 483.0441.

[BDI^{QQ}Ni][SO$_3$CF$_3$] (2). Under inert atmosphere, compound **1** (0.133 g, 0.41 mmol) was dissolved in 30 mL of dry THF. Potassium bis(trimethylsilyl) amide (0.235 g, 1.18

mmol) in 10 mL of dry THF was added dropwise to a solution of compound **1.** An immediate color change from yellow to pink was observed. In a separate vial, nickel(II) triflate (0.149 g , 0.42 mmol) was dissolved in 20 mL of THF. The deprotonated ligand solution was added dropwise to the metal solution. It was stirred overnight and red solids precipitated. Under ambient atmosphere, the solution was filtered using a glass fiber filter. The resulting solids were washed with THF and redissolved in MeOH. The solvent was evaporated using rotary evaporation and solids were dried under vacuum (0.054 g, 25%). UV (MeOH) λ_{max}, nm (ε/dm^3 mol^{-1} cm^{-1}): 212, 234, 287 (10400 ± 500), 343 (14600 ± 200), 524 (15900 ± 500), 631 (2200 ± 200). IR (Nujol Mull) $\tilde{\upsilon}_{max}$ (cm^{-1}): 2922 (s), 2852 (s), 1580 (m), 1493 (m), 1446 (s), 1376 (s), 1353 (w), 1324 (w), 1296 (m), 1267 (s, asym. SO_3), 1219 (w, sym. CF_3), 1141 (br. m, asym. CF_3), 1027 (s, sym. SO_3), 827 (s), 771 (s), 633 (s). ^{1}H NMR (500 MHz, CD_3CN): δ 8.58 (4 H, br d, *J* = 9.0 Hz, ar. CH); 7.89 (2 H, d, *J* = 7.5 Hz, ar. CH); 7.85 (2 H, d, *J* = 6.0 Hz, CH); 7.68 (6 H, m, ar. CH); 5.70 (1 H, t, *J* = 6.5 Hz, CH). ^{13}C NMR (125 MHz, CD_3CN): δ 153.3, 148.4, 147.4, 143.5, 141.4, 130.4, 130.2, 124.1, 116.4, 100.4, one quaternary resonance not observed. ^{19}F NMR (292 MHz, CD_3CN): δ -77.58. ESI-HRMS-TOF *m/z*: $[M - SO_3CF_3]^+$ calc. for $C_{21}H_{15}N_4Ni$, 381.0650; found, 381.0640.

[BDI^{QQ}NiCl] (3). Under ambient atmosphere, compound **2** (0.040 g, 0.07 mmol) was dissolved in 60 mL of MeOH. A solution of tetrabutylammonium chloride (0.042 g, 0.15 mmol) in 20 mL of MeOH was added dropwise to compound **2**. It was stirred overnight. Solution was filtered using a glass fiber filter and the solvent from the filtrate was removed using a rotary evaporator. Solids were washed with THF and dried under

vacuum (0.031 g, 98%). UV (MeOH) λ_{max}, nm (ε/dm^3 mol^{-1} cm^{-1}): 212, 235, 289 (3800 ± 200), 343 (6300 ± 300), 525 (6400 ± 400). IR (Nujol Mull) $\tilde{\upsilon}_{max}$ (cm^{-1}): 2924 (s), 2853 (s), 1494 (w), 1455 (s), 1376 (s), 1323 (w), 1311 (m), 1274 (w), 825 (w), 757 (w), 722 (w). ^{1}H NMR (800 MHz, CD_3CN): δ 8.73 (2 H, d, *J* = 5.6 Hz, ar. CH); 8.65 (2 H, d, *J* = 8.0 Hz, ar. CH); 8.21 (2 H, d, *J* = 4.8 Hz, CH); 7.97 (2 H, dd, *J* = 1.6 and 7.2 Hz, CH); 7.78 (2 H, dd, *J* = 5.6 and 8.0 Hz, ar. CH); 7.76 (4 H, m, ar. CH); 5.74 (1 H, t, *J* = 5.6 Hz, CH). ^{13}C NMR (200 MHz, CD_3CN): δ 155.0, 150.2, 149.8, 145.0, 142.8, 131.8, 131.6, 126.8, 125.4, 118.0, 102.2. ESI-HRMS-TOF *m/z*: $[M - Cl]^+$ calc. for $C_{21}H_{15}N_4Ni$, 381.0650; found, 381.0654.

[BDI^{QQ}CuCl] (4). Under ambient atmosphere, compound **1** (0.032 g, 0.10 mmol) was dissolved in 30 mL of MeOH. A solution of copper(II) chloride dihydrate (0.016 g, 0.09 mmol) in 10 mL of MeOH was added dropwise to the ligand solution. An immediate color change to red metal was observed. Three equivalents of 1.0 M sodium hydroxide (280 μL, 0.28 mmol) were added dropwise to the metal complex solution. The solution was stirred for another five minutes and was then filtered using a glass fiber filter. The solvent from the filtrate was removed via a rotary evaporator. The red residue was washed with THF and redissolved in MeOH. Further purification was obtained by layering the MeOH solution with diethyl ether (1:2). Solids and green crystals isolated from purification were dried under vacuum (0.016 g, 40%). UV (MeOH) λ_{max}, nm (ε/dm^3 mol^{-1} cm^{-1}): 215, 235, 284 (10100 ± 500), 493 (15300 ± 900), 514 (17500 ± 1100). ESI-HRMS-TOF *m/z*: $[M - Cl]^+$ calc. for $C_{21}H_{15}N_4Cu$, 386.0593; found, 386.0589. X-ray

quality crystals were obtained by layering a saturated MeOH solution of the complex with diethyl ether (1:2).

[BDI^{QQ}ZnCl] (5). Under ambient atmosphere, compound **1** (1.871 g, 5.8 mmol) was dissolved in 80 mL of MeOH. A solution of anhydrous zinc(II) chloride (0.787 g, 5.8 mmol) in 20 mL of MeOH was added dropwise to the ligand solution. Three equivalents of 1.0 M sodium hydroxide (17.3 mL, 17.3 mmol) were then added dropwise to the solution. An immediate color change was observed from yellow to red. The solution was immediately filtered using a glass fiber filter and the solvent removed from the filtrate by rotary evaporation. The resulting red solid was dried under vacuum (1.80 g, 73%). UV (DMSO) λ_{max}, nm (ε/dm^3 mol^{-1} cm^{-1}): 262, 282, 325, 369 (3700 ± 210), 509 (24900 ± 190), 530 (27600 ± 100). ^{1}H NMR (500 MHz, d$_6$-DMSO): δ 9.24 (2 H, dd, *J* = 1.0 and 4.5 Hz, ar. CH); 8.69 (2 H, d, *J* = 8.5 Hz, ar. CH); 8.52 (2 H, d, *J* = 6.0 Hz, CH); 7.92 (2 H, dd, *J* = 1.5 and 6.5 Hz, ar. CH); 7.87 (2 H, dd, *J* = 4.5 and 8.5 Hz, ar. CH); 7.74 (2 H, dd, *J* = 8.5 and 8.5 Hz, ar. CH); 7.73 (2 H, dd, *J* = 7.5 and 14.5 Hz, ar. CH); 5.32 (1 H, t, *J* = 6.0 Hz, CH). ^{13}C NMR (125 MHz, d$_6$-DMSO): δ 153.1, 148.7, 142.7, 139.8, 139.1, 138.4, 128.5, 122.7, 121.1, 112.4, 97.4. ESI-HRMS-TOF *m/z*: [M – Cl]$^+$ calc. for $C_{21}H_{15}N_4Zn$, 387.0588; found, 387.0585. X-ray quality crystals were obtained by layering a saturated MeOH solution of the complex with pure MeOH and diethyl ether.

BDI$^{Q'Q'}$ZnCl (5a). Complex **5a** was prepared using the same method as complex **5** except using compound **1a** (0.050 g, 0.10 mmol) and anhydrous zinc(II) chloride (0.014 g, 0.10 mmol). The resulting solid was dichromatic red and gold (0.067 g, 98%). UV

(MeOH) λ_{max}, nm (ε/dm^3 mol^{-1} cm^{-1}): 226, 266 (32000), 282 (sh.), 302 (sh.), 349, 382, 538 (29000), 560 (34000). ^{1}H NMR (500 MHz, d_6-DMSO): δ 9.44 (dd, *J* = 1.5, 8.7 Hz, 2H); 9.23 (dd, *J* = 1.5, 4.5 Hz, 2H); 8.52 (d, *J* = 6.6 Hz, 2H); 8.04 (d, *J* = 8.1 Hz, 2H); 7.91 (dd, *J* = 4.5, 8.7 Hz, 2H); 7.83 (d, *J* = 8.1 Hz, 2H); 5.35 (t, *J* = 8.3 Hz, 1H). ESI-HRMS-TOF *m/z*: $[M - 2H + 2Na - Cl]^+$ calc. for $C_{21}H_{11}N_4O_6S_2Na_2Zn$, 590.9363; found, 590.9364.

[(BDI^{QQ})$_2$Co]I (6). Under ambient atmosphere, compound **6** was prepared by dissolving compound **1** (0.101 g, 0.31 mmol) into 10 mL of MeOH. Three equivalents of 1.0 M sodium hydroxide (0.93 mL, 0.93 mmol) were added dropwise to compound **1**. A solution of cobalt(II) iodide (0.097 g , 0.31 mmol) in 10 mL of MeOH was added dropwise to the solution of compound **1**. An immediate color change from yellow orange to brown was observed. Solution was stirred overnight. Solution was filtered using a glass fiber filter and the solvent was removed from the filtrate by rotary evaporation. The resulting brown solids were washed with hexanes, redissolved in MeOH, dried under vacuum (0.145 g, 83%). ^{1}H NMR (500 MHz, d_6-DMSO): δ ppm 8.35 (2 H, d, *J* = 8.0 Hz, ar. CH); 8.09 (2 H, dd, *J* = 1.5 and 8.5 Hz, ar. CH); 8.07 (2 H, dd, *J* = 0.5 and 5.5 Hz, ar. CH); 7.80 (2 H, dd, *J* = 0.5 and 8.0 Hz, ar. CH); 7.76 (2 H, dd, *J* = 1.0 and 7.0 Hz, ar. CH); 7.56 (2 H, dd, *J* = 2.0 and 4.5 Hz, ar. CH); 7.51 (2 H, dd, *J* = 8.0 and 8.0 Hz, ar. CH); 7.50 (2 H, d, *J* = 2.0 and 8.0 Hz, ar. CH); 7.45 (2 H, d, *J* = 7.0 Hz, CH); 7.22 (4 H, d, *J* = 8.0 Hz, ar. CH); 7.07 (2 H, t, *J* = 8.0 Hz, ar. CH); 7.04 (2 H, dd, *J* = 4.0 and 8.0 Hz, ar. CH); 6.57 (2 H, d, *J* = 6.5 Hz, CH); 5.21 (2 H, t, *J* = 6.5 Hz, CH). ^{13}C NMR (125 MHz, d_6-DMSO): δ 161.3 (CH), 151.3, 149.8, 148.7, 147.8, 146.0, 144.0, 143.9 (CH),

143.0, 137.9, 135.1, 128.2, 127.9, 125.8, 125.7, 125.3, 125.2, 120.8, 120.7, 113.5, 93.5 (CH). ESI-HRMS-TOF *m/z*: $[M - I]^+$ calc. for $C_{42}H_{30}N_8Co$, 705.1925; found, 705.1920.

Conductivity Study. Solutions of complexes **2**, **3** and **4** were prepared in acetonitrile at a concentration of 5×10^{-4} M. Tetrabutylammonium chloride was used a standard. All solutions were measured using a conductivity probe.

Fluorescence Studies. For all fluorescence runs, a UV-vis spectrum was first acquired. The excitation spectra were scanned between 300 nm and 560 nm with the emission set at 575 nm while the emission spectra, which were excited at 485 nm, were collected between 495 nm and 800 nm. It should be stated that special care was taken to minimize the impact of trace metal for these studies.

For the quantum yield determination, stock solution of **5** (5.1×10^{-5} M) and fluorescein (3.1×10^{-5} M with 14 µL of triethylamine) were made with HPLC grade methanol. Five dilutions of the stock were preparing thus the concentration range for samples and standard were 1.48×10^{-6} M - 7.40×10^{-6} M and 6.12×10^{-7} M - 3.06×10^{-6} M respectively.

For the competition studies, methanol stock solutions of the cations (1.3×10^{-3} M) were made prepared from $MgCl_2 \cdot 6H_2O$, $CaCl_2$, $BaCl_2 \cdot 2H_2O$, $FeCl_2 \cdot 4H_2O$, $CoCl_2 \cdot 6H_2O$, $NiCl_2 \cdot 6H_2O$, $CuCl_2 \cdot 2H_2O$ and $ZnCl_2$. The concentration of the stock solution of **5** was 5.52×10^{-5} M in methanol while for **1**, it was 7.83×10^{-5} M. For the competition study between **5** and each cation, 250 µL of stock solution of **5**, 250 µL of a cation stock and 1.5 mL of methanol were added to a disposable cuvette. For the ligand study, each cation

run consisted of 10 µL of cation stock, 150 µL of 1, 1 µL of 0.5 M NaOH and 1.85 mL of methanol in a disposable cuvette.

Crystallography. Crystal data for **4** and **5** were collected on a Bruker SMART Platform CCD diffractometer at 173(2) K using Mo Kα radiation and a graphite monochromator. Structures were solved using SHELXS-97 and refined using SHELXL-97.[31] Crystallographic data for **4** and **5** are summarized in Table 1.

The structure of **5** was solved using a Patterson map to place the zinc and chloride atoms while all other non hydrogen atoms were placed using difference Fourier. Considering the similarities between the unit cells of **4** and **5**, the structure of **4** was solved using the solution structure of **5** as a model with substitution of the metal. Complex **4** showed nonmerohedral twinning and the data was corrected for this using Cell Now program.[32] The twin law was found to be 180º rotation of the reciprocal [0,1,0] axis. The ratio of its twin components was determined to be 56:44.

Computional Methods. All density functional calculations made use of the M06-L density functional and were carried out in Gaussian03 via the Minnesota Gaussian Functional Module (MN-GFM).[29, 33-34] As M06-L is a local functional, the resolution of the identity approximation with a fitting basis set was used for greater computational efficiency in the calculation of Coulomb integrals.[35-37] A pruned grid with 99 radial shells and 590 angular points per shell was used for all calculations. Stuttgart basis sets and effective core potentials were used for all metals and the 6-31G(d) basis set was used for all other atoms.[38-39] Where appropriate, molecular geometries were optimized in C_2 point-

group symmetry, and all geometries were verified as local minima by the computation of analytical vibrational frequencies. Ligand distortion energies (LDE) were calculated by subtracting the electronic energy of the BDI^{QQ} anion in its optimized, bare gas phase geometry from the electronic energies of BDI^{QQ} anions held at geometries obtained from optimized geometries of $BDI^{QQ}M^{n+}$ or $BDI^{QQ}MCl$ complexes.

-Chapter Three-

Synthesis and Reactivity of an Isolable Cobalt (I) Complex Containing a β-diketiminate-based Acyclic Tetradentate Ligand

In part from:

Marlier, E. E.; Ulrich, B. A.; McNeill, K. *Inorg. Chem*. Accepted.

3.1 Overview

A model for cobalamin was synthesized using a new monoanionic tetradentate nitrogen donor ligand; 2-(4-tolyl)-1,3-bis(2-isopropylpyridyl)propenediimine (Tol-BDI$^{(2\text{-}pp)2}$H) (**1**), which utilizes isopropylpyridines as pendant arms on a β-diketiminate (BDI) backbone. During the synthesis of **1**, the rearrangement product, Tol-BDI$^{(2\text{-}pp)(4\text{-}pp)}$H (**2**) was observed. Metallation of **1** with zinc iodide and cobalt chloride yielded the corresponding Tol-BDI$^{(2\text{-}pp)2}$ZnI (**3**) and Tol-BDI$^{(2\text{-}pp)2}$CoCl (**4**) complexes. The redox properties of **4** in comparison to cobalamin were examined though electrochemical studies. Electrochemical and bulk reduction of complex **4** gave a diamagnetic cobalt(I) complex, Tol-BDI$^{(2\text{-}pp)2}$Co (**5**). Reactivity of **5** towards C-X bonds was investigated using methyl iodide, 1-iodo-2-(trimethylsilyl)acetylene and *trans*-1-bromo-1-propene, yielding Tol-BDI$^{(2\text{-}pp)2}$Co(CH_3)I (**6**), Tol-BDI$^{(2\text{-}pp)2}$Co($C_2Si(CH_3)_3$)I (**7**) and Tol-BDI$^{(2\text{-}pp)2}$Co(CH=CH(CH_3))Br (**8**) respectively. Synthesis and characterization details for these complexes, including the crystal structure of **3**, are reported.

3.2 Introduction

Cobalamin is an established catalyst for reductive dehalogenation reactions that can transform highly chlorinated substrates into less chlorinated species.[1-4] In an effort to understand the scope and limitations of cobalamin's ability to remediate groundwater polluted with chlorinated ethylene and benzene compounds, several groups in addition to our own have examined dimethylglyoxime- and porphyrin-containing model complexes.[5-12] Cobaloxime, (bis(dimethylglyoximato)cobalt), complexes have been used to gain mechanistic insights and to model proposed intermediates involved in reductive dehalogenation reactions, due to their similar reactivity towards halogenated substrates.[5-7, 10-12] Cobalt porphyrin complexes also have been successfully used as dechlorination catalysts; with the discovery of water-soluble cobalt porphyrin complexes having higher rate constants of dechlorination than vitamin B_{12}.[8, 13] While both cobaloxime and (porphyrin)cobalt complexes have proven useful in modeling the chemistry of cobalamin, there is room for improvement. In particular, the porphyrin and glyoxime-based systems mimic the tetraaza coordination environment of the cobalamin corrin, but do not match its monoanionic charge.

An additional shortcoming of the glyoxime- and porphyrin-based model compounds is the difficulty in preparing and isolating cobalt(I) complexes in these systems. While examples of Co(I) have been prepared in these systems, the complexity in synthesizing these compounds has hindered their use in further studies.[14-16] Researchers have opted instead to generate the Co(I) oxidation state *in situ*. This is unfortunate from the standpoint of studying the mechanism of cobalamin-mediated dechlorination reactions, given that the Co(I) oxidation state is thought to play a central role.[4] The ligand

choice is clearly important as isolable cobalt(I) complexes supported by a variety of nitrogen donor ligands such as N_2P_2, bidentate BDI and iminopyridine pincers have become more common in the literature in recent years.[17-21] With this in mind, we set out to prepare a ligand system that would allow the isolation of a Co(I) complex that effectively models cobalamin.

Our approach to preparing a potentially improved structural model for the corrin has focused on using a β-diketiminate ligand with two pendant donor arms (Chart 1). This strategy has previously been employed by Roesky and coworkers with pendant trialkylamine donors and by Zatka *et al.* with pendant quinoline donors to create a variety of metal complexes.[22-26] Our initial attempts to prepare similar ligands with methylpyridine pendant arms prompted the discovery of a new route to pyridylpyrroles due to intramolecular cyclization of the ligand.[27] The cyclization is thought to occur through a nucleophilic attack by the carbon atom α to the pyridine on the neighboring ketone (or imine). To avoid the cyclization, we followed the lead of Zatka et al., and chose quinolines as pendant arms for our second generation ligand.[28] Subsequent study revealed that a ligand equipped with quinoline pendant arms was too rigid to accommodate the different oxidation states of cobalt.[29] Considering that all three oxidation states of cobalt are likely involved in the process of reductive dehalogenation, a more flexible ligand was devised.[4]

In this work, we report the synthesis and characterization of a new monoanionic tetradentate nitrogen donor ligand; 2-(4-tolyl)-1,3-bis(2-isopropylpyridyl)propenediimine (Tol-BDI$^{(2\text{-pp})_2}$H) (**1**), which employs isopropylpyridines as pendant arms on a β-diketiminate backbone (Chart 3.1).

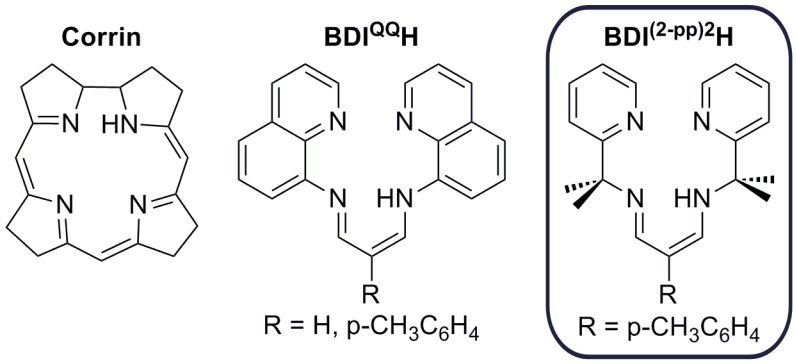

Chart 3.1. Tetradentate monoanionic ligands with the ligand reported here shown boxed.

Learning from our prior work, we have introduced greater flexibility by switching from an sp^2-hybridized carbon to an sp^3-hybridized carbon between the pyridyl group and the BDI backbone. Furthermore, gem-dimethyl substitution on the carbon atom α to the pyridine prevents pyrrole formation through intramolecular cyclization.

Compound **1** was used to prepare zinc iodide (**3**) and cobalt chloride (**4**) complexes. Most notably, we report the synthesis and characterization of an isolable cobalt(I) complex, Tol-BDI$^{(2\text{-pp})2}$Co (**5**) from the reduction of **4** with sodium amalgam. Lastly, we probed the ability of compound **5** to model cobalamin by exploring its reactivity towards carbon-halogen bonds. Substrates investigated were methyl iodide (**6**), 1-iodo-2-(trimethylsilyl)acetylene (**7**) and *trans*-1-bromo-1-propene (**8**). In addition, we report a ligand rearrangement product; Tol-BDI$^{(2\text{-pp})(4\text{-pp})}$H (**2**), which is formed during the synthesis of **1**.

3.3 Results & discussion

Ligand Synthesis

Compound **1** was prepared through the condensation of 2-(4-tolyl)-malondialdehyde and 2-amino-2-(2-pyridyl) propane (Scheme 3.1).

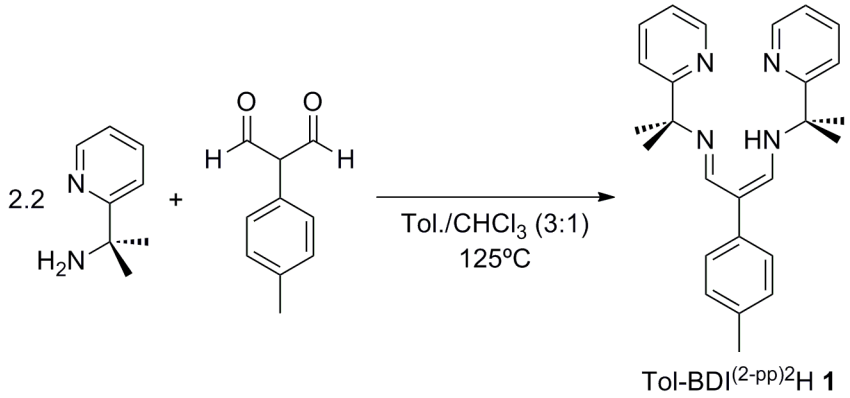

Scheme 3.1. Synthetic route to Tol-BDI$^{(2\text{-pp})2}$H, **1**.

The former starting material was synthesized in four steps from published procedures.[30-31] The condensation to **1** was conducted in a toluene/chloroform solvent mixture heated to reflux for one week. This yielded a mixture of **1** and the intermediate mono-imine, in which only one aldehyde had undergone reaction. Compound **1** was purified by flash chromatography and was isolated in 67% yield.

Compound **1** was characterized by ^{1}H NMR and ^{13}C NMR spectroscopy, electrospray ionization high-resolution mass spectrometry (ESI-HRMS) and UV-vis spectroscopy. The ^{1}H NMR spectrum shows a singlet at 11.6 ppm for the amine proton and seven resonances in the aromatic region including a singlet at 7.73 ppm belonging to the proton α to the imine on the β-diketiminate backbone (Figure 3.1).

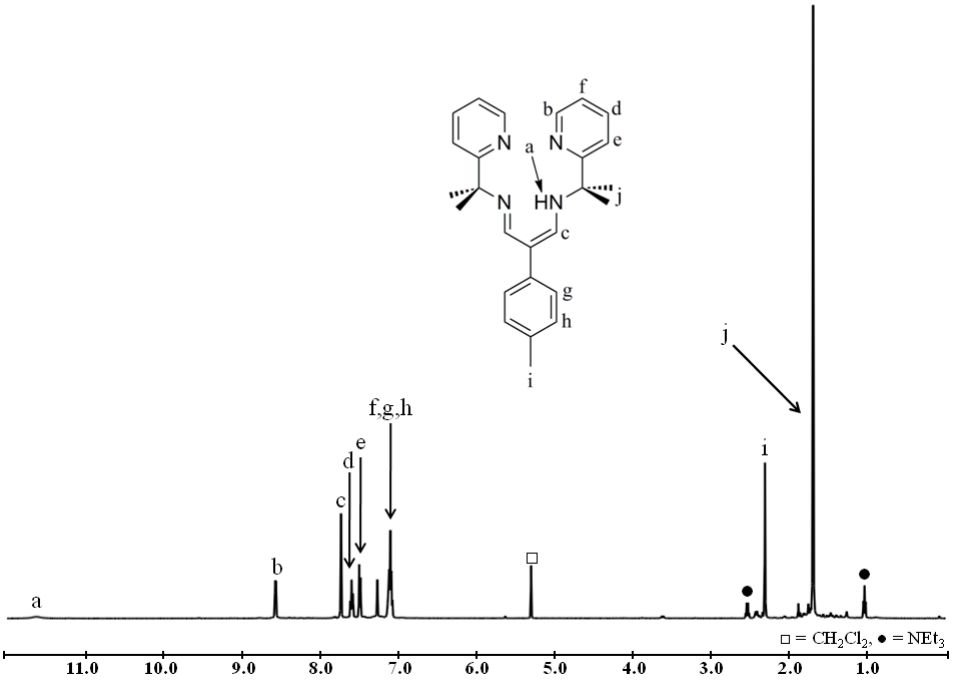

Figure 3.1. ^{1}H NMR spectrum of Tol-BDI$^{(2\text{-pp})2}$H, **1** in $CDCl_3$.

In the methyl region, a 1:4 ratio is observed between the tolyl methyl (2.31 ppm) and the isopropylpyridyl methyl resonances (1.70 ppm). This indicates that the two isopropylpyridine arms of compound **1** are symmetric on the NMR timescale.

Interestingly, a rearrangement is observed during the synthesis of **1** when the reaction concentration is around 0.11 M. Optimization of the synthesis of **1** shows that no rearrangement occurs when the reaction concentration is under 0.07 M. The ligand rearrangement product, **2**, only differs from **1**, in that one pendant arm contains a 4-pyridyl group instead of a 2-pyridyl group. Compound **2** was isolated from the flash chromatography purification of **1** in 14 % yield.

Compound **2** was fully characterized by ^{1}H NMR and ^{13}C NMR spectroscopy, ^{1}H/^{1}H COSY, and ESI-HRMS. The ^{1}H NMR spectrum of **2** does not contain a singlet for the proton α to the imine as is seen for **1** (Figure 3.2).

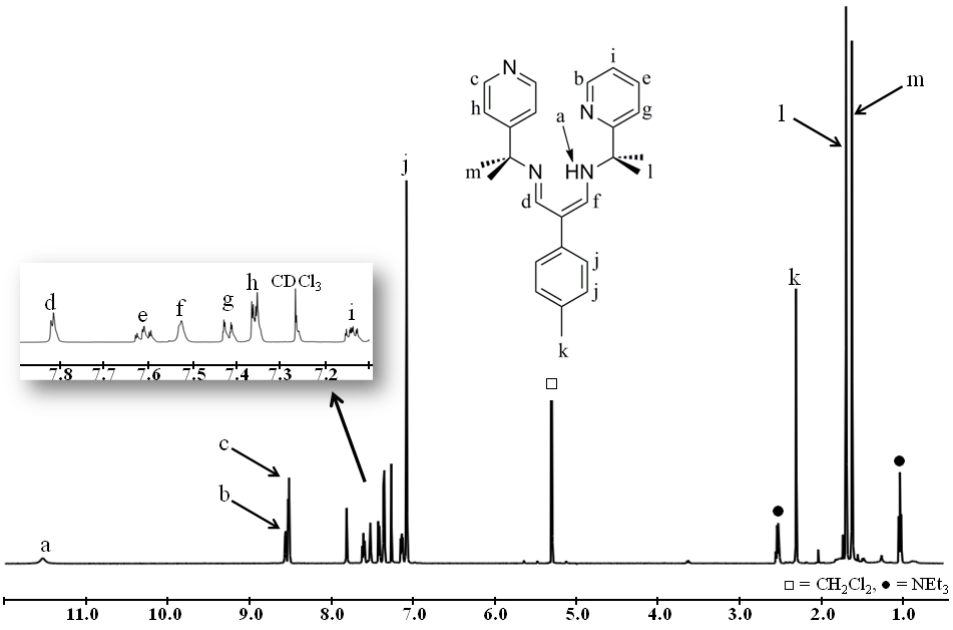

Figure 3.2. ^{1}H NMR spectrum of rearranged ligand, **2** (Tol-BDI$^{(2\text{-pp})(4\text{-pp})}$H) in $CDCl_3$.

Rather, it has two doublets (7.82 and 7.53 ppm) that share a 2.5 Hz coupling constant, confirmed by ^{1}H/^{1}H COSY. Furthermore, the isopropylpyridyl methyls give rise to two separate resonances (1.70 and 1.63 ppm), each integrating to 6H against the tolyl methyl proton signal (2.31ppm, 3H). The assignment of a 4-pyridyl group comes from the two second-order doublets each integrating to 2H at 8.52 and 7.36 ppm.

Metal Complexes Synthesis

Metallation of compound **1** was achieved by deprotonating the ligand with potassium bis(trimethylsilyl)amide, followed by the addition of the desired metal halide salt (Scheme 3.2).

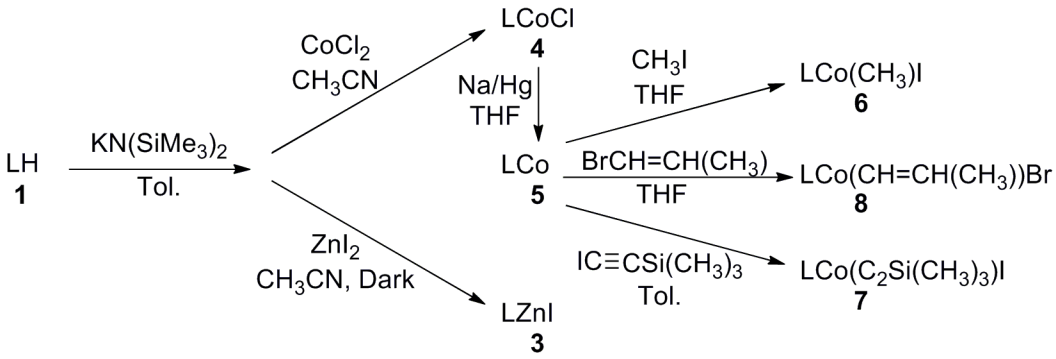

Scheme 3.2. Synthetic routes to Tol-BDI$^{(2\text{-pp})2}$ Zn and Co complexes, **3-8**, where L is Tol-BDI$^{(2\text{-pp})2}$.

Zinc (**3**) and cobalt (**4**) complexes were synthesized in 29% and 98% yield using zinc iodide and cobalt chloride respectively. The large difference in isolated yield is due in part to the superior ability of compound **3** to form a zinc dimer, [Tol-BDI$^{(2\text{-pp})}$ZnI]$_2$ where the ligand has been partially hydrolyzed. A crystal structure of the zinc dimer was obtained while attempting to crystallize compound **3** (Figure 3.3).

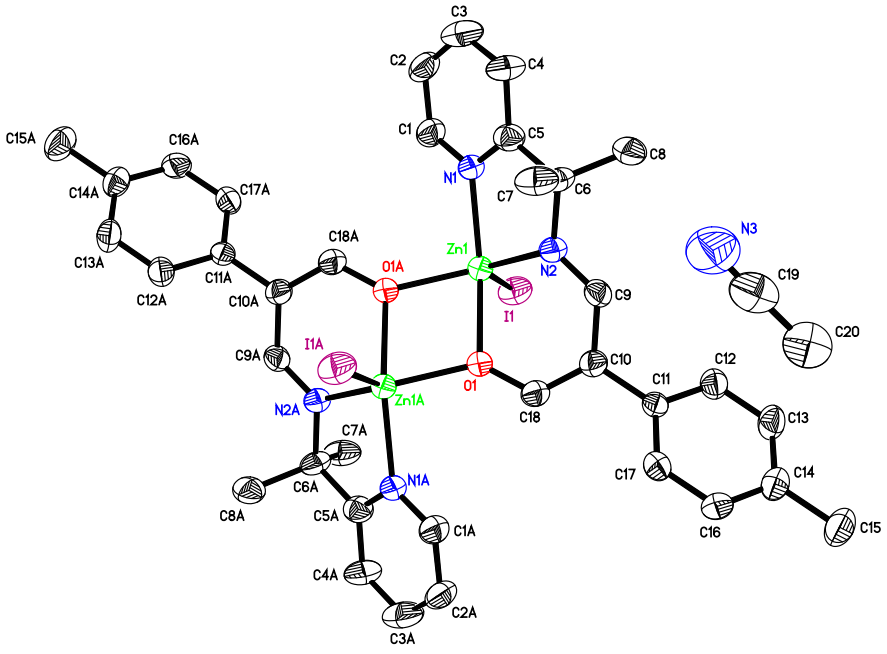

Figure 3.3. ORTEP diagram of [Tol-BDI$^{(2\text{-pp})}$ZnI]$_2$ with thermal ellipsoids drawn at the 50% probability level. Crystals were grown from a concentrated CH_3CN solution.

Compound **3** was characterized by ^{1}H NMR, ^{13}C NMR spectroscopy, ESI-HRMS, UV-vis spectroscopy, cyclic voltammetry and X-ray crystallography. The ^{1}H NMR spectrum is similar to compound **1**, apart from the disappearance of the amine proton and a downfield shift of the proton α to the imine which is now located at 8.16 ppm (Figure 3.4). A 1:4 ratio is still observed between the tolyl methyl (2.33 ppm) and the isopropylpyridyl methyl resonances (1.73 ppm).

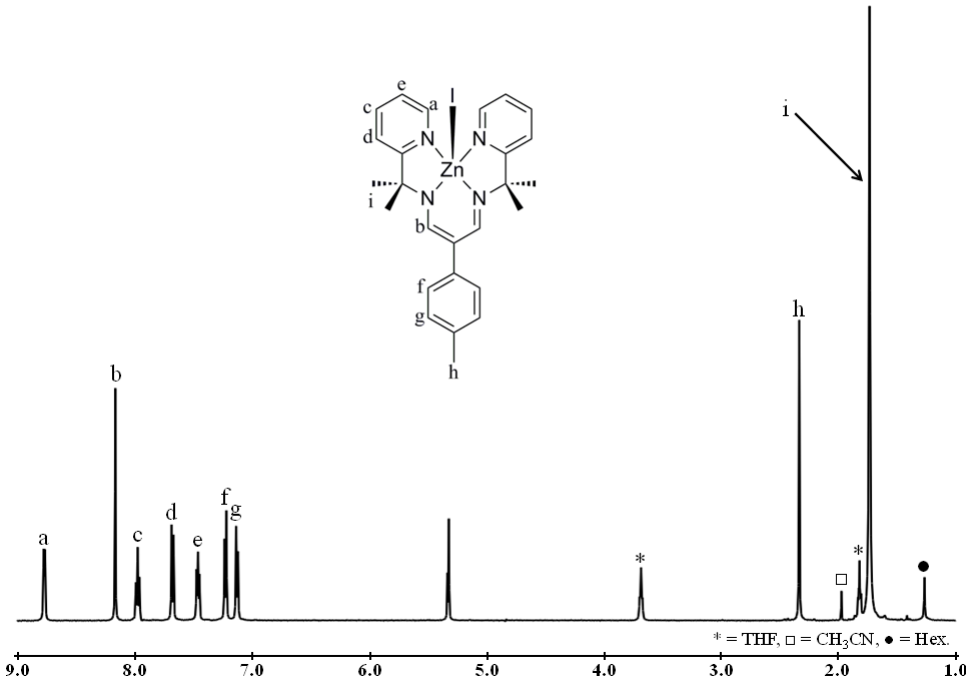

Figure 3.4. ^{1}H NMR spectrum of Tol-BDI$^{(2\text{-pp})2}$ZnI, **3** in CD_2Cl_2.

The UV-vis spectrum of **3** in CH_2Cl_2 showed three bands at 263, 297 and 393 nm which were also observed in the UV-vis absorbance spectrum of **1** in THF at 210, 262, 279 (shoulder) and 344 nm (Figure 3.5).

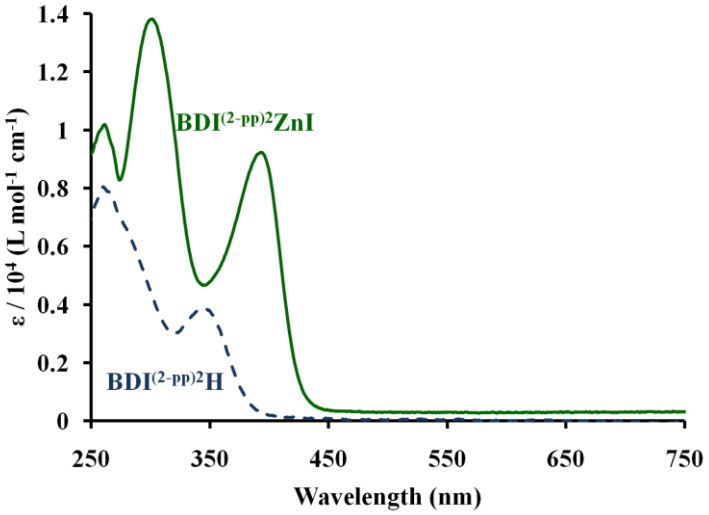

Figure 3.5. Electronic absorption spectrum of compounds **1** and **3**.

These transitions are likely ligand-based, as they resemble the transitions observed in the absorbance spectrum of **1**. X-ray quality crystals were grown from slow vapor diffusion of diethyl ether into a solution of **3** in CH_2Cl_2 (Figure 3.6).

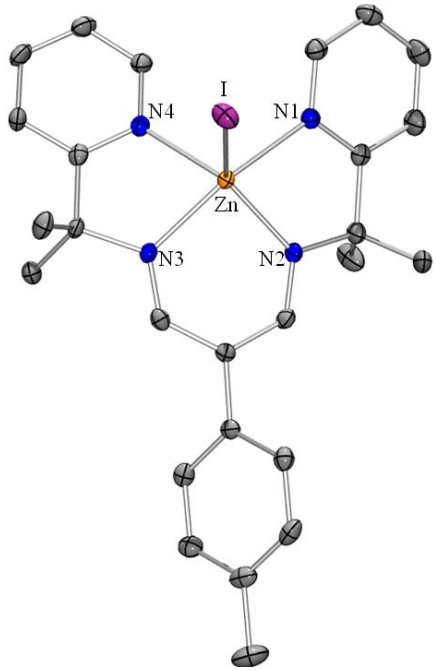

Figure 3.6. ORTEP diagram of Tol-BDI$^{(2\text{-pp})2}$ZnI, **3** with thermal ellipsoids drawn at the 50% probability level. Hydrogen atoms have been omitted for clarity.

The geometry of compound **3** can be described as distorted square pyramidal with a tau value of 0.32.[32] We have previously reported two similar BDI zinc complexes which use quinolines for pendant arms.[28-29] The structures for these complexes are very similar with Zn-N bonds matching within 0.03Å (Table 3.1 and 3.2).

Table 3.1. Crystallographic Data for Tol-BDI$^{(2\text{-pp})2}$ZnI and [Tol-BDI$^{(2\text{-pp})}$ZnI]$_2$.

Compounds	$C_{26}H_{29}IN_4Zn$	$C_{40}H_{44}I_2N_6O_2Zn_2$
Compounds Abbreviation	tolyl-BDI$^{(2\text{-pp})2}$ZnI, **3**	[tolyl-BDI$^{(2\text{-pp})}$ZnI]$_2$
Morphology	Block	Block
Color	Yellow	Orange
Lattice Type	Triclinic	Monoclinic
Space Group	P-1	$P2_1/c$
a, Å	8.942(1)	9.6672(7)
b, Å	11.743(2)	10.3710(7)
c, Å	12.458(2)	20.964(2)
α, deg	78.483(2)	90
β, deg	76.823(2)	94.831(2)
γ, deg	88.283(2)	90
V, Å	1247.9(3)	2094.4(3)
Z	2	2
formula wt, g mol^{-1}	589.80	1025.35
Dc,g cm^{-3}	1.570	1.626
μ, mm^{-1}	2.241	2.660
F(000)	592	1016
θ range, deg	1.71 to 27.54	1.95 to 27.53
reflns collected	14992	17744
unique reflns	5658	4751
data/restraint/parameters	5658 / 0 / 294	4751 / 0 / 239
R1, wR2 [I>2σ(I)]	0.0288, 0.0629	0.0441, 0.1151
R1, wR2 [all data]	0.0404, 0.0675	0.0754, 0.1306
GOOF	1.048	1.072
largest diff peak, hole, e Å^{-3}	0.611, -0.598	1.416, -0.956

Table 3.2. Experimental bond distances and angles for Tol-BDI$^{(2\text{-pp})2}$ZnI and [Tol-BDI$^{(2\text{-pp})}$ZnI]$_2$.

	Tol-BDI$^{(2\text{-pp})2}$ZnI, **3**	[Tol-BDI$^{(2\text{-pp})}$ZnI]$_2$
Bond Lengths (Å)		
Zn-N$_{pyr.}$	2.173(2)	2.114(3)
Zn-N$_{imi.}$	2.018(2)	2.036(4)
Zn-N$_{imi.}$/Zn-O$_{lig.\ 1}$	2.051(2)	2.113(3)
Zn-N$_{pyr.}$/Zn-O$_{lig.\ 1A}$	2.153(2)	2.024(3)
Bond Angles (deg)		
N$_{imi.}$-Zn-N$_{imi.}$/N$_{imi}$-Zn-O$_{lig.1}$	89.66(8)	84.9(1)
Tau, τ	0.32	0.33

Compound **4** was characterized by ^{1}H NMR spectroscopy, ESI-HRMS and UV-vis spectroscopy. The ^{1}H NMR spectrum of **4** exhibits broadened resonances, which are expected for a paramagnetic cobalt(II) complex. The elemental composition of **4** (456.2 *m/z*) was checked by ESI-HRMS with a polyethylene glycol exact mass internal standard. The UV-vis spectrum of **4** showed four transitions at 211, 256, 287 and 355 nm (Figure 3.7). All four of these transitions are assigned as ligand-based transitions.

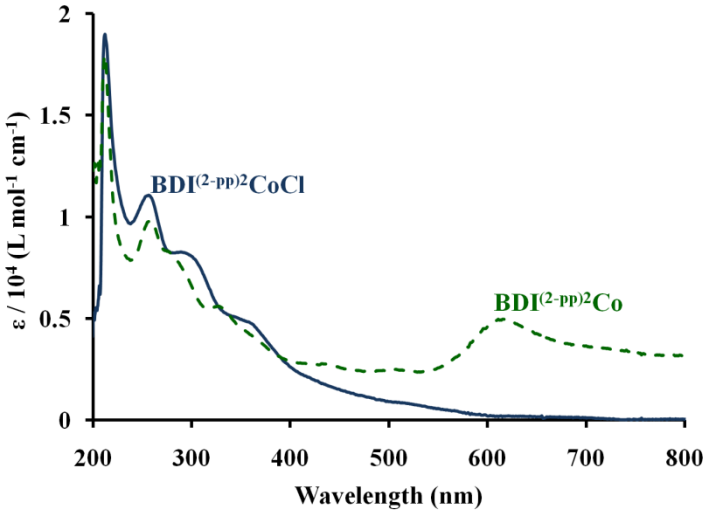

Figure 3.7. Electronic absorption spectrum of complexes **4** and **5**.

Reduction of compound **4** using sodium amalgam in THF yields the diamagnetic, cobalt(I) complex, Tol-BDI$^{(2\text{-pp})2}$Co(I) (**5**). Compound **5** was characterized by ^{1}H NMR, ^{13}C NMR spectroscopy, UV-vis spectroscopy and electron-impact high-resolution mass spectrometry (EI-HRMS). The ^{1}H NMR spectrum of **5** shows seven resonances in the aromatic region while two resonances at 2.29 and 1.52 ppm can be observed in the methyl region belonging to the tolyl methyl and the pyridyl methyl groups (Figure 3.8).

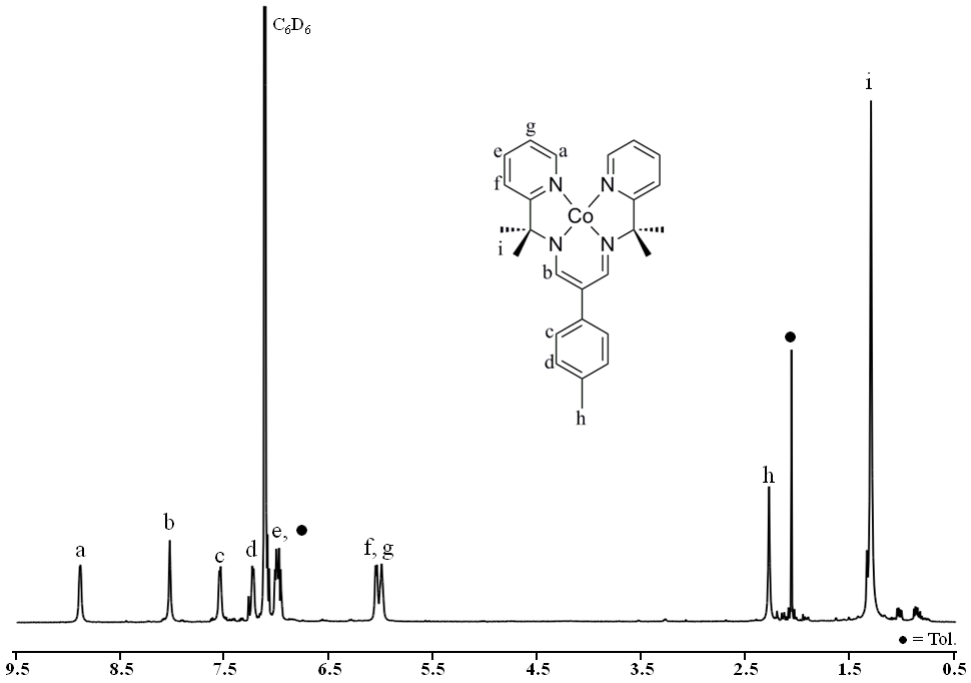

Figure 3.8. ^{1}H NMR spectrum of Tol-BDI$^{(2\text{-pp})2}$Co, **5** in C_6D_6.

Compound **5** has a unique teal color. The UV-vis spectrum of **5** is similar to **4**. In addition to the four ligand-based transitions at 210, 257, 270 and 318 nm, a distinctive transition is observed at 610 nm (Figure 5). This transition is associated with a molar absorptivity of 5000 M^{-1} cm^{-1} and is assigned as a MLCT transition. A similar broad MLCT transition at 650 nm with a molar absorptivity of 1000 M^{-1} cm^{-1} was observed for an electrochemically generated Co(I) species with a tetradentate pyridylpyrazole ligand.[33]

Cyclic Voltammetry

As previously mentioned, a cobalt complex with a high reduction potential is desirable to reduce a wide-range of halogenated organic substrates. To investigate the reducing power of complex **5**, cyclic voltammetry experiments in 0.1 M $[^nBu_4N]PF_6$ THF solution were performed on both **3** and **4** with the aim of finding the $Co^{I/II}$ couple (Figure 3.9).

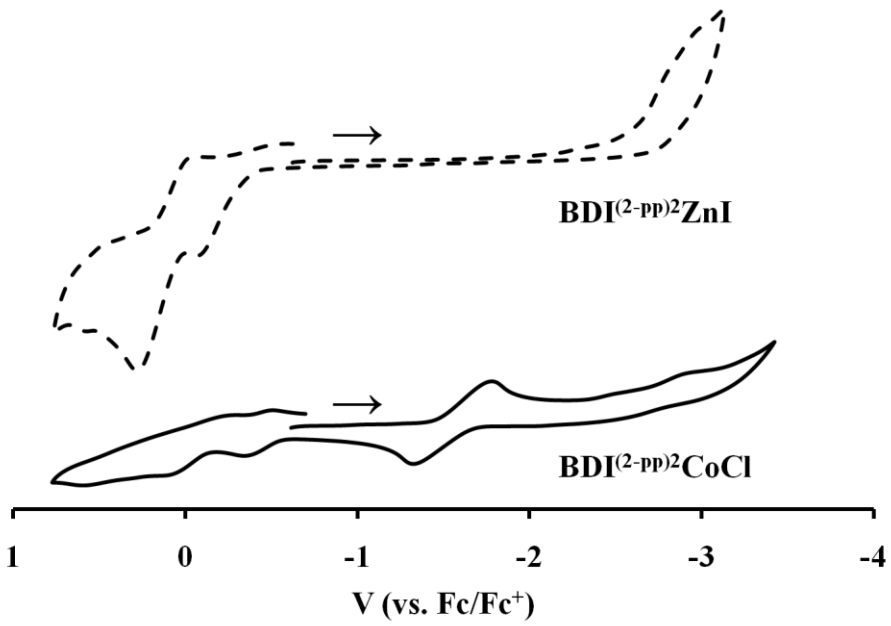

Figure 3.9. Cyclic voltammograms of $BDI^{(2\text{-}pp)2}ZnI$ (**3**) at a rate of 50 mV and $BDI^{(2\text{-}pp)2}CoCl$ (**4**) at a rate of 200 mV in 0.1 M $[^nBu_4N]PF_6$ in THF.

Although the cyclic voltammogram of **4** is complex, a quasi-reversible electron transfer wave was observed at -1.55 V with a peak-to-peak separation of 300 mV (vs. Fc/Fc^+) when scanning at 50 mV (Figure 3.10).

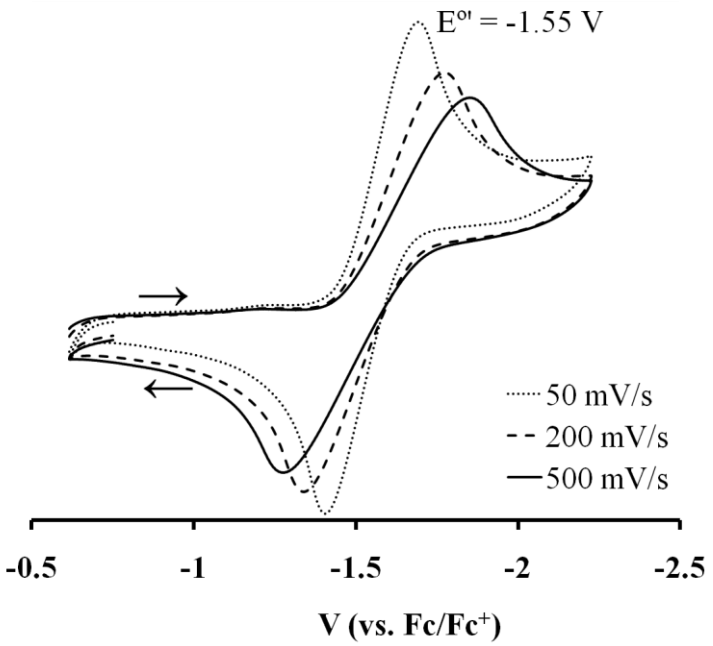

Figure 3.10. Cyclic voltammograms of **4** at various scan rates (50, 200, 500 mV/s; 0.1 M $[^{n}Bu_4N]PF_6$ in THF). Currents were multiplied by $(\text{scan rate})^{-1/2}$.

This separation increases to 600 mV and the peak potential shifts slightly cathodically to -1.56 V at the faster rate of 500 mV/s. The reduction/oxidation wave centered at -1.55 V is assigned to the $Co^{I/II}$ couple. This is slightly lower than the $Co^{I/II}$ couple observed for cobalamin (-1.38 V vs. Fc/Fc^{+}), indicating that **5** is a slightly stronger reductant than cob(I)alamin.[34-37]

*Reactivity of Tol-BDI$^{(2\text{-}pp)2}$Co, **5***

In addition to being a strong reductant, nucleophilicity of the cobalt(I) center is believed to be important in reductive dehalogenation reactions. The reaction of cobalt(I) with methyl iodide has previously been used to measure the nucleophilicity of the metal center.[38-39] For this reason, complex **5** was treated with methyl iodide, which produced an immediate color change from teal to green upon mixing. The product of this reaction was

isolated and found to be the cobalt(III)(CH_3)I complex, **6**, which was characterized by ^{1}H NMR and ^{13}C NMR spectroscopy, ESI-HRMS and UV-vis spectroscopy. The ^{1}H NMR spectrum of **6** has the expected seven resonances in the aromatic region while three resonances in a 1:4:1 ratio are present in the alkyl region (Figure 3.11).

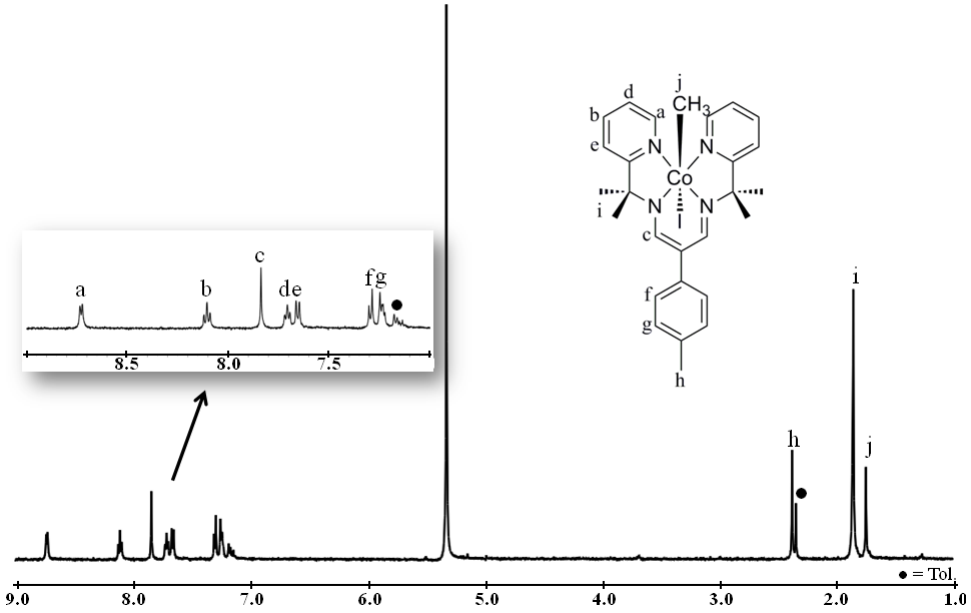

Figure 3.11. ^{1}H NMR spectrum of Tol-BDI$^{(2\text{-pp})2}$Co(CH_3)I, **6** in CD_2Cl_2.

While the resonances at 2.37 ppm and 1.85 ppm could be identified as belonging to the methyl of the tolyl group and the methyl groups on the pendant arms respectively, the resonance at 1.74 ppm was tentatively assigned as the methyl bound to the cobalt center. This assignment was verified through the reaction of **5** with CD_3I and observation of the methyl resonance by ^{2}H NMR spectroscopy. The ^{2}H NMR spectrum showed two resonances: one at 2.17 ppm belonging to residual CD_3I and one at 1.74 ppm, verifying the shift of the cobalt-bound methyl. The shift of the methyl is notably downfield compared to those of methyl groups bound to cobalamin and cobaloxime, which have been reported at -0.12 ppm in D_2O and 0.82 ppm in $CDCl_3$, respectively.[40-41] For the

assignment of the carbon resonance of the methyl cobalt, it was necessary to use ^{13}C-labeled methyl iodide, as the carbon shift could not be unambiguously assigned with unlabeled material. Using $^{13}CH_3I$, the carbon resonance for the cobalt methyl was observed at -4.67 ppm. The UV-vis spectrum of **6** has a total of four transitions (Figure 3.12). These ligand-based transitions are similar to those in complexes **4** and **5**.

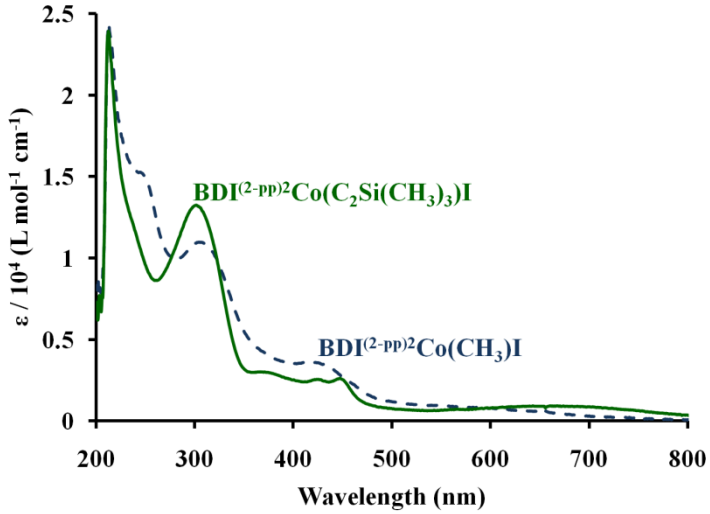

Figure 3.12. Electronic absorption spectrum of complexes **6** and **7**.

In addition to methyl iodide, complex **5** reacts with 1-iodo-2-(trimethylsilyl)acetylene to form complex **7** which was characterized by ^1H NMR and ^{13}C NMR spectroscopy, ESI-HRMS, IR and UV-vis spectroscopy. The ^1H NMR spectrum revealed five resonances in the aromatic region, integrating to a total of 14 protons and three resonances in the alkyl region in a 1:4:3 ratio (Figure 3.13). The methyl resonances from the trimethylsilyl group are shifted downfield from the starting material from 0.17 ppm to -0.24 ppm.

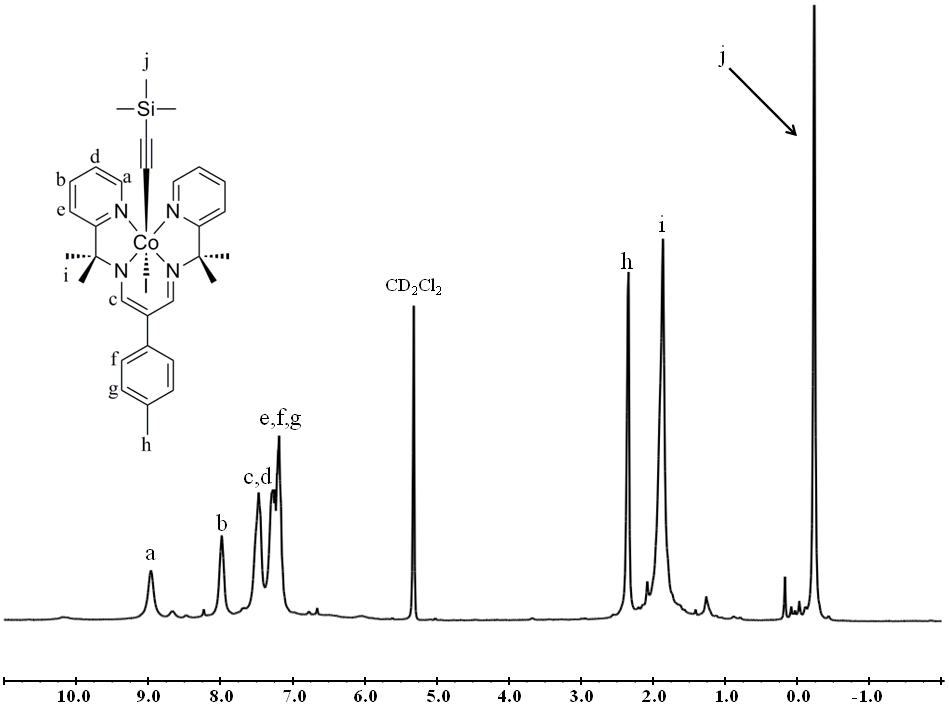

Figure 3.13. ^{1}H NMR spectrum of Tol-BDI$^{(2\text{-pp})2}$Co($C_2Si(CH_3)_3$)I, **7** in CD_2Cl_2.

Similarly, the IR spectrum shows a shift from 2099 cm^{-1} to 2046 cm^{-1} from starting material to complex **7** for the carbon-carbon triple bond stretching mode. In addition, a band at 840 cm^{-1} was observed and assigned to the C(methyl)-Si stretch. These values are similar to those reported for a [(PP_3)Co(H)(C≡C$SiMe_3$]BPh_4 complex where bands at 2023 cm^{-1} and 851 cm^{-1} were reported for the C≡C and $SiMe_3$ groups.[42] In addition to having the similar ligand-based transitions as previously mentioned compounds, the UV-vis spectrum of **7** also has peaks at 425 nm and 447 nm. Through its reactivity towards methyl iodide and 1-iodo-2-(trimethylsilyl)acetylene, complex **5** has been shown to be nucleophilic, similar to cobalamin.

We further investigated the reactivity of complex **5** towards vinyl C-X bonds. Complex **5** was observed to react with vinyl bromide and *trans*-1-bromo-1-propene. These reactions are slower than the reactions of **5** with methyl iodide and 1-iodo-2-

(trimethylsilyl)acetylene. Moreover, complex **5** did not react with *cis*-1-bromo-1-propene at room temperature. In both the reactions with vinyl bromide and *trans*-1-bromo-1-propene, the reaction gives a bromo vinyl species and is plagued with the production of Tol-BDI$^{(2\text{-pp})2}$Co^{II}Br as a side product. Complex **8** (Tol-BDI$^{(2\text{-pp})2}$Co(CH=CH(CH$_3$))Br) was isolated with complex **4** as an impurity and was characterized by ^{1}H NMR spectroscopy and ESI-HRMS (Figure 3.14).

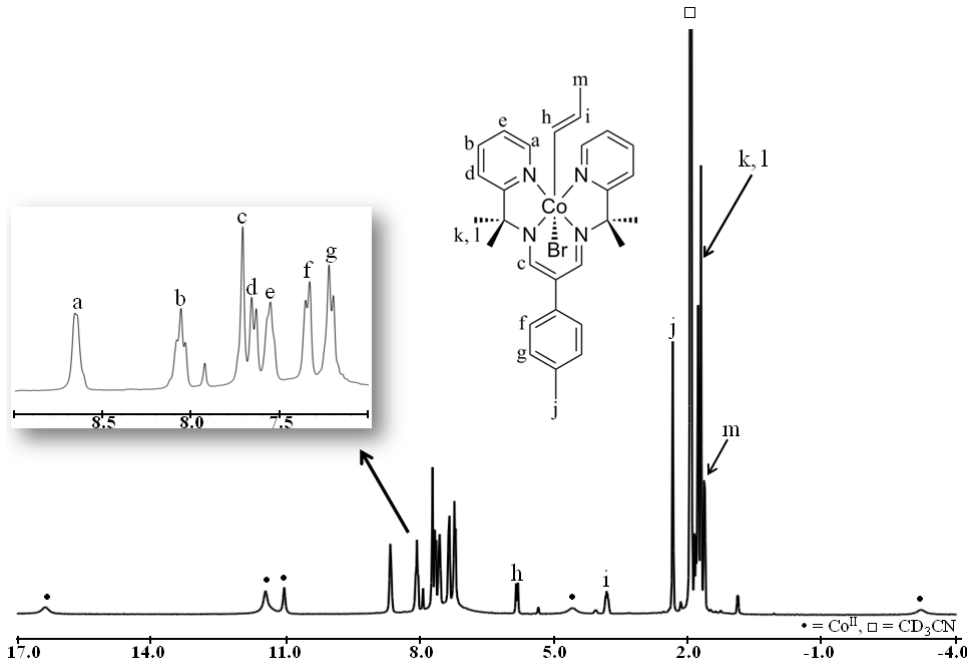

Figure 3.14. ^{1}H NMR spectrum of Tol-BDI$^{(2\text{-pp})2}$Co(CH=CH(CH$_3$))Br, **8** in CD$_3$CN.

The ^{1}H NMR spectra has seven aromatic resonances as expected. In the vinyl region, a doublet (*h*) at 5.82 ppm with a coupling constant of 11.4 Hz is observed, corresponding to the vinyl proton closest to the cobalt center. A second vinyl resonance (*i*), a doublet of doublets is located at 3.81 ppm with coupling constants of 6.3 Hz and 11.4 Hz, belonging to the other proton on the vinyl group. The methyl group on the vinyl group is a doublet with a coupling constant of 6.0 Hz located 1.63 ppm, whose coupling to the proton *i* was

confirmed by $^{1}H/^{1}H$ COSY. In this complex, the pyridyl methyl groups are split into two inequivalent sets based on their orientation with respect to the vinyl and bromide group.

Other vinyl substrates were observed to react with **5**. With an aim at the remediation of chlorinated water, complex **5** was revealed to dechlorinate TCE to *cis*-DCE, however this reaction appeared to have poor efficiency by GC-MS.

3.4 Conclusions

A monoanionic, tetraaza ligand was prepared in an effort to model the monoanionic corrin ligand in cobalamin. The ligand reported here, Tol-BDI$^{(2\text{-pp})2}$H, is a third-generation ligand that is the product of an iterative design process. The ligand is composed of a β-diketiminate backbone with isopropylpyridine pendant arms. It is both flexible enough to support the three important oxidation states of Co (I, II, III) and stable with respect to decomposition to pyridylpyrrole products. An isolable Co(I) complex of Tol-BDI$^{(2\text{-pp})2}$ was prepared and was found to be comparable to cobalamin(I) both in terms of its Co(I)/Co(II) redox couple and in its reactions as a nucleophile.

3.5 Experimental procedures

General Considerations. Experiments were conducted under anhydrous and anaerobic (dinitrogen) conditions using a glovebox or Schlenk line at the exception of the ligand synthesis which was conducted in air. Reagents with the exception of 2-amino-2-(2-pyridyl) propane were purchased commercially and used without further purification. 2-Amino-2-(2-pyridyl) propane was synthesized in four steps from published procedures.[30-31] Solvents were purchased commercially and dried under standard procedures.[43] UV-vis absorbance data was collected with an OceanOptics CHEMUSB2 spectrophotometer using a quartz cuvette. Infrared (IR) spectra were collected with a Midac M series spectrometer. ^{1}H NMR and 2D NMR spectra were acquired on Varian Inova instruments at 300 MHz and 500 MHz.^{13}C shifts were established from 2D HMQC (Heteronuclear Multiple Quantum Correlation) and HMBC (Heteronuclear Multiple Bond Correlation) NMR experiments. The assignment of the carbon shifts can be found in the supporting information (Table 3.3). ^{13}C NMR spectrum for the $^{13}CH_3I$ experiment was acquired on Varian Inova instrument at 75 MHz. ^{2}H NMR spectrum was acquired on a Varian Inova instrument at 300 MHz. Mass spectrometry (MS) data were acquired on a Bruker BioTOF ESI-MS under positive mode. Polyethylene glycol (PEG) and polypropylene glycol (PPG) standards were used for ESI-HRMS. A Finnigan MAT 95 double-focusing mass spectrometer with BE-geometry was used to collect EI-HRMS with sample introduction using a solids probe. Perfluorokerosene (PFK) was used as an internal standard for EI-HRMS.

Table 3.3. ^{13}C NMR assignment from HMQC and HMBC experiments. NMR spectra were taken in following solvents: $CDCl_3$ (**1** & **2**), CD_2Cl_2 (**3**, **6** & **7**) and d_8-thf (**5**).

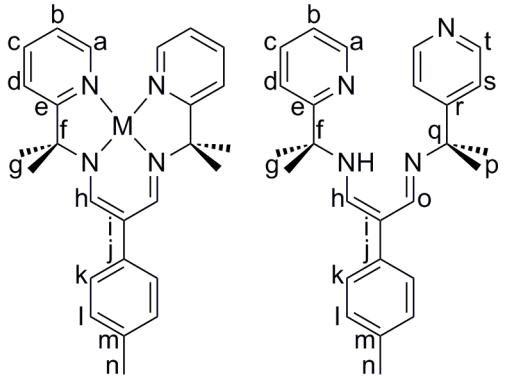

Compound	1	2	3	5	6	7
	M = H	NA	M = ZnI	M = Co	M = Co(CH_3)I	M = Co($C_2Si(CH_3)_3$)I
a	149.5	148.7	147.3	148.5	151.9	152.2
b	121.7	121.6	123.1	123.7	124.9	124.2
c	136.7	136.5	139.6	126.3	139.4	139.0
d	120.4	119.8	123.4	120.2	122.2	121.7
e	167.3	166.5	166.9	173.4	173.1	173.0
f	61.7	60.6	61.6	71.3	75.5	75.8
g	29.4	29.1	31.3	30.9	29.4	33.4
h	150.5	147.8	156.8	140.0	151.1	152.0
i	105.7	105.6	104.6	112.1	112.8	108.7
j	138.7	138.6	141.5	142.4	137.9	138.8
k	125.5	125.3	125.9	126.9	126.8	126.0
l	129.3	129.1	129.5	129.6	130.0	129.8
m	134.2	134.5	133.2	132.7	135.9	134.5
n	21.0	20.9	21.2	21.2	21.2	22.1
o	-	153.6	-		-4.7 (Co-**C**H_3)	89.6 (Co-**C**≡C-Si$(CH_3)_3$)
p	-	29.7	-			118.8 (Co-C≡**C**-Si$(CH_3)_3$)
q	-	59.7	-			1.2 (Co-C≡C-Si(**C**$H_3)_3$)
r	-	158.2	-			
s	-	121.3	-			
t	-	149.8	-			

Tol-BDI$^{(2\text{-pp})_2}$H (**1**) Under ambient atmosphere, 2-amino-2-(2-pyridyl) propane (0.200 g, 1.47 mmol) was dissolved in toluene (22 mL) in a round bottom flask. 2-(4-tolyl)-malondialdehyde (0.107 g, 0.66 mmol) was dissolved in $CHCl_3$ (7 mL) and was added to

the solution of 2-amino-2-(2-pyridyl)propane. A concentration of 0.070 M was found to be optimal to prevent the formation of compound **2**. The reaction was heated to reflux with a bath temperature of 125ºC for one week. The reaction was cooled to room temperature and solvent was removed using a roto-evaporator. A silica column (99:1 CH_2Cl_2:Et_3N eluent mixture) was used to separate compound **1** from the mono-condensed intermediate, 2-(4-tolyl)-1-(2-isopropylpyridyl)propeneimine-3-aldehyde. A brown oil was isolated and dried under vacuum (0.176 g, 67%). UV (THF) λ_{max}, nm (ε, L mol^{-1} cm^{-1}): 210, 262 (9200), 279 sh., 344 (4700). ^{1}H NMR (500 MHz, $CDCl_3$): δ ppm 11.62 (1 H, br. s, HN); 8.57 (2 H, d, *J* 4.0, pyr. CH); 7.73 (2 H, s, CH); 7.60 (2 H, ddd, *J* 2.0, 8.0 and 9.0, pyr. CH); 7.49 (2 H, d, *J* 8.0, pyr. CH); 7.12 (2 H, m, pyr. CH); 7.10 (2 H, m, tolyl CH); 7.10 (2 H, m, tolyl CH); 2.31 (3 H, s, tolyl CH_3); 1.70 (12 H, s, CH_3). ^{13}C NMR (125 MHz, $CDCl_3$): δ ppm 167.3, 150.3, 149.5, 138.7, 136.7, 134.1, 129.3, 125.5, 121.7, 120.4, 105.7, 61.7, 29.4, 21.0. ESI-TOF HRMS (MeOH) with PEG-400-600 *m/z*: $[M + H]^+$ calcd. for $C_{26}H_{31}N_4$, 399.2543; found, 399.2538; 1.25 ppm error.

Tol-BDI$^{(2\text{-pp})(4\text{-pp})}$H (**2**) Compound **2** was synthesized as a side product of the synthesis of compound **1**. Under high reaction concentration (approximately 0.110 M), compound **2** was observed. Under ambient atmosphere, 2-amino-2-(2-pyridyl) propane (0.318 g, 2.33 mmol) was dissolved in toluene (15 mL) in a round bottom flask. 2-(4-tolyl)-malondialdehyde (0.178 g, 1.10 mmol) was dissolved in $CHCl_3$ (5 mL) and was added to the solution of 2-amino-2-(2-pyridyl) propane. The reaction was heated to reflux with a bath temperature of 125ºC for one week. The reaction mixture was cooled to room temperature and the solvent was removed using a roto-evaporator. Compound **2** was

isolated using a silica column (99:1 CH_2Cl_2:Et_3N eluent mixture). A brown oil was isolated and dried under vacuum (0.050 g, 14%). ^{1}H NMR (500 MHz, $CDCl_3$): δ ppm 11.54 (1 H, br. s, HN); 8.57 (1 H, d, *J* 3.5, pyr. CH); 8.52 (2 H, d, *J* 6.0, pyr. CH); 7.82 (1 H, d, *J* 2.5, CH); 7.61 (1 H, t, *J* 8.0, pyr. CH); 7.53 (1 H, d, *J* 2.5, CH); 7.42 (1 H, d, *J* 8.0, pyr. CH); 7.36 (2 H, d, *J* 6.0, pyr. CH); 7.15 (1 H, dd, *J* 5.0 and 7.0, pyr. CH); 7.09 (4 H, br s, tolyl CH); 2.31 (3 H, s, tolyl CH_3); 1.70 (6 H, s, CH_3); 1.63 (6 H, s, CH_3). ^{13}C NMR (125 MHz, $CDCl_3$): δ ppm 166.5, 158.2, 153.6, 149.8, 148.7, 147.8, 138.6, 136.5, 134.5, 129.1, 125.3, 121.6, 121.3, 119.8, 105.6, 60.6, 59.7, 29.7, 29.1, 20.9. ESI-TOF HRMS (MeOH) with PPG-425 *m/z*: $[M + H]^+$ calcd. for $C_{26}H_{31}N_4$, 399.2543; found, 399.2544; 0.25 ppm error.

Tol-BDI$^{(2\text{-pp})2}$ZnI (**3**) Under inert atmosphere, compound **1** (0.028 g, 0.07 mmol) was dissolved in toluene (10 mL). A solution of potassium bis(trimethylsilyl)amide was prepared by dissolving $KN(SiMe_3)_2$ (0.016 g , 0.08 mmol) into toluene (5 mL). Upon addition of $KN(SiMe_3)_2$, a slight color change from brown to reddish brown was observed. After 10 minutes of stirring, a solution of ZnI_2 (0.026 g, 0.08 mmol) was prepared in the dark by dissolving ZnI_2 in CH_3CN (5 mL) and was added dropwise to the deprotonated ligand solution. The solution became orange when left stirring overnight. The solvent was removed under vacuum. The residue was extracted into minimal CH_3CN and was placed in the freezer overnight. The solids precipitated and were dried under vacuum (0.012 g, 29%). X-ray quality crystals were grown from vapor diffusion of diethyl ether into a solution of **3** in CH_2Cl_2. UV (CH_2Cl_2) λ_{max}, nm (ε, L mol^{-1} cm^{-1}): 263, 297, 393 (8500). ^{1}H NMR (500 MHz, CD_2Cl_2): δ ppm 8.77 (2 H, d, *J* 5.0, pyr. CH); 8.16

(2 H, s, CH); 7.97 (2 H, dd, *J* 1.5 and 8.5, pyr. CH); 7.67 (2 H, d, *J* 8.5, pyr. CH); 7.46 (2 H, dd, *J* 6.0, pyr. CH); 7.22 (2 H, d, *J* 8.0, tolyl CH); 7.12 (2 H, d, *J* 8.0, tolyl CH); 2.33 (3 H, s, tolyl CH_3); 1.73 (12 H, s, CH_3). ^{13}C NMR (125 MHz, CD_2Cl_2): δ ppm 166.9, 156.8, 147.3, 141.5, 139.6, 133.2, 129.5, 125.9, 123.4, 123.1, 104.6, 61.6, 31.1, 21.2. ESI-TOF HRMS (CH_3CN) with PEG-400-600 *m/z*: $[M - I]^+$ calcd. for $C_{26}H_{29}N_4Zn$, 461.1684; found, 461.1680; 0.87 ppm error.

Tol-BDI$^{(2\text{-}pp)2}$CoCl (**4**) Under inert atmosphere, compound **1** (0.389 g, 0.98 mmol) was dissolved in toluene (50 mL). A solution of potassium bis(trimethylsilyl)amide was prepared by dissolving $KN(SiMe_3)_2$ (0.187 g , 0.94 mmol) into toluene (25 mL). Upon addition of $KN(SiMe_3)_2$, a slight color change from brown to reddish brown was observed. After 10 min. of stirring, a solution of $CoCl_2$ (0.129 g, 0.99 mmol) was prepared by dissolving it in CH_3CN (25 mL) and was added dropwise to the deprotonated ligand solution. No visible change of color was observed. The reaction was left stirring overnight. The solvent was removed on a Schlenk line and the residue was extracted using toluene, THF and CH_3CN. The extraction solutions were filtered and evaporated to dryness. The residues were combined and dried under vacuum (0.473 g, 98%). UV (THF) λ_{max}, nm (ε, L mol^{-1} cm^{-1}): 211 (21000), 256 (12000), 287 (8700), 355 (5300). ^1H NMR (300 MHz, CD_3CN): δ ppm 15.67, 12.24, 11.44, 11.12, 7.98, 7.19, 5.44, 2.32, 1.63, -2.87. ESI-TOF HRMS (CH_3CN) with PEG-400-600 *m/z*: $[M - Cl]^+$ calcd. for $C_{26}H_{29}N_4Co$, 456.1724; found, 456.1715; 1.97 ppm error.

Tol-BDI$^{(2\text{-pp})2}$Co (**5**) Under inert atmosphere, compound **4** (0.069 g, 0.14 mmol) was dissolved in THF (30 mL). Sodium amalgam was created by adding elemental mercury (1.093 g, 5.45 mmol) to sodium metal (0.013 g, 0.57 mmol). The solution of compound **4** was added to the sodium amalgam and was left stirring overnight. The brown solution became teal. The THF solution was filtered and filtrate was dried under vacuum. The residue was extracted using toluene and the extraction solution was dried under vacuum (0.046 g, 72%). UV (THF) λ_{max}, nm (ε, L mol^{-1} cm^{-1}): 210, 257 (10000), 270 sh., 318 (5900), 610 (5000). ^{1}H NMR (500 MHz, d_8-THF): δ ppm 9.02 (2 H, d, *J* 3.5, pyr. CH); 7.77 (2 H, s, CH); 7.56 (2 H, dd, *J* 7.0, pyr. CH); 7.11 (2 H, d, *J* 6.5, tolyl CH); 7.02 (2 H, d, *J* 6.5, tolyl CH); 6.72 (2 H, d, *J* 7.0, pyr. CH); 6.57 (2 H, dd, *J* 8.0, pyr. CH); 2.29 (3 H, s, tolyl CH_3); 1.52 (12 H, s, CH_3). ^{13}C NMR (125 MHz, d_8-THF): δ ppm 173.4, 150.5, 149.5, 142.4, 136.7, 132.7, 129.3, 125.5, 121.7, 120.4, 112.1, 71.3, 29.4, 21.0. EI-HRMS (70 eV) with PFK *m/z*: $[M]^+$ calcd. for $C_{26}H_{29}N_4Co$, 456.1724; found, 456.1700; 5.26 ppm error.

Tol-BDI$^{(2\text{-pp})2}$Co(CH$_3$)I (**6**) Under inert atmosphere, compound **5** (0.010 g, 0.02 mmol) was dissolved in THF (5 mL). While stirring, methyl iodide (13 µL, 0.02 mmol) was added dropwise. The solution changed color immediately to green. The solution was stirred for 1 hour before being filtered and dried under vacuum (0.012 g, 94%). UV (THF) λ_{max}, nm (ε, L mol^{-1} cm^{-1}): 212, 236, 304 (9800), 418 (3600). ^{1}H NMR (500 MHz, CD_2Cl_2): δ ppm 8.73 (2 H, dd, *J* 1.0 and 5.5, pyr. CH); 8.11 (2 H, dd, *J* 1.0 and 8.0, pyr. CH); 7.84 (2 H, s, CH); 7.71 (2 H, dd, *J* 1.0 and 7.0, pyr. CH); 7.65 (2 H, dd, *J* 1.0 and 8.0, pyr. CH); 7.29 (2 H, d, *J* 8.5, tolyl CH); 7.24 (2 H, d, *J* 8.0, tolyl CH); 2.37 (3 H, s,

tolyl CH_3); 1.85 (12 H, s, CH_3); 1.74 (3 H, s, $CoCH_3$). The ^{1}H NMR shift of the methyl bound to the cobalt was verified by reacting compound **5** with CD_3I. ^{2}H NMR (300 MHz, CH_3CN): δ ppm 1.74 (s, $CoCD_3$). ^{13}C NMR (125 MHz, CD_2Cl_2): δ ppm 173.1, 151.9, 151.1, 139.4, 137.9, 135.9, 130.0, 126.8, 124.9, 122.2, 112.8, 75.5, 31.7, 29.4, 21.2. The resonance for the methyl bound to the cobalt was not observed when using CH_3I, however, the use of $^{13}CH_3I$ allowed for its observation. ^{1}H NMR (500 MHz, CD_3CN): δ ppm 1.76 (d, J_{CH} 141, $Co^{13}CH_3$). ^{13}C NMR (125 MHz, CD_3CN): δ ppm -4.7. ESI-TOF HRMS (CH_3CN) with PPG-425 *m/z*: $[M - I]^+$ calcd. for $C_{27}H_{32}N_4Co$, 471.1959; found, 471.1957; 0.42 ppm error.

Tol-BDI$^{(2\text{-}pp)2}$Co($C_2Si(CH_3)_3$)I (**7**) Under inert atmosphere, compound **5** (0.010 g, 0.02 mmol) was dissolved in toluene (7 mL). While stirring, a solution of 1-iodo-2-(trimethylsilyl)acetylene (10 µL, 0.07 mmol) in toluene (3 mL) was added dropwise to the solution of compound **5**. The solution changed color immediately to red brown. The solution became green after stirring for an hour. It was filtered and dried under vacuum. The residue was washed heavily with hexanes to remove starting material and was dried under vacuum (0.013 g, 86%). UV (THF) λ_{max}, nm (ε, L mol^{-1} cm^{-1}): 205 (3900), 301 (13000), 367 (3200), 425 (2800), 447 (2800). IR $^{o}\upsilon_{max}$/cm^{-1}: 2046 (C≡C), 840 (Si-CH_3) (Nujol Mull). ^{1}H NMR (500 MHz, CD_2Cl_2): δ ppm 8.96 (2 H, br. d, pyr. CH); 7.97 (2 H, dd, *J* 7.0, pyr. CH); 7.49 (2 H, dd, *J* 6.0, pyr. CH); 7.45 (2 H, d, *J* 7.0, pyr. CH); 7.30 (2 H, s, CH); 7.28 (2 H, d, *J* 7.5, tolyl CH); 7.19 (2 H, d, *J* 7.5, tolyl CH); 2.35 (3 H, s, tolyl CH_3); 1.87 (12 H, s, CH_3), -0.23 (9 H, s, $Si(CH_3)_3$). ^{13}C NMR (125 MHz, CD_2Cl_2): δ ppm 173.0, 152.2, 152.0, 139.0, 138.8, 134.5, 129.8, 126.0, 124.2, 121.7, 118.8, 108.7, 89.6,

75.8, 33.4, 22.1, 1.2. ESI-TOF HRMS (CH_3CN) with PEG-400-600 *m/z*: $[M - I]^+$ calcd. for $C_{31}H_{38}N_4CoSi$, 553.2198; found, 553.2205; 1.27 ppm error.

Tol-BDI$^{(2\text{-}pp)2}$Co(CH=CH(CH_3))Br (**8**) Under inert atmosphere, complex 5 (0.029 g, 0.06 mmol) was dissolved in d_8-THF and placed in a sealable NMR tube. Trans-1-bromo-1-propene (55 μL, 0.06 mmol) was added. Reaction was monitored by NMR over 4 days. The reaction was filtered and the solvent of the filtrate was removed under reduced pressure. The resulting solids were washed with cold toluene and dried under vacuum (0.007 g, 20%, including Co^{II} impurity). ^{1}H NMR (300 MHz, CD_3CN): δ ppm 8.60 (2 H, d. *J* 3.0, pyr. CH); 8.06 (2 H, t, *J* 6.9, pyr. CH); 7.71 (2 H, s, CH); 7.65 (2 H, d, *J* 7.8, pyr. CH); 7.56 (2 H, d, *J* 6.0, pyr CH); 7.35 (2 H, d, *J* 7.2, tolyl CH); 7.21 (2 H, d, *J* 7.5, tolyl CH); 5.82 (1 H, d, *J* 11.4, Co-C*H*=CH(CH_3)); 3.82 (1 H, dd, *J* 6.3 & 11.4, Co-CH=C*H*(CH_3)); 2.34 (3 H, s, tolyl CH_3); 1.78 (6 H, s, CH_3), 1.71 (6 H, s, CH_3), 1.63 (3 H, d, *J* 6.0, Co-CH=CH(C*H*$_3$)). ESI-TOF HRMS (CH_3CN) with PGG-425 *m/z*: $[M - Br]^+$ calcd. for $C_{29}H_{34}N_4Co$, 497.2115; found, 471.2100; 3.02 ppm error.

Electrochemistry. Cyclic voltammetry experiments were performed inside a glovebox with a CHInstruments Model 600D potentiostat/galvanostat. A single-chamber cell was set up with a glassy carbon working electrode (3 mm diameter), a Pt wire as the auxiliary electrode, and a reference electrode consisting of a silver wire in 10 mM $AgNO_3$ solution (0.1 M $[^nBu_4N]PF_6$ in CH_3CN). The measurements were taken in a 0.1 M $[^nBu_4N]PF_6$ THF solution. The background cyclic voltammograms of the electrolyte solution were

taken prior to the addition of the sample. All measurements were calibrated to an internal ferrocene standard.

X-ray Crystallography. A single crystal of **3** was placed onto the tip of a 0.1 mm diameter glass capillary and mounted on a Bruker SMART Platform CCD diffractometer for data collection at 173(2) K. The data collection was carried out using Mo Kα radiation (graphite monochromator). The data intensity was corrected for absorption and decay (SADABS). Final cell constants were obtained from least squares fits of all measured reflections. The structure was solved using SHELXS-97 and refined using SHELXL-97.[44] A direct-methods solution was calculated which provided most non-hydrogen atoms from the E-map. Full-matrix least squares / difference Fourier cycles were performed to locate the remaining non-hydrogen atoms. All non-hydrogen atoms were refined with anisotropic displacement parameters. Hydrogen atoms were placed in ideal positions and refined as riding atoms with relative isotropic displacement parameters. Crystallographic data for complex **3** is summarized in Table 3.1 and 3.2.

-PART II-

Investigation into the Wide Bite-Angle Diphosphine ^{iPr}DPDBFphos through Preparation of First-Row Transition Metal Complexes and Catalysis with (^{iPr}DPDBFphos)NiCl

-Chapter Four-

Introduction

4.1 Wide bite-angle diphosphines

Since the development of 1,2-bis(diphenylphosphino)ethane (dppe) in 1959, diphosphines have been major players in homogeneous catalysis with applications such as cross-coupling reactions, enantioselective reactions, and hydroformylation.[1-5] In the early 1970's, diverse diphosphines were developed with the intent of stabilizing square-planar d^8 transition metal catalysts. While both *cis*- and *trans*- coordinating diphosphines were initially targeted, *cis*-diphosphines became the main focus for catalysis due to their relevancy to asymmetric hydrogenation.[4] Wide bite angle diphosphines were only revisited in the 1990's with the development of 2,2'-bis(diphenylphosphinomethyl)biphenyl (BISBI) and 9,9-dimethyl-4,6-bis(diphenylphosphino)xanthene (Xantphos). These two diphosphines have a bite angle of approximately 120°, which is ideal for occupying two equatorial positions in a trigonal bipyramidal complex. The use of these two diphosphine ligands in rhodium-catalyzed hydroformylation of α-olefins led to unprecedented selectivity of the linear aldehyde product over the branched aldehyde product.[6-7] This enhanced selectivity motivated the development of even wider bite angle diphosphine ligands, including exclusively *trans*-spanning diphosphines. *Trans*- coordination requires an optimal distance between the two phosphorous atoms, which can be obtained through the inclusion of large backbone between the two phosphines. However, these ligands have an increased flexibility that can lead to the formation of *cis* complexes, bimetallic complexes and/or even oligomers. Additionally, the backbone has been observed in some cases to coordinate the metal to create a tridentate P-X-P coordination motif.[4] Therefore, an exclusively *trans*-spanning phosphine remains a challenge. There have been advances towards this goal with the

synthesis of preferentially *trans*-binding phosphines such as 2,11-bis(diphenylphosphinomethyl) benzophenanthrene (TRANSphos) and 8,8'-bis(diphenylphosphino)-4,4,4',4',6,6'-hexamethylspiro-2,2'-bichroman (SPANphos). In their extensive study of TRANSphos, Venanzi and co-workers have observed mostly *trans*-complexes but they have characterized a few *cis*-complexes spectroscopically.[8-9] Considering its *trans*- and *cis*- binding modes, TRANSphos is more aptly classified as a wide bite angle diphosphine.

This class of phosphine ligands has become popular thanks to their ability to coordinate in both *cis*- and *trans*- fashions and their different catalytic capacities relative to *cis*-diphosphines (Figure 4.1).

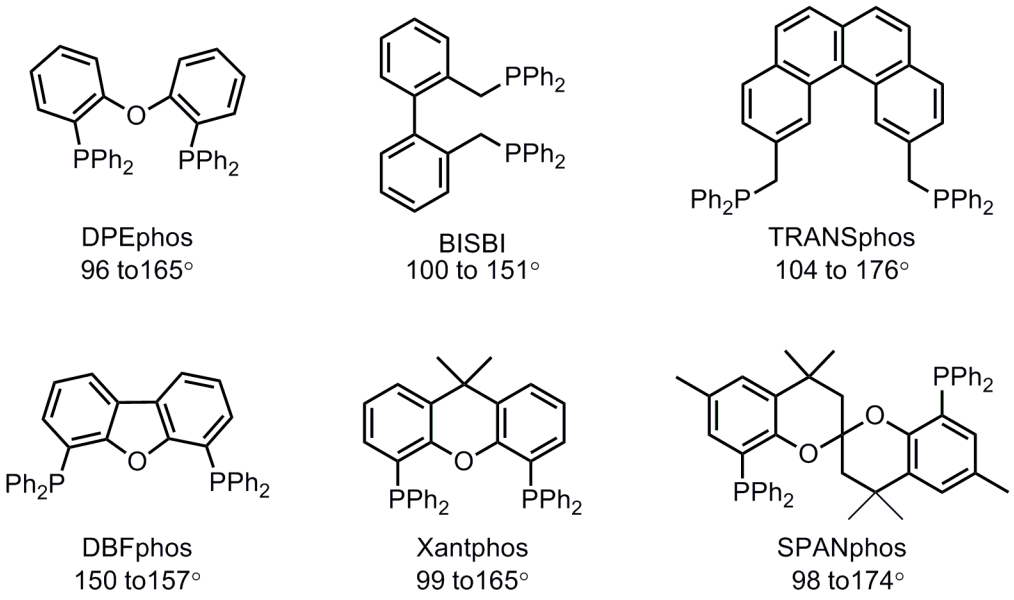

Figure 4.1. Examples of wide bite angle diphosphines. A corresponding bite angle range is listed based on structures from the Cambridge Structural Database.[10-11]

Specifically, wide bite angle diphosphines have proven to be useful in catalysis by alternating the energy profile of a reaction through *cis*-*trans* isomerization.[2-5, 12] Nickel-

catalyzed hydrocyanation of olefins is a well documented example of a catalytic system that benefits from the use of a wide bite angle diphosphine ligand.[3] In hydrocyanation, an alkene reacts with excess HCN to form a nitrile. On an industrial scale, Dupont has been using zero-valent nickel to catalyze the hydrocyanation of butadiene. However, the use of zero-valent nickel presents one major issue: with excess HCN, the formation of inactive nickel(II) cyanide complexes is competitive and leads to catalyst deactivation.[13] The use of wide bite angle diphosphines has remedied this concern by supporting tetrahedral nickel(0) complexes and disfavoring square planar nickel(II) cyanide complexes (Figure 4.2).[13]

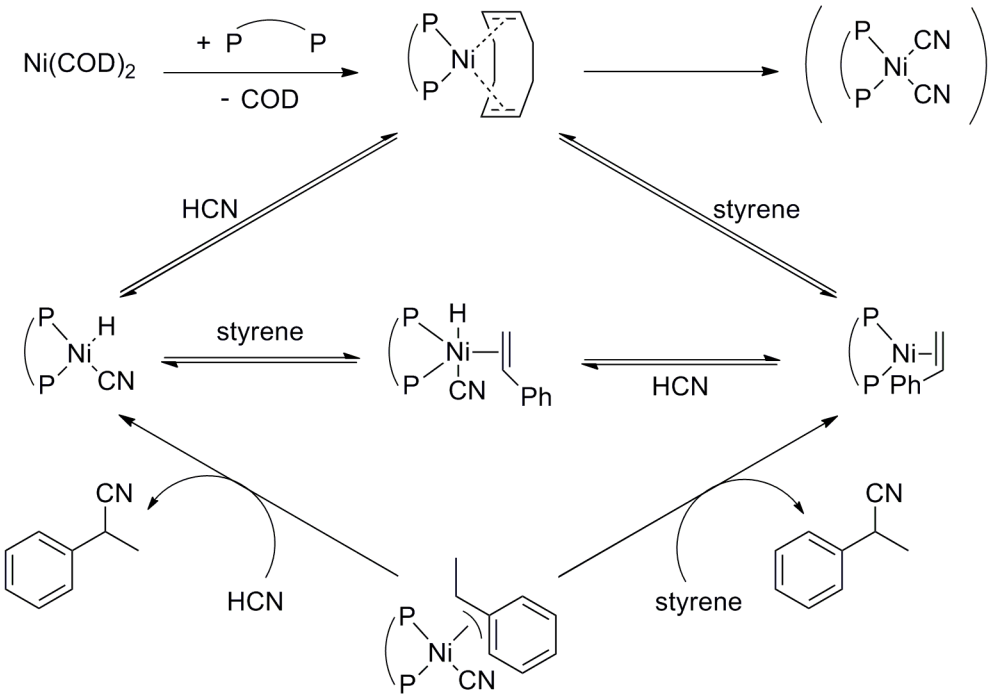

Figure 4.2. Simplified catalytic cycle of the nickel-catalyzed hydrocyanation reaction. Adapted from reference 3.

The key intermediate in hydrocyanation is likely a five coordinate trigonal bipyramidal complex where the nickel is bound to a hydride, a cyano group, an alkene and two

phosphines.[3] A wide bite angle diphosphine ligand such as Xantphos is able to accommodate this geometry and promote the reductive elimination step. This is further observed in the difference in regioselectivity between the smaller bite angle DPEphos and the more rigid thio-variant of Xantphos. The previously mentioned five-coordinate intermediate can easily allow for isomerization and β-elimination of a thermodynamically favored internal alkene.[13] The use of Xantphos over DPEphos results in higher regioselectivity for the terminal nitrile. In this case, the more rigid ligand favors the hydrocyanation pathway kinetically.[13]

The ability of a wide bite angle diphosphine to undergo *cis*-*trans* isomerization can also influence the catalytic pathway. For example in cross-coupling reactions, this characteristic has been shown to promote product formation by accelerating reductive elimination.[5, 14-15] Comparison studies between Xantphos and DPEphos have revealed that Xantphos is a better catalyst for the amination of aryl bromides due to differences in the conformations of the intermediates. Isolated intermediates for DPEphos have *cis*-geometries, while *trans*-intermediates are isolated for Xantphos. Considering that 1,1-reductive elimination from a *cis*-intermediate is necessary for product formation, it is thought that the reaction catalyzed by Xantphos must involve a *trans* to *cis* isomerization. The *trans* to *cis* isomerization is followed by a fast reductive elimination step due to the stability of the Xantphos palladium(0) species and the steric hindrance observed in the *cis*-conformation.[16] This appears to be more effective than the catalysis with DPEphos whose *cis*-intermediates do not need to isomerize, and undergo a slower elimination step.[4, 17-18] In order to get insight into the isomerization mechanism, one study looked at the effects of different wide bite angle phosphines and anion on the structure of neutral

and ionic 4-cyanophenylpalladium and methypalladium complexes in solution and in the solid state.[16] From this study, they proposed one mechanism for the *cis-trans* isomerization of Xantphos metal complexes focused on the participation of the oxygen on the backbone (Figure 4.3).[16]

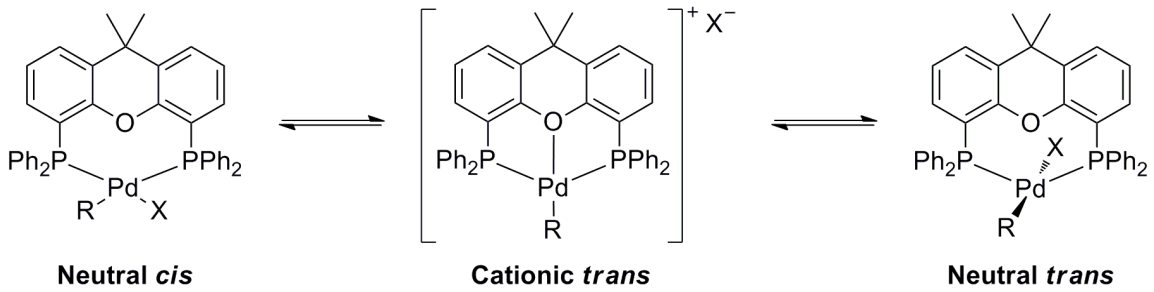

Figure 4.3. Possible mechanism for the *cis-trans* isomerization of Xantphos. Figure adapted from reference 16.

While the participation of the oxygen atom in the backbone of Xantphos is beneficial in the case of palladium cross-coupling reactions, sp^2 and sp^3 C-H bonds of the ligand backbone of other wide bite angle phosphines can be activated by the metal center.[19] This has been observed in rhodium complexes when a long $–CH_2$ chain is used to connect the two phosphines.[19] One solution to preventing unwanted interaction from the backbone is the use of an inflexible backbone. For instance, TRANSphos contains a benzophenanthrene π-system and SPANphos incorporates a fused spirobichroman ring (Figure 4.1).[20-21] Another approach has been lengthening the distance between the donor atoms and the backbone through the inclusion of phenyl linkers.[22-23] Using a similar approach, our group has synthesized a new wide bite angle diphosphine ligand 4,6-bis(3-diisopropylphosphinophenyl)dibenzofuran (^{iPr}DPDBFphos) with two alkylphosphine donors connected to a dibenzofuran backbone by phenyl linkers (Scheme 4.1).[22]

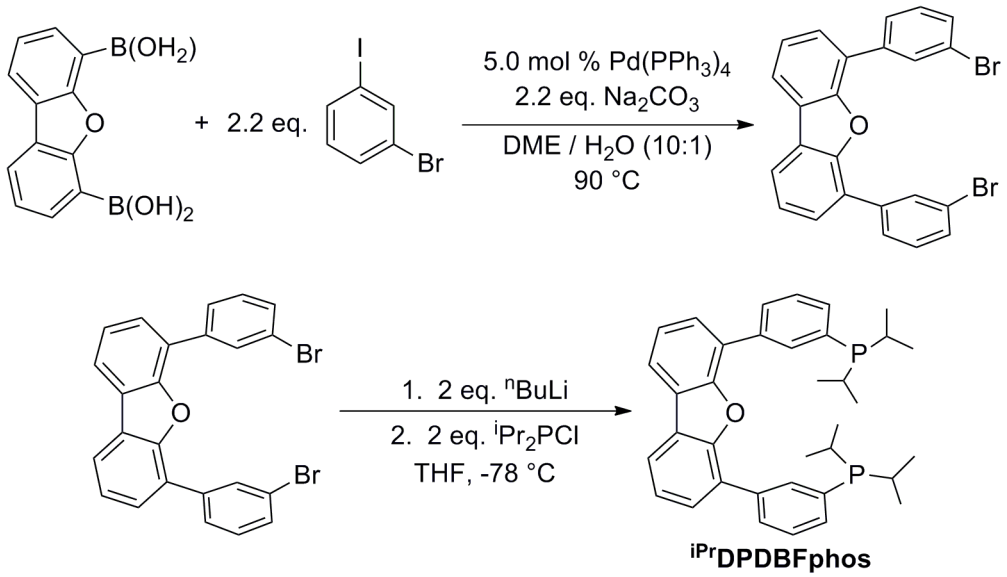

Scheme 4.1. Synthetic route to the diphosphine ligand ^{iPr}DPDBFphos. Figure adapted from reference 22.

The addition of the phenyl linkers should avert interactions between the metal and the ligand backbone.

The ^{iPr}DPDBFphos ligand is a wide bite angle diphosphine ligand with a calculated difference of 3.5 kcal/mol between its *cis* and *trans* conformations.[22] In fact, the ^{iPr}DPDBFphos ligand has been metallated with Rh(I) and Pd(II), resulting in both *cis* and *trans* structures.[22] While on-going investigations are currently looking into the catalytic capabilities of these noble metal ^{iPr}DPDBFphos complexes, first-row transition metals were targeted for metallation due to their lower costs and catalytic promise.

4.2 Catalysis with nickel diphosphines

Though strides have been made towards the use of a variety of first-row transition metals in catalysis, nickel-based catalysts have become most prominent in the field of catalysis employing wide bite-angle diphosphines.[2-3, 5, 12] Their use has been shown to enhance the yield and selectivity of a variety of catalytic reactions. For example, $Ni(COD)_2$ (COD = cycloocta-1-5-diene) in the presence of wide bite angle diphosphines can efficiently catalyze the hydrocyanation of alkenes.[7, 13]An in-depth look at the relationship between the bite angle and the efficiency of the catalyst revealed that wider bite angle diphosphines were favorable and gave improved yields and selectivity over monophosphines and diphosphines with bite angles smaller than 106°.[7, 13, 15] Additionally, the use of wide bite angle diphosphines is believed to stabilize tetrahedral nickel(0) intermediates, causing faster reductive elimination from nickel(II).[7]

Cross coupling reactions have also been catalyzed by nickel diphopshine complexes. Saito and co-workers have reported the coupling of chloroarenes with arylboronic acids with high yields using $NiCl_2$(dppf) (dppf = 1,1'-bis(diphenylphosphino)ferrocene) in the presence of *n*-butyl lithium as a reducing agent to yield a nickel(0) complex *in situ*.[24] Similarly, $NiCl_2$(dppe) catalyzes for the formation of styrene from the cross coupling of vinyl chloride and PhMgBr.[25]

While the key intermediates in these cross coupling reactions have been generally hypothesized to be nickel(0) species, recent studies of N-heterocyclic carbene nickel(I) complexes have revived the alternative proposal that nickel(I) species are involved in both Kumada and Suzuki cross coupling reactions.[26-28] Considering the continued ambiguities in the mechanisms of nickel-mediated cross coupling reactions, the

development of well-defined nickel(I) and nickel(II) complexes supported by a wide bite-angle ligand would be beneficial for gaining insight into the mechanism.

4.3 Scope of thesis

The objective of the second part of this dissertation is to synthesize nickel(I) and nickel(II) complexes supported by the wide bite angle diphosphine ^{iPr}DPDBFphos and to examine their reactivity and catalytic capability towards cross coupling reactions. In chapter 5, the synthesis and characterization of a series of first-row transition metal complexes with ^{iPr}DPDBFphos is described. Within this family of complexes, it is shown through X-ray crystallography that ^{iPr}DPDBFphos can accommodate a wide range of bite angles, allowing for a diverse set of geometries. Additionally, chapter 5 presents the synthesis and characterization of a low-valent three-coordinate nickel(I) complex (^{iPr}DPDBFphos)NiCl. Chapter 6 examines the reactivity of (^{iPr}DPDBFphos)NiCl including metathesis reactions, small-molecule binding, and C-X bond activation. Furthermore, the catalytic activity of Ni(II) versus Ni(I) is compared by probing (^{iPr}DPDBFphos)$NiCl_2$ and (^{iPr}DPDBFphos)NiCl, respectively, as potential catalysts in the Kumada cross coupling of vinyl bromide and phenyl Grignard reagent.

-Chapter Five-

First-Row Transition-Metal Complexes of the Wide Bite-Angle Diphosphine ^{iPr}DPDBFphos

In part from:

Marlier, E. E.; Tereniak, S. J.; Ding, K.; Mulliken, J. E.; Lu, C. C. *Inorg. Chem.* **2011**, *50*, 9290-9299.

5.1 Overview

The diphosphine 4,6-bis(3-diisopropylphosphinophenyl)dibenzofuran (^{iPr}DPDBFphos) has been metalated with transition metal dichlorides of zinc, cobalt, and nickel and iron pentacarbonyl to yield (^{iPr}DPDBFphos)MCl_2 and (^{iPr}DPDBFphos)$Fe(CO)_3$ complexes, respectively. Within these compounds, the diphosphine ^{iPr}DPDBFphos adapts a wide range of bite angles (115 to 180°) as determined by X-ray crystallography. A three-coordinate planar Ni(I) species was isolated from the reduction of (^{iPr}DPDBFphos)$NiCl_2$ with KC_8. Low-temperature EPR measurements of (^{iPr}DPDBFphos)NiCl allow the determination of g values (2.09, 2.14, 2.37) and hyperfine coupling constants to two ^{31}P nuclei, A_{iso} = 46 x 10^{-4} cm^{-1}, and one $^{37}Cl/^{35}Cl$ nucleus, A = (12, 0.7, 35) x 10^{-4} cm^{-1}. Density functional theory (DFT) studies reveal the nature of the magnetic orbital to be d_{xy}, which has σ-antibonding and $\pi_{//}$-antibonding interactions with the phosphorus and chloride atoms, respectively.

5.2 Introduction

In homogeneous transition-metal catalysis research, the reactivity of the metal center is often fine-tuned by modifications to the supporting ligand(s). The development of ligand scaffolds becomes invaluable when these scaffolds confer new reactivities at the metal center that result in advances in catalysis. We have reported a conformationally flexible diphosphine, ^{iPr}DPDBFphos and its *cis*- and *trans*-coordination complexes of Rh(I) and Pd(II) (Chart 5.1).[1]

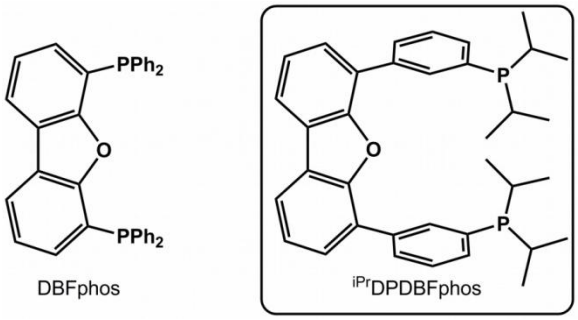

Chart 5.1. Ligands DBFphos and ^{iPr}DPDBFphos.

The ligand ^{iPr}DPDBFphos is analogous to (4,6-bis(diphenylphosphino)dibenzofuran (DBFphos)[2-3] but has a phenyl linker between the dibenzofuran backbone and the phosphine donors. One effect is to distance the backbone from the transition metal center and hence, to prevent binding of the O-atom to the metal. Another effect is to confer flexibility to the ligand's chelate properties.[4-5] Specifically, ^{iPr}DPDBFphos supports a wider range of bite angles within coordination complexes (compared to DBFphos, whose bite angle is limited to 150−157°)[6-7] and can switch from the *cis* to *trans* coordination mode with a calculated 3.5 kcal/mol driving force.[1]

Herein, we extend the coordination chemistry of ^{iPr}DPDBFphos to the first-row transition metals zinc, cobalt, and nickel. A long-standing goal in homogeneous catalysis is to replace precious transition-metal catalysts with their earth-abundant counterparts.[8-9] Notable organometallic examples include iron-mediated cross-coupling reactions,[10] hydroxylation of aliphatic C−H bonds,[11-14] and hydrogenation of alkenes[15-17] and ketones;[18-19] cobalt-mediated hydroformylation[20] and cross-coupling;[21] and nickel-mediated polymerization and oligomerization of olefins,[22-24] cross-coupling,[25-26] and cyclization reactions.[27] More relevant to the complexes reported here, P_2MX_2-type complexes of cobalt and zinc have been shown to be effective catalysts for the polymerization of methyl acrylate and CO_2/ethylene oxide, respectively.[28-29]

The (^{iPr}DPDBFphos)MCl_2 and (^{iPr}DPDBFphos)$M(CO)_3$ complexes are characterized by UV-Visible (UV-Vis) spectroscopy, heteronuclear NMR spectroscopies, and single-crystal X-ray diffraction studies. A three-coordinate nickel(I) chloride complex is presented with additional characterization from electron paramagnetic resonance (EPR) spectroscopy and density functional theory (DFT) calculations.

5.3 Results & discussion

Syntheses of (^{iPr}DPDBFphos)MCl_2, where M = Zn, Co, Ni

The diphosphine ligand ^{iPr}DPDBFphos is cleanly metalated with the anhydrous transition metal dichlorides to provide the zinc, cobalt, and nickel dichloride complexes, [(^{iPr}DPDBFphos)$ZnCl_2$] **1**, [(^{iPr}DPDBFphos)$CoCl_2$] **2**, and [*trans*-(^{iPr}DPDBFphos)$NiCl_2$] **3**, respectively (Scheme 5.1).

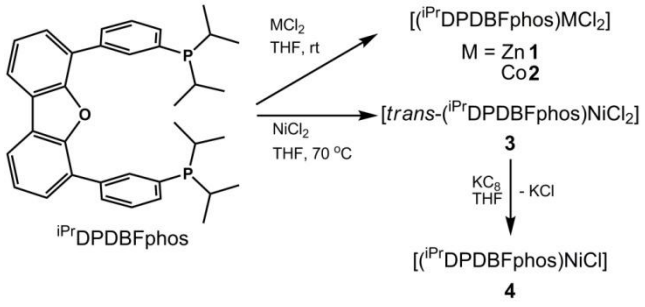

Scheme 5.1. Synthetic routes to coordination complexes **1** to **4**.

UV-Vis & NMR Characterization of (^{iPr}DPDBFphos)MCl_2, where M = Zn, Co, Ni

The UV-Vis spectra of compounds **1** – **3** were collected at room temperature in THF. All complexes have characteristic bands in the UV region from 275 to 330 nm (Figure 5.1). These bands are intense ($\varepsilon \sim 10^4$ L mol^{-1} cm^{-1}) and do not shift significantly for the different transition metal ions. These excitations primarily originate from the dibenzofuran group since the ligand ^{iPr}DPDBFphos has analogous absorbances in this range.

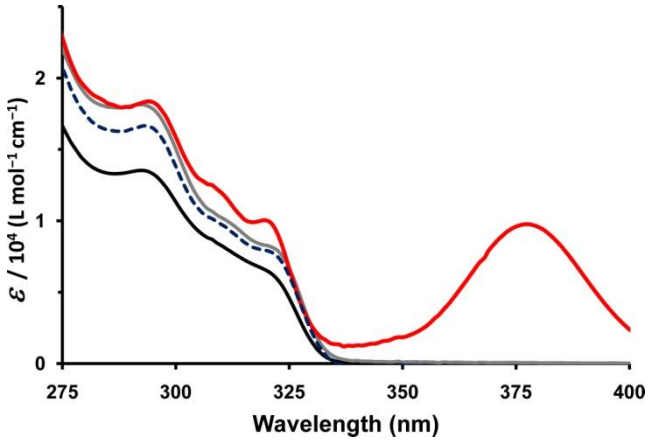

Figure 5.1. Electronic absorption spectra of Zn **1** (—, black), Co **2** (--, blue), Ni **3** (—, red), and ^{iPr}DPDBFphos (—, gray).

Between 330 and 800 nm, the colorless zinc complex **1** has no absorbances, which is consistent with its d^{10} electron count (Figure 5.2).

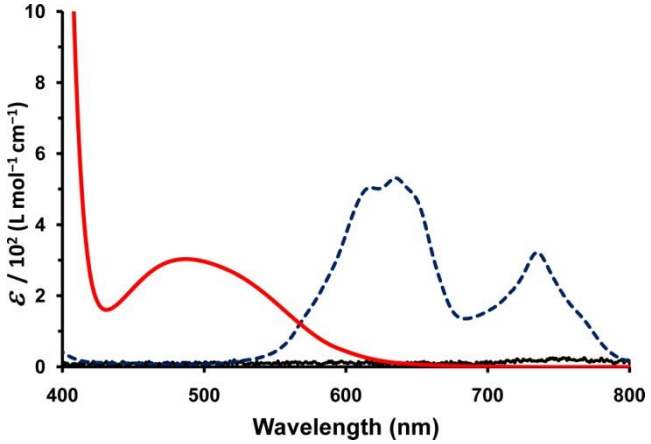

Figure 5.2. Electronic absorption spectra of Zn **1** (—, black), Co **2** (--, blue), and Ni **3** (—, red).

The brilliant blue cobalt complex **2** has several bands between 550 and 800 nm with molar absorptivity values between 320 and 530 L mol^{-1} cm^{-1}, which are typical of *d-d* transitions of a high-spin Co(II) center. The bright red nickel complex **3** has a prominent, intense transition with a maximum at 377 nm (ε = 9,500 L mol^{-1} cm^{-1}) and overlapping

broad features from 420 to 600 nm (ε ~ 300 L mol^{-1} cm^{-1}).[30] The broad features are likely *d-d* transitions, while the intense peak is tentatively assigned as a ligand-to-metal charge transfer band.

Compounds **1** – **3** have been characterized by NMR spectroscopy. For the two diamagnetic complexes, Zn **1** and Ni **3**, one type of phosphorus nucleus is observed at 2.7 and 26.5 ppm, respectively. In the corresponding ^{1}H NMR spectrum of **1**, half of the aryl protons of the ligand are unique, consistent with the approximate two-fold symmetry observed in its solid-state structure (vide infra) (Figure 5.3).

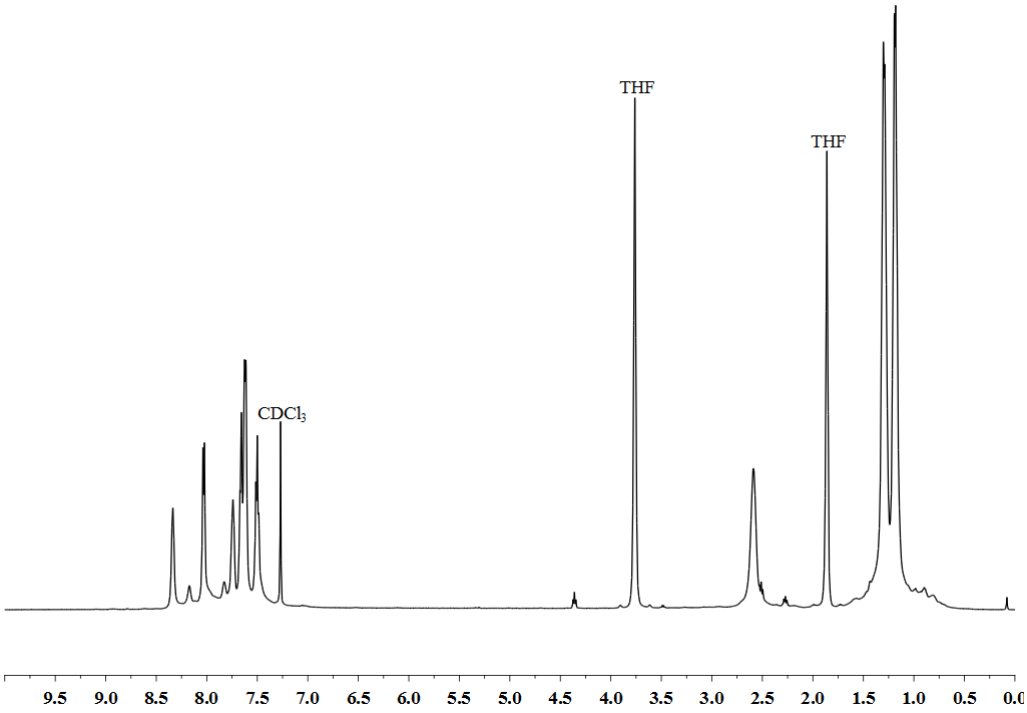

Figure 5.3. ^{1}H NMR spectrum of [(^{iPr}DPDBFphos)$ZnCl_2$] **1** in $CDCl_3$.

For the four isopropyl groups of the ligand, only one methine proton and two methyl resonances are seen. This is an unexpected observation since a two-fold axis should result in two chemically distinct methine types. Hence, their full equivalency must be rationalized by another mechanism (vide infra).

At room temperature, the ^{1}H NMR spectrum of the nickel compound **3** contains both sharp and broad resonances (Figure 5.4).

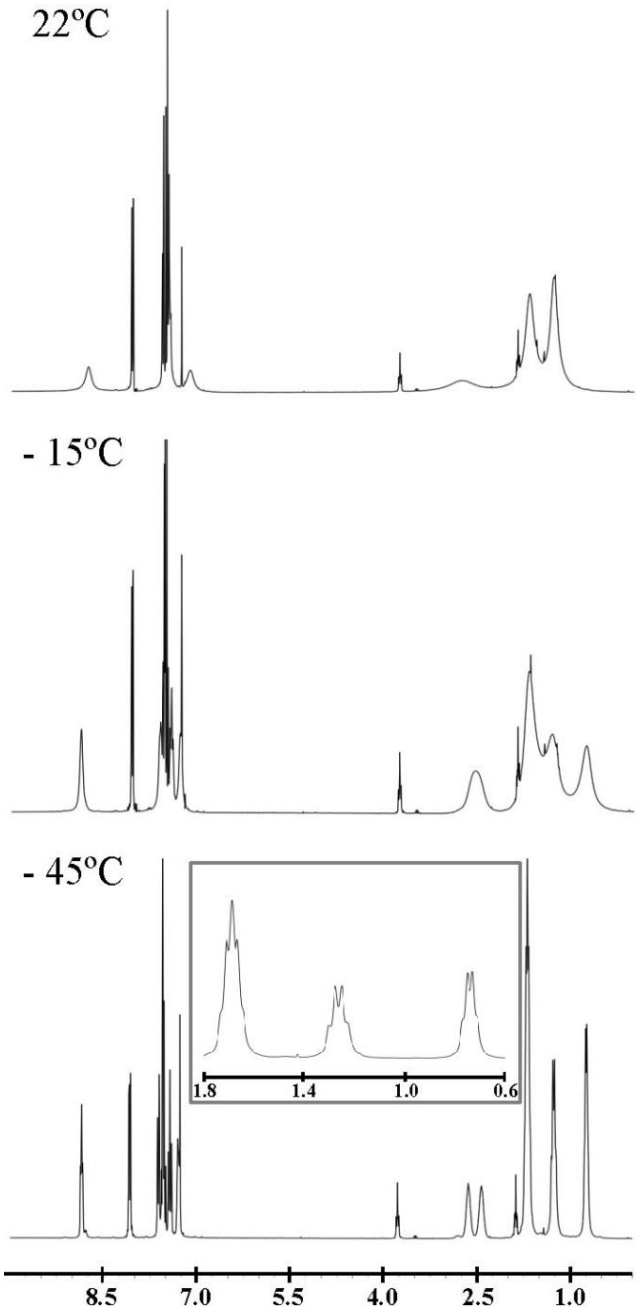

Figure 5.4. Variable-temperature ^{1}H NMR spectra (300 MHz, $CDCl_3$) of [*trans*-(^{iPr}DPDBFphos)$NiCl_2$] **3**. Inset is an expansion of the methyl region at –45 °C.

The sharp signals correspond to the dibenzofuran group, while those belonging to the isopropyl groups and the phenyl linkers are significantly broadened. Upon cooling to −45 °C, the ^{1}H NMR spectrum of **3** sharpens completely, and exactly half of the protons of the ligand are uniquely observed, consistent with the approximate mirror-plane symmetry of its molecular structure. At low temperature, the isopropyl groups resolve into two distinct methine and three methyl resonances. The presence of the mirror plane means that the two chemically different methine protons occur within the same phosphine group, ie. P(CHMe$_2$)(C'HMe$_2$). If P−C$_{methine}$ bond rotation is fast, then two methyl peaks would be expected; if slow, four. At −45 °C, only three methyl signals are apparent due to a coincidental overlap of two of the four possible methyl peaks.[31] At room temperature, the ^{1}H NMR spectrum of **3** shows one methine and two methyl signals, akin to that of **1**. Again, the higher symmetry solution-structure cannot be explained by a mirror plane alone. Additional fluxional processes will be described in the next section.

The cobalt dichloride compound **2** is characterized by a paramagnetic ^{1}H NMR spectrum, which is consistent with a Co(II) oxidation state. Its solution magnetic moment of μ_{eff} = 4.01 μ_B is slightly greater than the spin-only magnetic moment for an S = 3/2 state ($\mu_{S.O.}$ = 3.88 μ_B), which leads to the expected assignment of a high-spin Co(II) center.

Synthesis & Characterization of (^{iPr}DPDBFphos)Fe(CO)$_3$

When our attempts at metallating ^{iPr}DPDBFphos with iron dichloride did not lead to a highly purified material, we turned our attention towards metallating with iron pentacarbonyl. During a 6 hour photolysis using a mercury vapor lamp, ^{iPr}DPDBFphos

can be metallated with iron pentacarbonyl to yield [(^{iPr}DPDBFphos)Fe(CO)$_3$] **5** in nearly quantitative yield.

Complex **5** was characterized by NMR and IR spectroscopy. The ^{31}P NMR spectrum shows one peak, located at 90.4 ppm while the ^{1}H NMR spectrum displays the same two fold symmetry observed in complexes **1** and **3** (Figure 5.5).

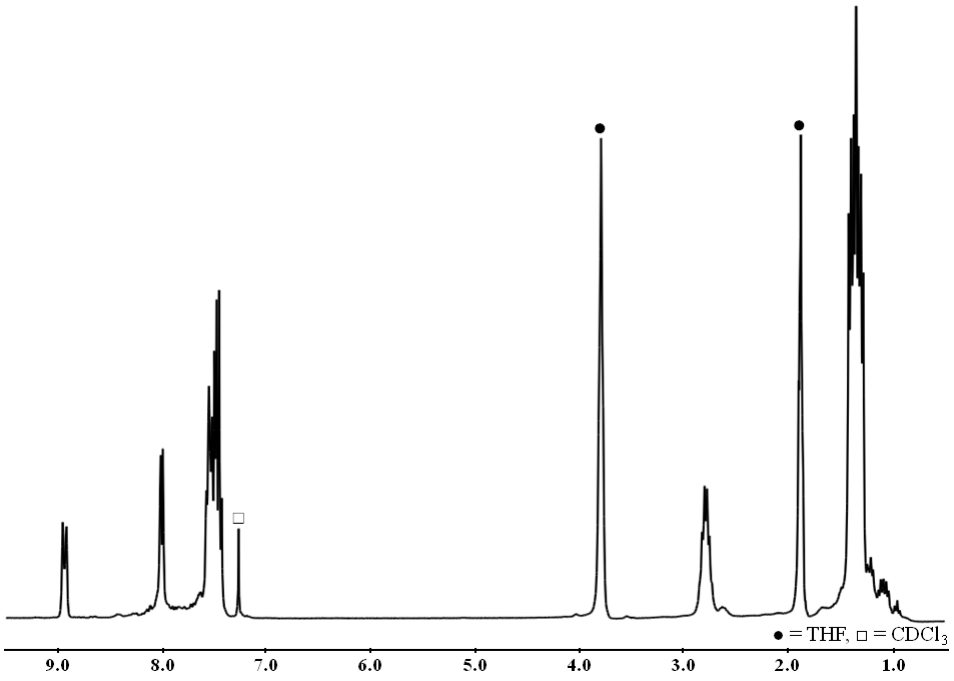

Figure 5.5. ^{1}H NMR spectrum of [(^{iPr}DPDBFphos)Fe(CO)$_3$] **5** in $CDCl_3$.

A total of three resonances are observed in the aromatic region, integrating to the 14 protons of the benzofuran backbone and phenyl linkers. For the four isopropyl groups of the ligand, only one methine proton and two methyl resonances are seen.

The IR spectrum of **5** has two different signals; a strong resonance at 1869 cm^{-1} and a weak resonance at 1959 cm^{-1}. These are assigned as E´ and A_1´ stretching mode respectively, where the A_1´ stretching mode is weak considering it is forbidden. These stretching resonances are similar to those observed for *trans*-Fe(CO)$_3$(PR$_3$)$_2$.[32] When PR$_3$

is triphenylphosphine, three stretches at 1881 cm^{-1}, 1886 cm^{-1} and 1944 cm^{-1} are observed in the IR spectrum.[32] In this case, the E´ stretching mode is split into two different resonances, which is a common characteristic when chloroform is used as a solvent.[32] Additionally the ^{31}P NMR shift of *trans*-$Fe(CO)_3(PPh_3)_2$ is similar to **5**, as it is located at 82.5 ppm versus 90.4 ppm for **5**.[32]

Solid-state Structures of (^{iPr}DPDBFphos)MCl_2, where M = Zn, Co, Ni

The geometry of the zinc and cobalt centers in **1** and **2**, respectively, are tetrahedral. The structures of **1** and **2** are highly homologous, and their unit cell dimensions are nearly identical (Figure 5.6 and Table 5.1).

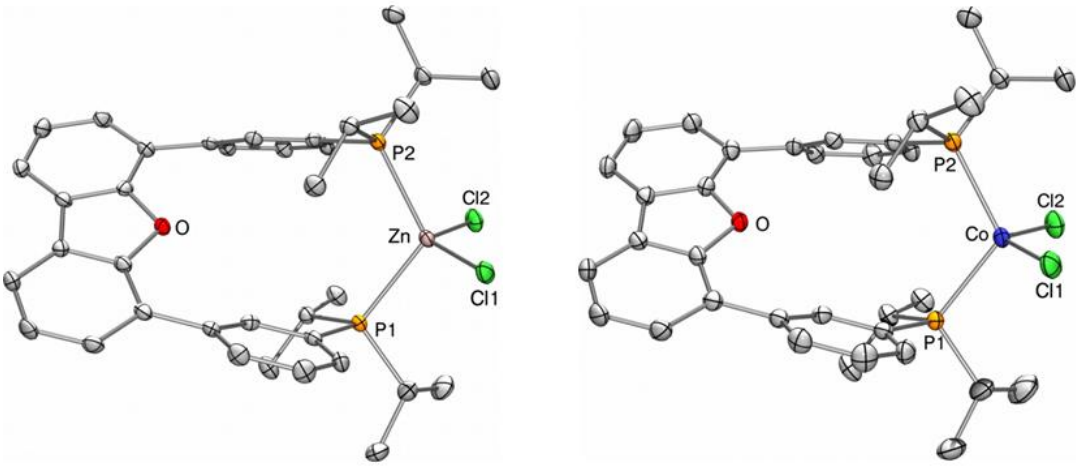

Figure 5.6. Solid-state structures of [(^{iPr}DPDBFphos)$ZnCl_2$] **1** and [(^{iPr}DPDBFphos)$CoCl_2$] **2** at 50% probability level.
Hydrogen atoms were omitted for clarity.

Table 5.1. Crystallographic data for **1** – **5**.

Compounds	$C_{36}H_{42}Cl_2ZnOP_2$	$C_{36}H_{42}Cl_2CoOP_2$	$C_{36}H_{42}Cl_2NiOP_2$	$C_{36}H_{42}ClNiOP_2$	$C_{39}H_{42}FeO_4P_2$
Compounds Abbreviation	**1**	**2**	**3**	**4**	**5**
Morphology	Plate	Block	Plate	Plate	Plate
Color	White	Blue	Red	Yellow	Yellow
Lattice Type	Triclinic	Triclinic	Monoclinic	Monoclinic	Monoclinic
Space Group	P-1	P-1	P2(1)/c	P2(1)/c	P2(1)/n
a, Å	9.772(3)	9.7720(10)	19.181(3)	24.277(4)	10.656(2)
b, Å	10.024(3)	10.0197(10)	9.0591(13)	17.431(3)	9.466(2)
c, Å	17.882(6)	17.9389(19)	21.040(3)	16.052(3)	33.610(7)
α, deg	80.286(5)	80.377(2)	90	90	90
β, deg	75.748(5)	76.0060(10)	115.196(2)	105.405(2)	97.770(3)
γ, deg	85.834(5)	85.940(2)	90	90	90
V, Å	1672.6(9)	1679.5(3)	3308.0(8)	6548.6(18)	3359(1)
Z	2	2	4	8	4
formula wt, g mol^{-1}	688.91	682.47	682.25	646.8	692.52
Dc,g cm^{-3}	1.368	1.350	1.370	1.312	1.369
μ, mm^{-1}	1.017	0.793	0.873	0.799	0.585
F(000)	720	714	1432	2728	1456
θ range, deg	1.19 to 26.37	1.18 to 27.52	1.17 to 27.49	1.46 to 26.37	1.22 to 25.10
reflns collected	16699	20155	31527	56856	30187
unique reflns	6815	7590	7531	13372	5959
data/restraint/parameters	6815 / 0 / 387	7590 / 0 / 387	7531 / 0 / 387	13372 / 0 / 755	5959 / 0 / 423
R1, wR2 [I>2σ(I)]	0.0428, 0.0959	0.0372, 0.0830	0.0295, 0.0669	0.0540, 0.0904	0.0545, 0.0858
R1, wR2 [all data]	0.0712, 0.1083	0.0583, 0.0928	0.0432, 0.0777	0.1100, 0.1043	0.0997, 0.0980
GOOF	1.050	1.021	1.043	1.029	1.017
largest diff peak, hole, e $Å^{-3}$	0.925, -0.519	0.781, -0.428	0.466, -0.312	0.413, -0.409	0.345, -0.329

Both structures contain an approximate two-fold rotation axis. The P-M-P bond angle is 115.27(3)° and 114.62(2)° in the zinc and cobalt complexes, respectively (Table 5.2).

Table 5.2. Experimental bond distances (Å) and angles (deg) for **1** – **5**.

	1, Zn(II)	**2, Co(II)**	**3, Ni(II)**	**4, Ni(I)[a]**		**5, Fe(0)**
				A	*B*	
Bond Distances (Å)						
M-P_1	2.420(1)	2.3920(7)	2.2410(5)	2.209(1)	2.243(1)	2.217(1)
M-P_2	2.416(1)	2.3844(7)	2.2413(5)	2.217(1)	2.233(1)	2.220(1)
M-Cl_1	2.255(1)	2.2331(7)	2.1748(5)	2.163(1)	2.180(1)	-
M-Cl_2	2.2641(9)	2.2435(7)	2.1609(5)	-		-
M-CO	-	-	-	-		1.767(4), 1.761(4), 1.765(4)
Bond Angles (deg)						
P_1-M-P_2	115.27(3)	114.62(2)	176.55(2)	115.53(4)	119.49(4)	115.27(3)
Cl_1-M-Cl_2	117.38(3)	118.55(3)	175.10(2)	-		-
CO-M-CO	-	-	-	-		117.7(2), 130.2(2), 112.0(2)

[a] Two values are reported because two independent molecules (*A*, *B*) are present in the unit cell.

Previously, we observed a more acute bite angle of 104.5° for ^{iPr}DPDBFphos in the distorted square planar complex, [*cis*-(^{iPr}DPDBFphos)Rh(nbd)]BF_4.[1] The Co−P and Zn−P bond distances in **1** and **2**, respectively, are comparable to other diphosphine dichloride coordination complexes with the corresponding transition metal centers.

The geometry of the nickel center in **3** is square planar with a *trans*-spanning ^{iPr}DPDBFphos ligand (P−Ni−P = 176.55(2)°) (Figure 5.7).

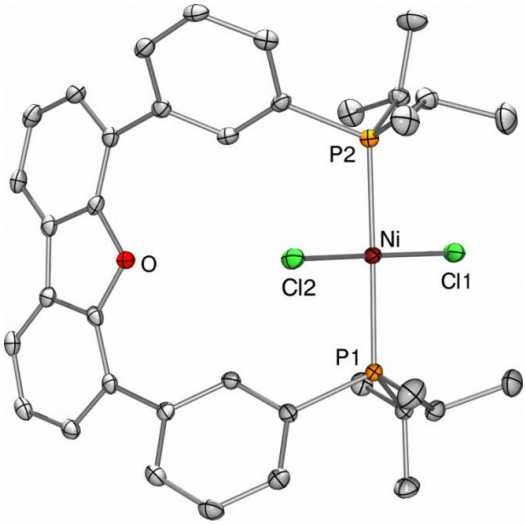

Figure 5.7. Solid-state structure of [(^{iPr}DPDBFphos)$NiCl_2$] **3** at 50% probability level. Hydrogen atoms were omitted for clarity.

The Ni−P bond distances in **3** (2.2410(5), 2.2413(5) Å) are unremarkable compared to other *trans*-diphosphine nickel dichloride complexes (average P−Ni = 2.24 Å, Cambridge Structural Database).[6-7] An approximate mirror plane bisects the solid-state structure of **3**. The two chloride atoms in **3** reside in the mirror plane and are nonequivalent. One chloride is near the dibenzofuran backbone while the other chloride is sandwiched between the isopropyl substituents. At room temperature, the ^{1}H-NMR peaks representing the isopropyl groups coalesce into one methine and two methyl resonances. The coalescence requires a combination of two dynamic motions (Scheme 5.2): (1) canting of the phenyl linkers, which flips the relative bent orientation of the dibenzofuran group, and (2) rotation of the P−Ni−P vector, equalizing the two chlorides.

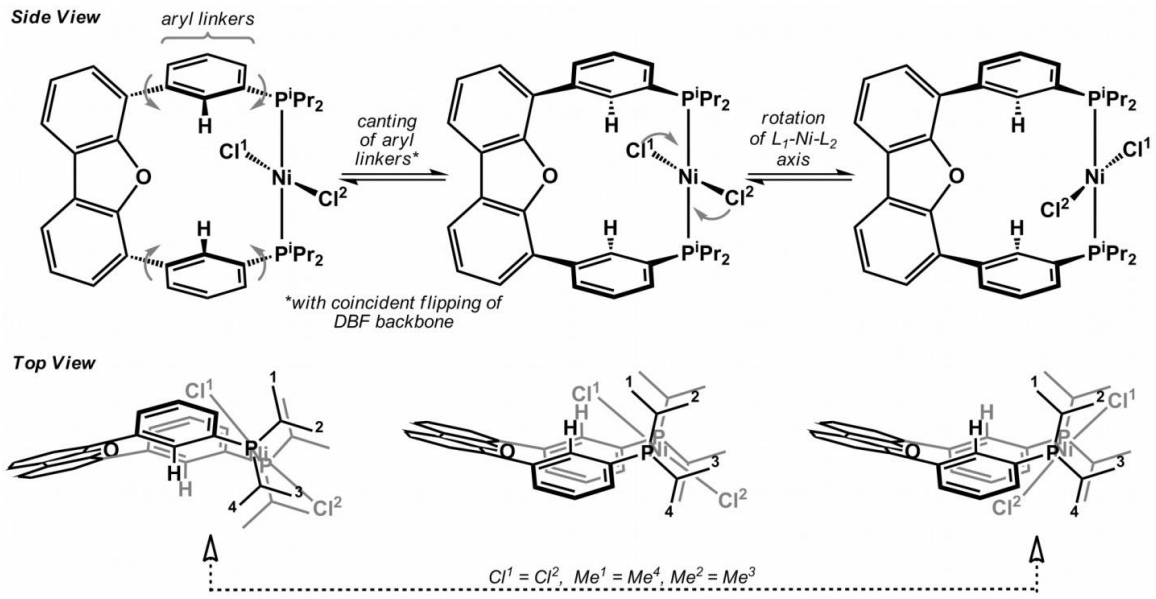

Scheme 5.2. Fluxional processes in **3**.

Similar fluxional behavior has been previously described for the analogous square-planar complexes, [*trans*-(^{iPr}DPDBFphos)Rh(NCMe)$_2$]BF$_4$ and [*trans*-(^{iPr}DPDBFphos)Pd(NCMe)$_2$](BF$_4$)$_2$.[1] We propose that canting of the phenyl linkers would also occur in tetrahedral **1** to rationalize the solution-structure equivalency of all the methine protons of the ligand.

Solid Structure of (^{iPr}DPDBFphos)M(CO)$_3$, where M = Fe

X-ray quality crystals of **5** were grown from vapor diffusion of pentane into a concentrated CH_2Cl_2 solution of **5**. The geometry of the iron(0) center is trigonal bipyramidal, with *trans*-spanning diphosphine ligand and the three carbonyl groups occupying the axial and equatorial positions respectively (Figure 5.8).

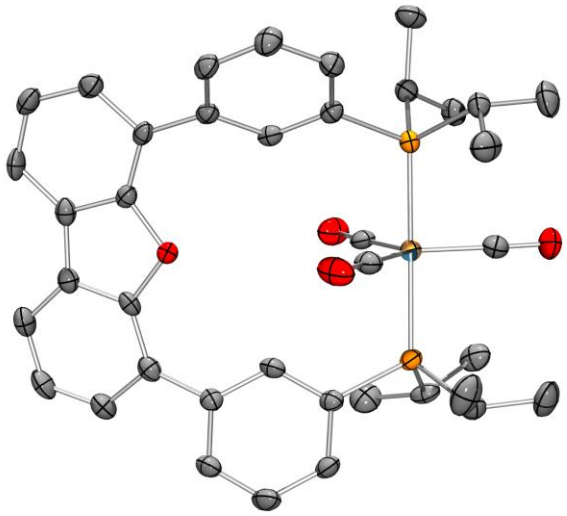

Figure 5.8. Solid-state structure of [(^{iPr}DPDBFphos)Fe(CO)$_3$] **5** at 50% probability level. Hydrogen atoms were omitted for clarity.

In this case, the bite angle of ^{iPr}DPDBFphos is 171.94(4)°, which shows some slight distortion from the expected 180° angle. The Fe-P bond distances are 2.217(1) Å and 2.220(1) Å while the Fe-CO bond distances are 1.767(4) Å, 1.761(4) Å and 1.765(4) Å.

Synthesis and Characterization of (^{iPr}DPDBFphos)Ni^{I}Cl

The redox properties of compounds **1** – **3** were investigated by cyclic voltammetry (0.1 M [^{n}Bu$_4$]PF$_6$ in THF), but no reversible redox events were found (Figure 5.9). Interestingly, the nickel dichloride complex **3** exhibited two irreversible events when scanning cathodically, whereas only one reductive signal was seen for the zinc and cobalt dichloride complexes, presumably a ligand-based reduction. Therefore, the chemical reduction of compound **3** was investigated.

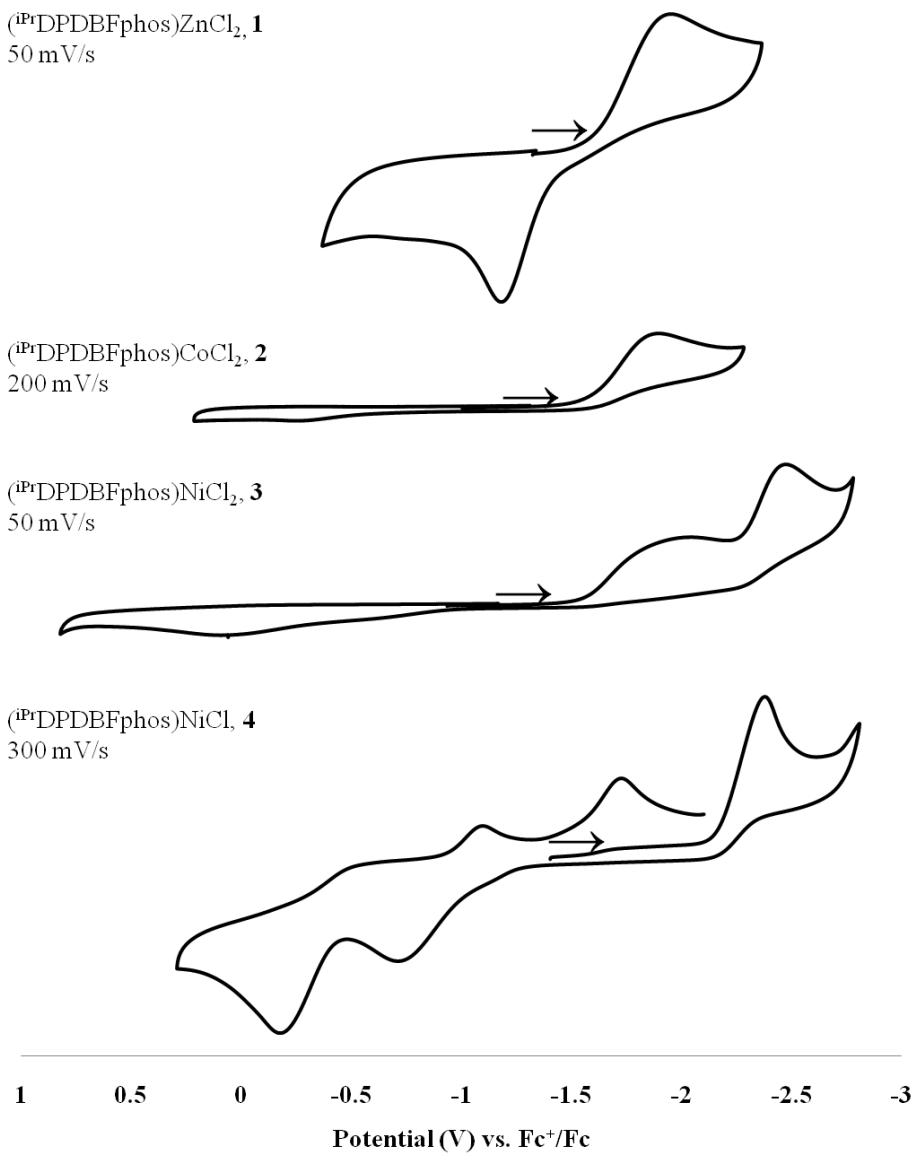

Figure 5.9. Cyclic voltammograms of (^{iPr}DPDBFphos)MCl_2, **1 – 4**, taken in 0.1 M [TBA]PF_6 THF solution. Scan rate studies were performed on each complex but only one rate is shown for each complex in the negative direction.

Sodium-based reducing agents such as sodium metal, sodium amalgam, and sodium naphthalide resulted in decomposition of **3** and formation of the free ligand by ^{31}P NMR spectroscopy. Mixing potassium graphite with **3** in THF resulted in an immediate color change from red to yellow (Figure 5.10).

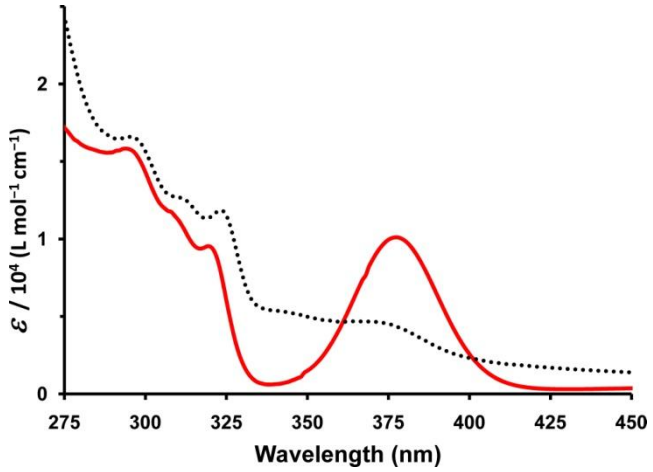

Figure 5.10. Electronic absorption spectra of the nickel compounds **3** (—, red) and **4** (···, black).

The resulting product is paramagnetic, and a single-crystal X-ray diffraction study reveals a three-coordinate, formally 15-electron Ni(I) complex, [(^{iPr}DPDBFphos)]NiCl **4** (Figure 5.11).

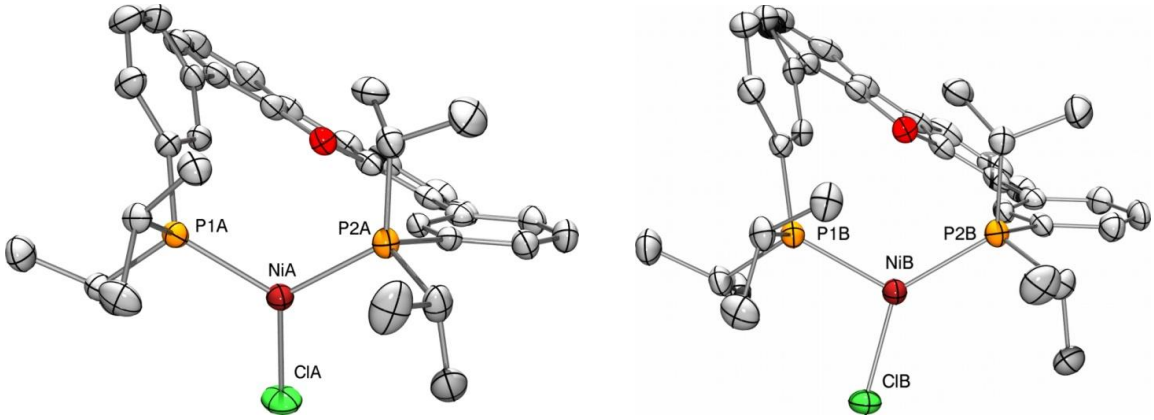

Figure 5.11. Solid-state structures of [(^{iPr}DPDBFphos)NiCl] **4** at 50% probability level. Both independent molecules in the unit cell are shown. Hydrogen atoms were omitted for clarity. Selected bond angles: P1A−NiA−P2A 115.53(4), P1A−NiA−ClA 122.94(9), P2A−NiA−ClA 121.53(4), P1B−NiB−P2B 119.49(4), P1B−NiB−ClB 104.61(4), P2B−NiB−ClB 135.00(4).

Yellow crystals of [(^{iPr}DPDBFphos)NiCl] **4** were grown from a concentrated CD_3CN solution at room temperature. Two independent molecules of **4** are found in the unit cell. Both nickel centers are three-coordinate and planar. The L−Ni−L angles sum to 359 and 360°. There are, however, significant variations in the bond and angle metrics between these two molecules (Table 5.2, *A* and *B*). For instance, the Ni−L bond distances within the two molecules differ from each other by 0.02 to 0.03 Å. One may normally expect to see a shortening of Ni–P bonds upon reduction of the Ni center (from **3** to **4**) because of increased π-back bonding into the phosphine ligands. However, this is not necessarily the case here. While molecule *A* does have significantly shorter Ni–P bond lengths relative to [*trans*-(^{iPr}DPDBFphos)$NiCl_2$] **3**, molecule *B* has essentially identical Ni–P bond lengths to those in **3**. The diphosphine bite angle in molecule *A*, 115.53(4)°, is nearly identical to that in the tetrahedral [(^{iPr}DPDBFphos)MCl_2] compounds reported here, but molecule *B* has a wider bite angle of 119.49(4)°. Moreover, the NiA center is nearly trigonal planar with similar P(1)−NiA−Cl and P(2)−NiA−Cl bond angles of 122.94(4) and 121.53(4)°, respectively. The NiB center has a more distorted trigonal geometry with the chloride ligand positioned asymmetrically between the two phosphorus atoms. The P(1)−NiB−Cl and P(2)−NiB−Cl bond angles are quite different at 104.61(4) and 135.00(4)°, respectively. The origin of the distortion is unclear. We looked for indications of crystal packing forces, but the shortest non-bonded contact distances to the chloride atom in the more distorted molecule (*B*) are too long (> 2.88 Å for Cl----H)[33] to have much impact (Table 5.3).[34]

Table 5.3. Shortest non-bonded contact distances near the Cl atoms in the two independent molecules of **4**.

Non-Distorted Molecule (NiA)			Distorted Molecule (NiB)		
Atom	**Symcode**	**Distance (Å)**	**Atom**	**Symcode**	**Distance (Å)**
H2AB	1555	2.761	H1BB	1555	2.993
H5AB	4556	2.900	H8BA	4576	2.902
H26B	1555	2.762	H32A	3656	2.893
H31C	1555	2.912			
H34A	4556	2.677			

Of relevance, the molecular structure of $Ni(PPh_3)_2Cl$ is slightly distorted trigonal planar, and the observed asymmetry was attributed to a first-order Jahn Teller effect.[35] This rationale, however, is inherently flawed because no degenerate *d*-orbitals can exist for NiP_2X species, even with idealized D_{2h} symmetry. Instead, we propose that the chloride atom wiggles within the NiP_2-plane, and that these structural perturbations cost little energy.

The X-band EPR spectrum of **4** was taken in frozen toluene at 20 K (Figure 5.12). A slightly rhombic signal is observed with *g*-values of 2.09, 2.14, and 2.37 (g_{iso} = 2.20), which are consistent with the assignment of a S = ½ Ni(I) center.[36-38] EPR spectra of three-coordinate Ni(I) complexes typically have rhombic anisotropy with $g_3 - g_2 > g_2 - g_1$.[39-40] The spectrum was simulated using hyperfine coupling constants to two ^{31}P (I = ½) nuclei of (43, 40, 55) x 10^{-4} cm^{-1} (A_{iso} = 46 x 10^{-4} cm^{-1}) and to one $^{37}Cl/^{35}Cl$ nucleus (I = 3/2, abundance ratio = 0.3196) of (12, 0.7, 35) x 10^{-4} cm^{-1}.

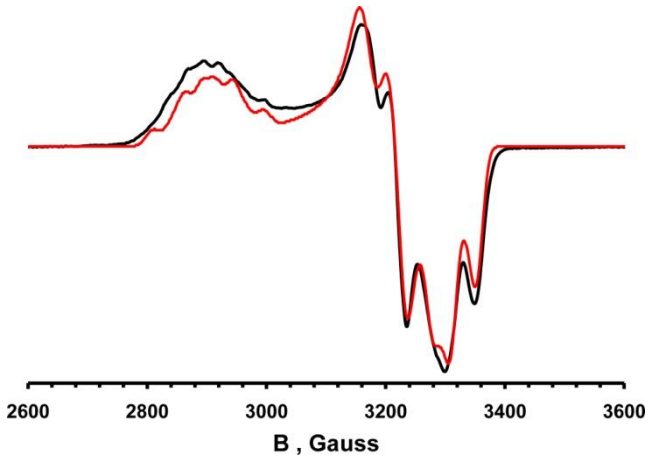

Figure 5.12. X-band EPR spectrum (dX″/dB) of [(^{iPr}DPDBFphos)NiCl] **4** in toluene glass shown in black (1mM, 20.0 K, frequency = 9.65 GHz, modulation to 10.0 G, power = 0.02 mW). The spectrum was simulated (shown in red) by adopting the following values: g = (2.09, 2.14, 2.37); line widths, W = (12, 21, 13.5) G; A(two ^{31}P, I = ½) = (43, 40, 55) x 10^{-4} cm^{-1}; A(^{37}Cl/^{35}Cl, I = 3/2) = (12, 0.7, 35) x 10^{-4} cm^{-1}.

Large hyperfine coupling constants to the two ^{31}P nuclei are observed for all three g-values, while the hyperfine splitting caused by ^{37}Cl/^{35}Cl coupling is significant only for g_3. The equivalence of the two phosphorus nuclei in the frozen solution EPR of **4** stands in contrast to the classical work of Nilges *et al.* on the single-crystal EPR study of Ni(I)-doped $Cu(PPh_3)_2Cl$, in which the hyperfine coupling constants of the two phosphorus nuclei are remarkably inequivalent, A_{iso}(^{31}P) = 38 and 59 x 10^{-4} cm^{-1}.[41] Of note, our ^{31}P hyperfine coupling constant is midway between these two values determined for $Ni(PPh_3)_2Cl$.

Theoretical Studies of (^{iPr}DPDBFphos)Ni^{I}Cl

DFT calculations were performed on the Ni(I) complex **4** using the BP86 and M06-L functionals. The optimized geometries compare favorably with the experimental structure, whose NiA coordinates were used as the initial geometry (Table 5.4).

Table 5.4. Comparison of calculated and experimental geometric parameters for **4**.

	Experimental	BP86	M06-L
bond distances			
Ni-P(1)	2.209(1)	2.211	2.216
Ni-P(2)	2.217(1)	2.221	2.229
Ni-Cl(1)	2.163(1)	2.154	2.177
bond angle			
P(1)-Ni-P(2)	115.53(4)	117.72	115.35

All calculated Ni–L bond distances are within 0.015 Å of their experimental values. The optimized bite angles were also remarkably close to the experimental value, differing at most by 2°.

The molecular-orbital (MO) diagram showing the splitting of the *d*-orbital manifold was generated from the DFT calculations (Figure 5.13). Because the MO diagrams derived from the two functionals are very similar, only the results from the BP86 optimization were used to generate the MO diagram. For the following discussion, the molecular trigonal plane is defined as the xy-plane with the Ni−Cl vector along the x-axis.

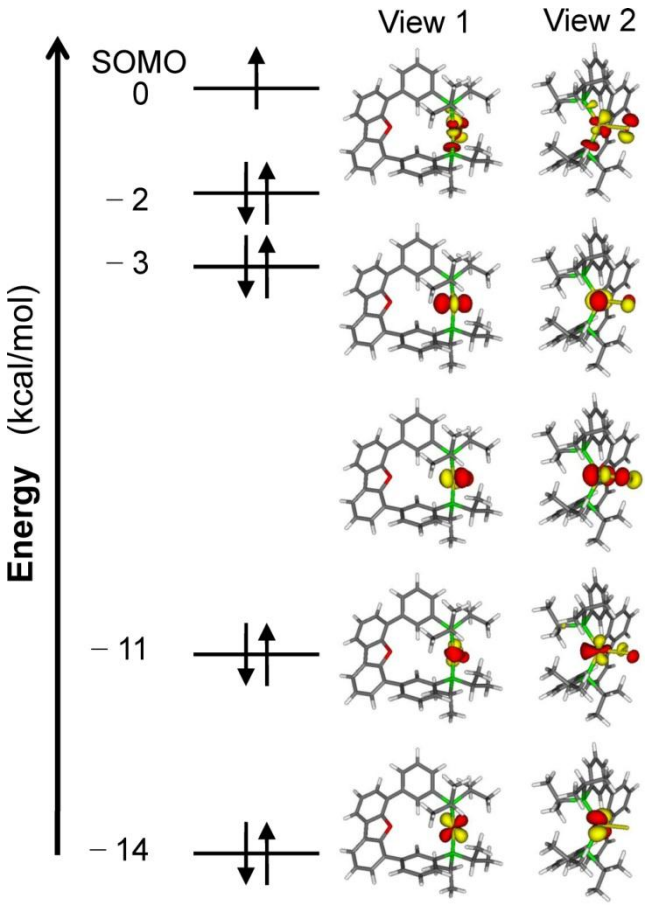

Figure 5.13. Qualitative MO diagram of the *d*-orbital manifold derived from a DFT-BP86 calculation of [(^{iPr}DPDBFphos)NiCl] **4**.

The *d*-orbital manifold comprises three energetically high-lying *d*-orbitals and two low-lying *d*-orbitals. The singly occupied MO (SOMO) is predominantly d_{xy} in composition and is σ-antibonding with respect to the phosphorus atoms and $\pi_{//}$-antibonding with the chloride atom. This magnetic orbital description[42] is consistent with the EPR spectrum of **4**, which is characterized by a large hyperfine coupling constant to both phosphorus nuclei and a smaller interaction with the chloride nucleus. The next two MO's, which have d_{z2} and d_{xz} parentage, are characterized by $\pi_{\perp}$-antibonding interactions with the chloride. Significantly lower in energy are the d_{x2-y2} and d_{yz} orbitals. The former is

slightly σ-antibonding with respect to chloride, and the latter is formally non-bonding. The calculated electronic structure is fully consistent with monovalent nickel. The LUMO (not shown) is ligand-based and is characterized by delocalized electron density throughout the π-system of the dibenzofuran backbone.

5.4 Conclusions

The diphosphine ^{iPr}DPDBFphos was successfully used as a supporting ligand in tetrahedral Zn(II), tetrahedral Co(II) and trigonal bipyramidal Fe(0) complexes, as well as in square-planar Ni(II) and distorted trigonal planar Ni(I) compounds. The breadth of coordination geometries as exemplified by these complexes is enabled by the conformationally flexible backbone in ^{iPr}DPDBFphos. Compared to *cis*-chelating diphosphines, non-rigid *trans*-spanning diphosphines may be advantageous when a non-labile ligand platform is required that must also accommodate different coordination geometries, such as during a catalytic cycle. The reactivity of the (^{iPr}DPDBFphos)NiCl **4** and its use in catalysis will be discussed in the next chapter.

5.5 Experimental procedures

Synthetic Considerations. Unless otherwise stated, all manipulations were performed under a dinitrogen atmosphere in a MBraun glovebox or using standard Schlenk techniques. Standard solvents were deoxygenated by sparging with dinitrogen and dried by passing through activated alumina columns of a SG Water solvent purification system. Deuterated solvents were purchased from Cambridge Isotope Laboratories, Inc., dried over CaH_2, distilled, and stored over activated 4 Å molecular sieves. Elemental analyses were performed by Atlantic Microlab. The synthesis of 4,6-bis(3-diisopropylphosphinophenyl)dibenzofuran, referred to as ^{iPr}DPDBFphos, was previously reported.[1] Other reagents were purchased commercially and used without further purification.

Synthesis of [(^{iPr}DPDBFphos)$ZnCl_2$] (1). A solution of zinc (II) chloride (0.026 g, 0.19 mmol) in 10 mL of THF was added dropwise to a solution of ^{iPr}DPDBFphos (0.102 g, 0.18 mmol) in 10 mL of THF. The reaction solution was stirred overnight. After 12 hours, the solvent was removed under reduced pressure, and the resulting solids were washed with Et_2O and then extracted into THF. The THF solution was layered with hexane and stored at –35 ºC overnight to give a white precipitate, which was collected and dried under reduced pressure (0.089 g, 70%). Single crystals suitable for X-ray diffraction analysis were grown from Et_2O. UV (THF) λ_{max}, nm (ε, L mol^{-1} cm^{-1}): 294 sh (13,000), 310 sh (6,400). ^{1}H NMR (500 MHz, $CDCl_3$): δ 8.33 (2H, br, CH), 8.03 (2H, d, *J* = 7.0 Hz, CH), 7.74 (2H, br. s, CH), 7.66 (2H, d, *J* = 6.5 Hz, CH), 7.62 (4H, m, *J* = 6.5 Hz, CH), 7.50 (2H, t, *J* = 7.5 Hz, CH), 2.59 (4H, m, PC*H*$(CH_3)_2$), 1.29 (12H, dd, J_{HH} =

8.0 Hz, J_{HP} = 15 Hz, PCH(CH_3)(C′H$_3$)), 1.19 (12H, dd, J_{HH} = 8.0 Hz, J_{HP} = 15 Hz, PCH(CH$_3$)(C′H_3)). ^{31}P NMR (121 MHz, $CDCl_3$): δ 2.7. ESI-MS-TOF *m/z* : $[M - Cl]^+$ calc. for $C_{36}H_{42}ClZnOP_2$, 651.1691; found, 651.3.

Synthesis of [(^{iPr}DPDBFphos)CoCl$_2$] (2). A suspension of cobalt (II) chloride (0.026 g, 0.20 mmol) in 20 mL of THF was added dropwise to a solution of ^{iPr}DPDBFphos (0.109 g, 0.20 mmol) in 20 mL of THF. The reaction solution was stirred overnight. After 12 hours, the solvent was removed under reduced pressure, and the resulting solids were washed with Et_2O and then extracted into THF. The THF solution was filtered and then evaporated to dryness under reduced pressure to give a blue powder (0.133 g, 99 %). Single crystals suitable for X-ray diffraction analysis were grown from Et_2O. UV (THF) λ_{max}, nm (ε, L mol^{-1} cm^{-1}): 295 sh (16,000), 322 sh (7,600), 618 sh (500), 636 (530), 735 (320). ^{1}H NMR (300 MHz, C_6D_6): δ 21.36, 13.54, 7.95, 7.64, 6.79, 4.19, 1.83, −14.03. Evans' method ($CDCl_3$/$CHCl_3$, 300 MHz): μ_{eff} = 4.01 μ_B. Anal. Calcd. for $C_{36}H_{42}Cl_2OP_2Co$: C, 63.35; H, 6.20; N, 0. Found: C, 62.83; H, 6.05; N, 0.0.

Synthesis of [(^{iPr}DPDBFphos)NiCl$_2$] (3). A suspension of nickel (II) chloride (0.068 g, 0.52 mmol) in 20 mL of THF was added dropwise to a solution of ^{iPr}DPDBFphos (0.250 g, 0.45 mmol) in 20 mL. The reaction solution was heated at 70 ºC with stirring. After 12 hours, the solvent was removed under reduced pressure, and the resulting solids were washed with Et_2O and then extracted into THF. The THF solution was filtered and then stored at –35 ºC overnight to give red crystals, which were collected and dried under reduced pressure (0.202 g, 65%). Single crystals suitable for X-ray diffraction analysis

were grown from a CH_2Cl_2/Et_2O (1:3) solution. UV (THF) λ_{max}, nm (ε, L mol^{-1} cm^{-1}): 295 sh (18,000), 322 sh (9,300), 377 (9,500), 487 (280). ^{1}H NMR (300 MHz, $CDCl_3$): δ 8.74 (2H, br, CH), 8.06 (2H, d, *J* = 7.5 Hz, CH), 7.57 (2H, d, *J* = 7.5 Hz, CH), 7.50 (6H, m, *J* = 7.5 Hz, CH), 7.13 (2H, br, CH), 2.75 (4H, br, PC*H*$(CH_3)_2$), 1.67 (12H, br, PCH(C*H*$_3$)(C′H$_3$)), 1.27 (12H, br, PCH(CH_3)(C′*H*$_3$)). ^{31}P NMR (121 MHz, $CDCl_3$): δ 26.5 (br). Anal. Calcd. for $C_{36}H_{42}Cl_2OP_2Ni$: C, 63.37; H, 6.20; N, 0. Found: C, 63.16; H, 6.20; N, 0.0.

Synthesis of [(^{iPr}DPDBFphos)NiCl] (4). A THF solution of **3** (0.095 g, 0.14 mmol) was added to KC_8 (0.020 g, 0.15 mmol) and stirred overnight. An immediate color change from red to yellow was observed. The reaction solution was filtered, and the filtrate was evaporated to dryness under reduced pressure. The resulting crude was dissolved in toluene, filtered, and then stored at –35 ºC. The resulting yellow precipitate was collected and dried under reduced pressure (0.080 g, 90%). Single crystals suitable for X-ray diffraction analysis were obtained from a concentrated CD_3CN solution. UV (THF) λ_{max}, nm (ε, L mol^{-1} cm^{-1}): 263 (37,000), 298 (16,000), 314 sh (12,000), 324 (11,000), 346 sh (5,200), 375 (4,500). ^{1}H NMR (300 MHz, d_8-THF): δ 13.98, 9.03, 8.62, 7.97, 3.14. Anal. Calcd. for $C_{36}H_{42}ClOP_2Ni$: C, 66.85; H, 6.54; N, 0. Found: C, 67.00; H, 6.48; N, 0.0.

Synthesis of [(^{iPr}DPDBFphos)Fe(CO)$_3$] (5). Iron pentacarbonyl (50 μL, 0.37 mmol) was added to a 10 mL THF solution of ^{iPr}DPDBFphos (0.205 g, 0.37 mmol) in bomb flask. The flask was evacuated and photolyzed for 6 hours using a mercury vapor lamp. The THF solution was filtered and then evaporated to dryness under reduced pressure to

give a yellow powder (0.235 g, 92 %). Single crystals suitable for X-ray diffraction analysis were grown from a vapor diffusion of pentane into a concentrate CH_2Cl_2 solution of **5**. IR $^{o}\upsilon_{max}/cm^{-1}$: 1959 ($A_1'$ CO), 1869 (E´ CO) ($CDCl_3$: CH_2Cl_2). ^{1}H NMR (500 MHz, $CDCl_3$): δ 8.94 (2H, d, J = 11.1 Hz, CH), 8.00 (2H, dd, J = 1.8 & 7.5 Hz, CH), 7.75 – 7.43 (10H, m, CH), 2.79 (4H, m, PCH(CH_3)$_2$), 1.38 (12H, dd, J_{HH} = 6.9 Hz, J_{HP} = 15.0 Hz, PCH(CH_3)(C′H$_3$)), 1.62 (12H, dd, J_{HH} = 6.6 Hz, J_{HP} = 14.1 Hz, PCH(CH_3)(C′H_3)). ^{31}P NMR (121 MHz, $CDCl_3$): δ 90.4.

Crystallography. A colorless plate of **1**, a blue block of **2**, a red plate of **3**, a yellow plate of **4**, and a yellow plate of **5** were placed onto the tip of a 0.1 mm diameter glass capillary and mounted on a Bruker or a Siemens SMART Platform CCD diffractometer for data collection at 123(2) K for complexes **1 – 3** or 173(2) K for complexes **4** and **5**. The data collection was carried out using Mo Kα radiation (graphite monochromator). The data intensity was corrected for absorption and decay (SADABS). Final cell constants were obtained from least squares fits of all measured reflections. The structure was solved using SHELXS-97 and refined using SHELXL-97. For complexes **1 - 4**, a direct-methods solution was calculated which provided most non-hydrogen atoms from the E-map while complex **5** was solved using a Patterson map. Full-matrix least squares / difference Fourier cycles were performed to locate the remaining non-hydrogen atoms. All non-hydrogen atoms were refined with anisotropic displacement parameters. Hydrogen atoms were placed in ideal positions and refined as riding atoms with relative isotropic displacement parameters. Crystallographic data are summarized in Table 1.

Physical Measurements. ^{1}H and ^{31}P NMR spectra were acquired on Varian Inova 300 and 500 MHz spectrometers at ambient temperature unless otherwise stated. Chemical shifts were referenced to residual solvent in ^{1}H NMR spectra, while ^{31}P NMR spectra were referenced to an external reference of 85% H_3PO_4 set to 0 ppm. Solution magnetic susceptibilities were determined by the Evans method[43-44] and were corrected for underlying diamagnetism using tabulated Pascal's constants.[45] Electronic spectra of complexes were recorded on a Cary 300 Bio UV-Visible spectrophotometer. Infrared (IR) spectra were collected with a Bruker TENSOR 37 spectrometer. Perpendicular-mode X-band EPR spectra were recorded on a Bruker EPP 300 spectrometer equipped with an Oxford ESR 910 liquid helium cryostat and an Oxford temperature controller. X-band EPR spectra were simulated using EPR program (version W95) written by Professor Frank Neese (University of Bonn, Germany). Cyclic voltammetry experiments were performed inside a glovebox with a CHInstruments Model 600D potentiostat/galvanostat. A single-chamber cell was set up with a glassy carbon working electrode (3 mm diameter), a Pt wire as the auxiliary electrode, and a reference electrode consisting of a silver wire in 10 mM $AgNO_3$ solution (0.1 M $[^{n}Bu_4N]PF_6$ in CH_3CN). All measurements were calibrated to an internal ferrocene standard. Mass spectrometry (MS) data were acquired on a Bruker BioTOF ESI-MS under positive mode.

Theoretical Calculations. DFT calculations (BP86,[46-47] M-06L[48-49]) were performed with the Gaussian09 program.[50] The all-electron Gaussian basis sets used were those reported by the Ahlrichs group.[51] For nickel, chloride, and phosphorus atoms, the triple-ξ-quality basis sets with one set of polarization functions was used (def2-TZVP). The

carbon, oxygen, and hydrogen atoms were described by smaller polarized split-valence def2-SV(P) basis sets.

-Chapter Six-

Reactivity Studies of the Monovalent Three-coordinate Nickel Complex ^{iPr}DPDBFphosNiCl

In part from:

Marlier, E. E.; Tereniak, S. J.; Ding, K.; Mulliken, J. E.; Lu, C. C. *Inorg. Chem.* **2011**, *50*, 9290-9299.

6.1 Overview

Following the isolation and characterization of a three-coordinate planar Ni(I) complex (^{iPr}DPDBFphos)NiCl (**1**), its reactivity towards nucleophiles, small molecules and organic halides was investigated. Through a metathesis reaction of **1** with lithium 2,6-di-*iso*-propylphenylamide (LiNH(2,6-$(CHMe_2)_2C_6H_3$), the paramagnetic aryl amido complex [(^{iPr}DPDBFphos)Ni{NH(2,6-$(CHMe_2)_2C_6H_3$)}] (**2**) was synthesized and oxidized with tropylium hexafluorophosphate to give the diamagnetic Ni(II) amido salt, [(^{iPr}DPDBFphos)Ni{NH(2,6-$(CHMe_2)_2C_6H_3$)}][PF_6] (**3**). A brief survey of small molecules found that (^{iPr}DPDBFphos)NiCl reacts with H_2(g) to yield a Ni(II) hydride [(^{iPr}DPDBFphos)Ni(H)Cl] (**4**). Lastly, (^{iPr}DPDBFphos)NiCl reacts with substrates containing C−X bonds, and in the case of vinyl chloride, a Ni(II) vinyl species (^{iPr}DPDBFphos)Ni(CH=CH_2)Cl (**5**) is generated along with the Ni(II) dichloride complex (^{iPr}DPDBFphos)$NiCl_2$ (**6**). Complex **1** is an active catalyst in the Kumada cross-coupling reaction of vinyl chloride and phenyl Grignard reagent.

6.2 Introduction

Three-coordinate nickel complexes constitute a rich area in coordination chemistry. Supported by the bulky monophosphine PCy_3, zero-valent nickel forms adducts with small molecules, as observed in the end-on dinitrogen dinickel compound $\{(PCy_3)_2Ni\}_2(\mu\text{-}N_2)$[1] and the first structurally characterized carbon dioxide complex, $(PCy_3)_2Ni(\eta^2\text{-}CO_2)$.[2] Hillhouse has pioneered the area of divalent Ni=E complexes featuring multiply-bonded ligands (E = NR, PR, CR_2) using the bulky diphosphine, 1,2-bis(di-*tert*-butylphosphino)ethane (dtbpe).[3-5] Other notable three-coordinate nickel complexes have been supported by non-traditional phosphine ligands, including the Fryzuk-type tridentate bis(phosphine)amides,[6] diketiminates,[7-9] *N*-heterocyclic carbenes,[10-11] and the unusual *N*-heterocyclic silenes.[12] Typically, the oxidation state of the nickel center is mono-valent for the anionic ligands, and zero-valent for the neutral carbenes/silenes. The rare Ni(III) oxidation state has also been proposed in three-coordinate Ni(III) imides, which can be remarkably reactive and decompose via radical pathways.[13,14] A recent report from Hillhouse highlighted the synthesis and characterization of a Ni(III)-imide complex synthesized from the oxidation of an arylimido nickel(II) complex.[15]

Herein, we explore the reactivity of the three-coordinate planar Ni(I) complex (^{iPr}DPDBFphos)NiCl (**1**) through metathesis reactions, small-molecule binding and C-X bond activation. Considering the reactivity of **1** towards vinyl halides, the cross-coupling reaction between vinyl chloride and phenyl Grignard reagent was investigated with **1** as a catalyst. These preliminary results join recent studies in demonstrating the relevance of monovalent nickel species in cross-coupling catalysis.[16, 17]

6.3 Results and discussion

Metathesis with (^{iPr}DPDBFphos)Ni^{I}Cl

Inspired by Hillhouse's work, the synthesis of an arylimido nickel(II) complex was targeted. Following the procedure established by Mindiola and Hillhouse, complex **1** was reacted with lithium 2,6-di-*iso*-propylphenylamide (LiNH(2,6-$(CHMe_2)_2C_6H_3$) (Scheme 6.1).[4]

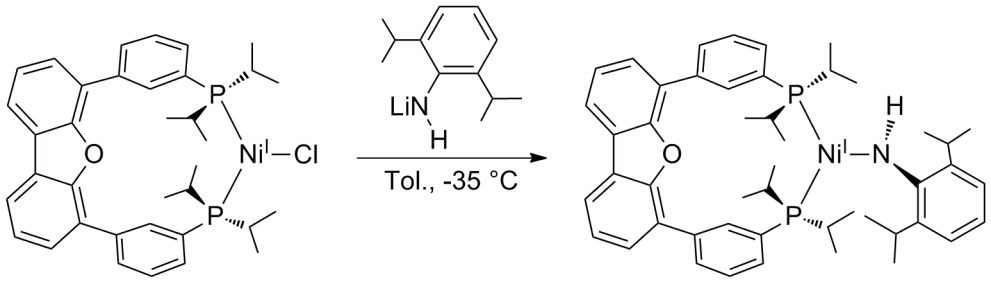

1 **2**

Scheme 6.1. Synthetic route for [(^{iPr}DPDBFphos)Ni{NH(2,6-$(CHMe_2)_2C_6H_3$)}] **2**.

Upon addition of LiNH(2,6-$(CHMe_2)_2C_6H_3$), an immediate color change from yellow to beet purple was observed. X-ray quality crystals revealed this species to be the three coordinate aryl amido complex [(^{iPr}DPDBFphos)Ni{NH(2,6-$(CHMe_2)_2C_6H_3$)}] **2**, which was also characterized by ^{1}H NMR spectroscopy (Table 6.1 and Figure 6.1).

Table 6.1. Crystallographic data for **2** and **5**.

Compounds	$C_{48}H_{60}NNiOP_2$	$C_{38}H_{45}ClNiOP_2$
Compounds Abbreviation	**2**	**5**
Morphology	Block	Block
Color	Purple red	Yellow
Lattice Type	Monoclinic	Triclinic
Space Group	P2(1)/c	P-1
a, Å	12.280(3)	11.952(3)
b, Å	15.743(4)	15.245(3)
c, Å	28.565(6)	20.695(5)
α, deg	90	88.084(3)
β, deg	99.601(5)	73.958(2)
γ, deg	90	89.567(3)
V, Å	5445(2)	3622(1)
Z	4	4
formula wt, g mol^{-1}	787.62	673.84
Dc,g cm^{-3}	0.961	1.236
μ, mm^{-1}	0.443	0.725
F(000)	1684	1424
θ range, deg	1.45 to 26.47	1.71 to 26.51
reflns collected	11216	26923
unique reflns	8908	14614
data/restraint/parameters	8908 / 0 / 490	14614 / 0 / 775
R1, wR2 [I>2σ(I)]	0.0493, 0.1149	0.0563, 0.1406
R1, wR2 [all data]	0.0910, 0.1255	0.0645, 0.1437
GOOF	0.761	1.128
largest diff peak, hole, e $Å^{-3}$	0.313, -0.337	1.056, -0.068

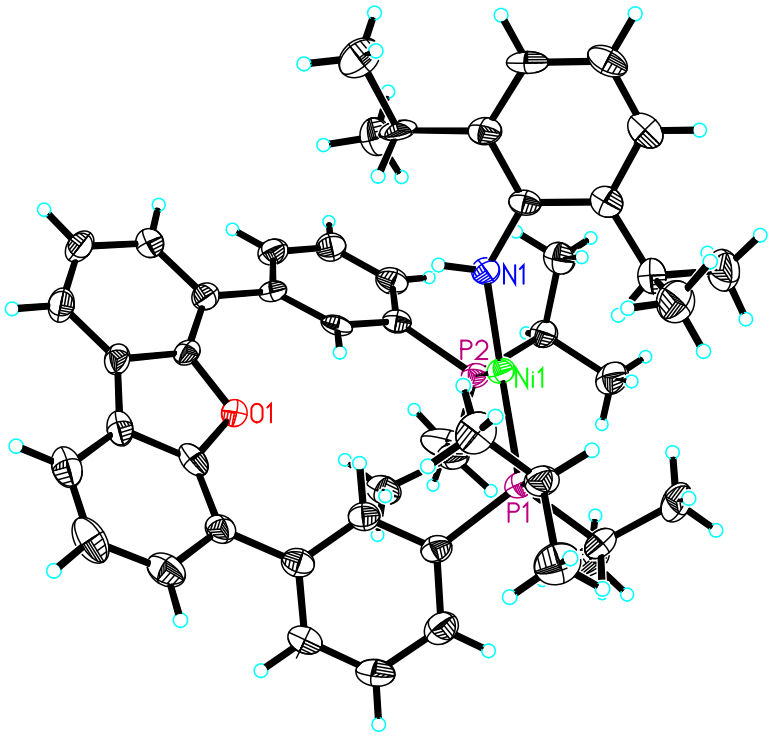

Figure 6.1. Solid-state structure of [(^{iPr}DPDBFphos)Ni{NH(2,6-$(CHMe_2)_2C_6H_3$)}] **2** at 50% probability level.

The diphosphine bite angle in **2** (113.98(5)°) is slightly smaller than the bite angle observed for the two independent molecules of **1** (115.53° and 119.49°). When comparing **2** to Hillhouse's amido Ni(I) [(dtbpe)Ni{NH(2,6-$(CHMe_2)_2C_6H_3$)}] where dtbpe is 1,2-bis(di-*tert*-butylphosphino)ethane, the two structures are very similar with bond lengths matching within 0.02 Å and angles showing similar trends given the vastly different bite angles for the diphosphines (Table 6.2).[4]

Table 6.2. Comparison of selected bond lengths (Å) and angles (°) for **2** and (dtbpe)NiNHAr, where Ar = 2,6-$(CHMe_2)_2C_6H_3$.

	2	**(dtbpe)NiNHAr***
Bond Distances (Å)		
$Ni\text{-}P_1$	2.211(1)	2.2012(7)
$Ni\text{-}P_2$	2.227(1)	2.2094(8)
$Ni\text{-}N_1$	1.878(3)	1.881(2)
$N_1\text{-}C$	1.380(5)	1.373(3)
Bond Angles (deg)		
$P_1\text{-}Ni\text{-}P_2$	113.98(5)	91.91(3)
$P_1\text{-}M\text{-}N_1$	135.6(1)	140.41(7)
$P_2\text{-}M\text{-}N_1$	109.4(1)	123.18(7)
$Ni\text{-}N_1\text{-}C$	140.7(3)	134.6(2)

*Values were obtained from reference 4.

For the following step, the paramagnetic arylamido nickel(I) complex **2** was oxidized with tropylium hexafluorophosphate to the diamagnetic arylamido nickel(II) complex **3** (Scheme 6.2).

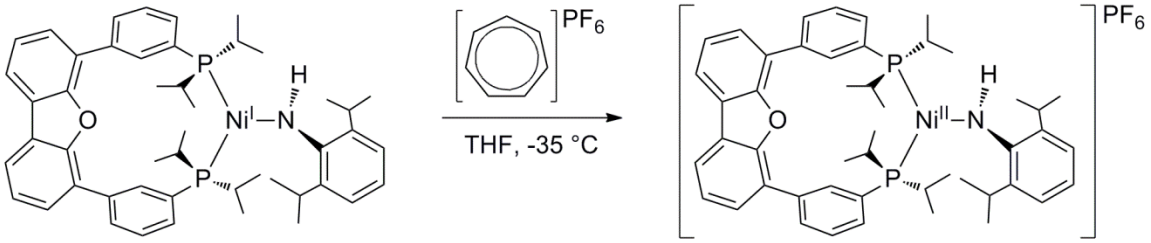

2 **3**

Scheme 6.2. Synthetic route for [(^{iPr}DPDBFphos)Ni{NH(2,6-$(CHMe_2)_2C_6H_3$)}][PF_6] **3**.

Though an immediate color change to blue was observed, the complex appeared sensitive to temperature and stirring time. Based on ^{31}P NMR spectroscopy, the oxidation also did not proceed cleanly with the observation of four different shifts located at 37.8, 32.3, 12.8 and -141.5 ppm. The resonance at 12.8 ppm is identified as free ligand while the peaks at 32.3 and -141.5 ppm belong to complex **3** for the phosphines on the ligand and the anion

PF_6 respectively. The last peak at 37.8 ppm is hypothesized to be a hydride species considering a triplet at -23.0 ppm was observed in the crude ^1H spectrum. In an attempt to optimize this reaction, other oxidants such as ferrocenium hexafluorophosphate were tested, but resulted in a larger amount of free ligand and hydride. Thus, the oxidation was carried out with tropylium hexafluorophosphate and a toluene wash was found to separate complex **3** from both the ligand and hydride species.

The last step in the synthesis of an imido nickel(II) complex following Hillhouse's route is the deprotonation of the nitrogen bound to the nickel center. For the deprotonation, Mindiola and Hillhouse report the use of sodium bis(trimethylsilyl)amide at -35 °C. This step was attempted several times on our system and produced free ligand each time. The reaction was modified by varying the temperature from -35 °C to -196 °C, changing the solvent from THF to toluene, surveying a range of bases (e.g. potassium bis(trimethylsilyl)amide, Hünig's base ($^iPr_2EtN$) and potassium *tert*-butoxide), and changing the number of equivalents of base added. Since these modifications led to either no reaction or free ligand, the synthesis of the nickel(II) imide was abandoned.

Reactivity of (^{iPr}DPDBFphos)Ni^{I}Cl with small molecules

The reactivity of **1** towards small molecules was surveyed with CO_2(g), NO(g) and H_2(g). While **1** did not react with CO_2(g), the reaction of **1** with excess NO(g), and also with excess H_2(g) led to the observation of new shifts in the ^{31}P NMR spectrum. In the case of NO(g), the reaction became blue upon addition, and two new shifts at 49.04 and 45.93 ppm were detected by ^{31}P NMR spectroscopy. A similar color change was observed by Mindiola and Hillhouse upon treatment of their Ni(I) dimer with 2.1

equivalents of NO(g).[18] They identified this species to be (dtbpe)Ni(NO)Cl where the nickel center is formally a nickel(0) nitrosyl complex.[18] It is likely a similar product was formed in our system, however this reaction was not investigated further due to a lack of access to NO(g).

The reaction of **1** with H_2(g) was slow and required heating, but it produced one major peak at 38.0 ppm by ^{31}P NMR spectroscopy (Figure 6.2). This appeared as a multiplet in the ^{31}P NMR spectrum due to an inaccuracy in the hydrogen decoupling frequency. The ^{1}H NMR spectrum had a triplet at -23.2 ppm, a shift characteristic of a hydride.

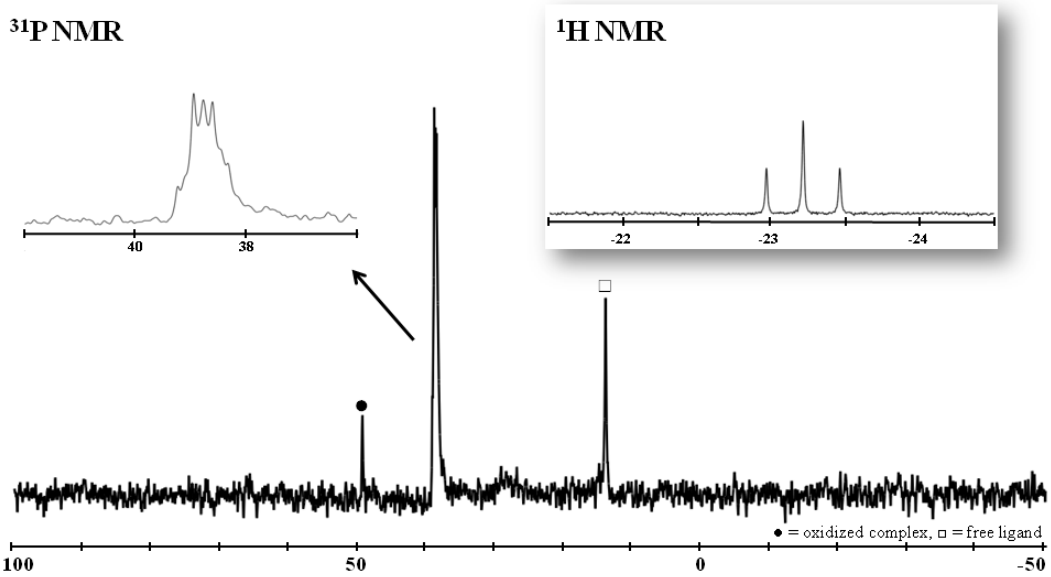

Figure 6.2. ^{31}P NMR spectrum of [(^{iPr}DPDBFphos)Ni(H)Cl] (**4**) from a crude reaction of **1** with H_2(g). Inset shows a zoom-in of the triplet at -23.2 ppm in ^{1}H NMR spectrum.

To check for the presence of a hydride, a phosphorus decoupling ^{1}H NMR experiment was performed. During this experiment, the triplet at -23.2 ppm collapsed to a singlet, showing the disappearance of phosphorus coupling. This phosphorous hydride coupling was determined to be 75.0 Hz. The product of this reaction is the Ni(II) hydride,

[(^{iPr}DPDBFphos)Ni(H)Cl] (**4**). This was verified against the bromo hydrido Ni(II) complex, [(^{iPr}DPDBFphos)Ni(H)Br] which was synthesized independently by reacting a Ni(0) benzophenone adduct complex with 2-bromomesitylene. The [(^{iPr}DPDBFphos)Ni(H)Cl] is currently being synthesized through β-hydride elimination in the reaction of *tert*-butyl chloride and the same Ni(0) precursor.

Although dihydrogen cleavage is common among early transition metals and 2nd and 3rd row transition metals, there are only a few examples with nickel complexes.[19-20] He and Caulton have reported the heterolysis of H_2 using a Ni(II) pincer complex.[21] In this system, the Brønsted basic character of the pincer nitrogen participates in the heterolysis via protonation while a hydride is added to nickel. A similar approach has been taken by Wilson and DuBois through the use of two PNP ligands (bis(diethylphosphinomethyl)methylamine) on a nickel(II) center.[22-23] While nickel(II) hydrides are fairly common, their synthesis usually entails the treatment of a nickel(0) source with HX or the use of a hydride source such as $NaBH_4$ on a nickel(II) complex.[24-26] One study by Chow does report the formation of a nickel hydride from the reaction of H_2(g) and an (acetylacetonato)nickel (I) complex. The Ni(I) complex is generated *in situ* from a xanthone-sensitized photoreduction of bis(acetylacetonato)nickel(II) in the presence of hydrogen gas which acts as hydrogen atom donor to give acetylacetone as a side product.[27] The photo-generated Ni(I) complex reacts with H_2(g) to form the nickel hydride in the dark. While used *in situ*, the nickel hydride catalyzed the isomerization and hydrogenation *of cis,cis*-1,5-cyclooctadiene (1,5-cod) and the hydrogenation of simple olefins.[27-28]

Interestingly, Nocera and co-workers recently used a photochemical approach to generate hydrogen gas from chloro and bromo hydrido nickel(II) complexes bearing N-heterocyclic carbene ligands.[29] In light of this, a study investigating the photolysis of complex **4** is currently ongoing.

Reactivity of (^{iPr}DPDBFphos)Ni^{I}Cl with C-X bonds

Preliminary reactivity studies reveal that the Ni(I) complex **1** can cleave C–X bonds. Benzyl bromide and **1** react instantly at room temperature to yield bibenzyl determined by ^{1}H NMR spectroscopy. The product mixture is characterized by a singularly broad signal in the ^{31}P NMR spectrum, which upon cooling to 0 °C resolves into three distinct peaks at 26.5, 29.0, and 31.2 ppm. The former corresponds to [*trans*-(^{iPr}DPDBFphos)NiCl$_2$] **6**. The latter two are assigned as the mixed halide [(^{iPr}DPDBFphos)NiClBr] and dibromide [(^{iPr}DPDBFphos)NiBr$_2$] compounds based on the following evidence. Metalation of (^{iPr}DPDBFphos) with NiBr$_2$ proceeds cleanly, giving rise to a single peak at 31.2 ppm in the ^{31}P NMR spectrum, corresponding to [(^{iPr}DPDBFphos)NiBr$_2$]. This shift matches well with the one observed in the benzyl bromide reaction mixture. The third peak in the ^{31}P NMR spectrum at 29.0 ppm is presumably the mixed halide species [(^{iPr}DPDBFphos)NiClBr] because its chemical shift is exactly half-way between that of the nickel dichloride **6** and of the nickel dibromide complexes.

Compound **1** reacts with excess vinyl chloride to cleanly produce [(^{iPr}DPDBFphos)NiCl$_2$] **6** and the vinyl complex, [(^{iPr}DPDBFphos)Ni(CH=CH$_2$)Cl] **5**. The nickel vinyl complex **5** was identified by combustion analysis, ^{1}H NMR

spectroscopy, UV-vis spectroscopy and a single-crystal X-ray diffraction experiment (Figure 6.3, Figure 6.4 and Table 6.1).

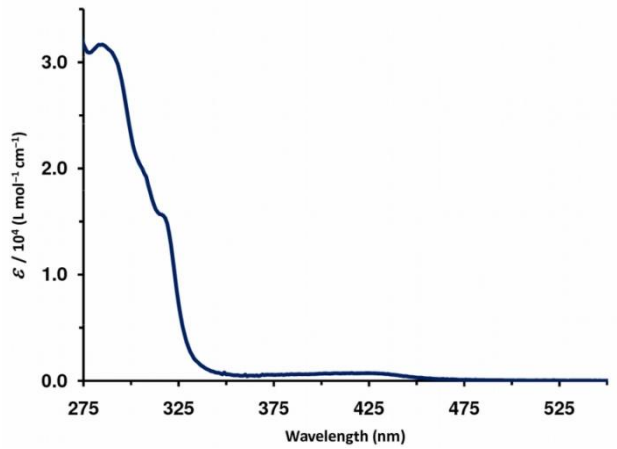

Figure 6.3. UV-vis spectrum of [(^{iPr}DPDBFphos)Ni(CH=CH$_2$)Cl] **5** at rt in THF.

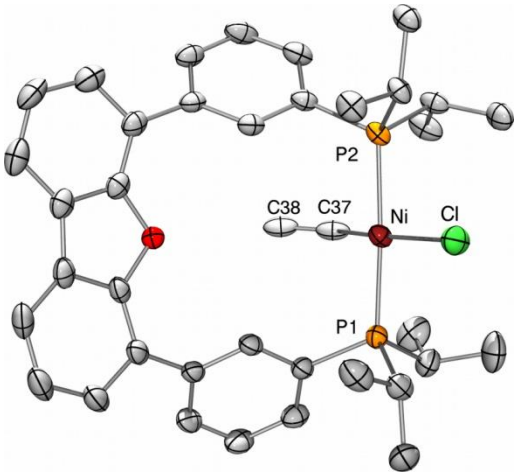

Figure 6.4. Solid-state structure of [(^{iPr}DPDBFphos)Ni(CH=CH$_2$)Cl] **5** at 50% probability level. Only one of the two independent molecules in the unit cell is shown. Hydrogen atoms were omitted for clarity. Selected bond lengths (Å) and angles (°): Ni−P1 = 2.204(1), Ni−P2 = 2.210(1), Ni−Cl = 2.241(1), Ni−C37 = 1.919(4), C37−C38 = 1.220(6), P1−Ni−P2 = 174.39(4), P1−Ni−Cl = 93.35(4), P2−Ni−Cl = 92.19(4), P1−Ni−C37 = 87.6(1), P2−Ni−C37 = 86.8(1), Ni−C37−C38 = 136.9(3).

The product ratio of **5**:**6** is 1:1 based on their relative integration in the ^{1}H NMR spectrum (Figure 6.5).

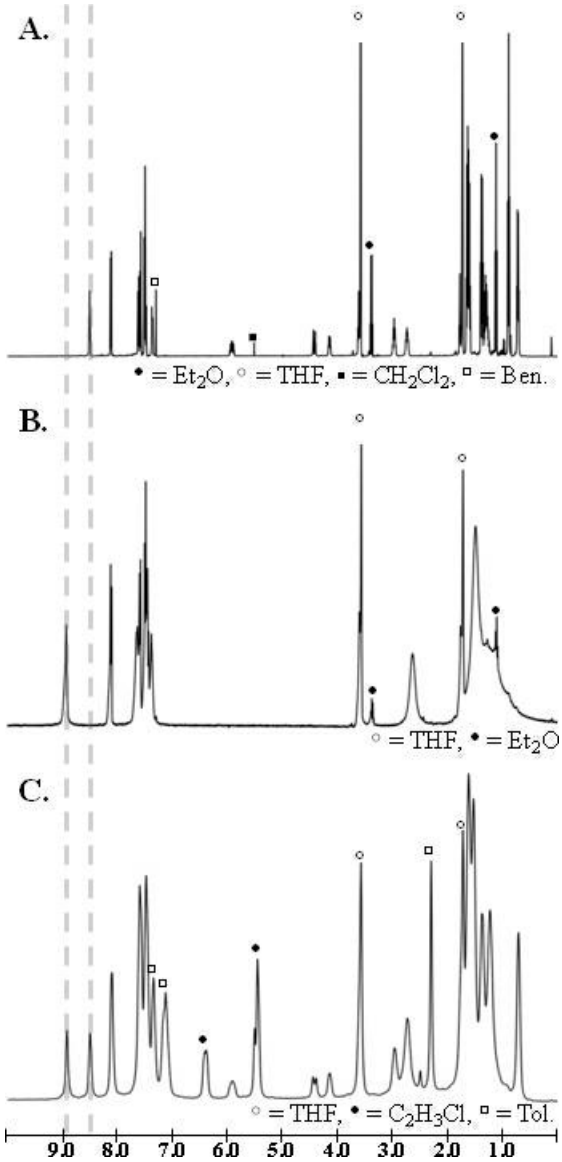

Figure 6.5. Stacked ^{1}H NMR spectra (300 MHz,d_8-THF) of (**A**) [(^{iPr}DPDBFphos)Ni(CH=CH$_2$)Cl], **5** at rt; (**B**) [(^{iPr}DPDBFphos)NiCl$_2$], **3** at 0° C; and, (**C**) the two-product mixture in the reaction of vinyl chloride and [(^{iPr}DPDBFphos)NiCl] at rt. The product distribution of the reaction (**C**) was determined by the relative integrations of the two most downfield peaks.

This ratio is consistent with two nickel(I) molecules reacting with one molecule of vinyl chloride to yield a mixture of **5** and **6** (Scheme 6.3).

Scheme 6.3. Reaction of [(^{iPr}DPDBFphos)NiCl] **1** and vinyl chloride.

Additionally, **1** also reacts with one equivalent of vinyl bromide to generate a mixture that contains the Ni(II) dihalide complexes, **5**, and a new species that is assigned as the bromide analogue of **5** because of their similar spectroscopic data. Collectively, these results demonstrate that Ni(I) **1** cleaves vinyl–X bonds to ultimately produce stable Ni(II) products.

Two limiting mechanisms are proposed for the cleavage of vinyl halide: (1) a radical chain process is initiated by an inner-sphere electron transfer to form a Ni(II)-alkene adduct, $Ni^{II}X–(\eta^2\text{-}CH_2CHX)^{\bullet-}$, which subsequently eliminates $X^{\bullet}$ and/or $CH_2CH^{\bullet}$, or (2) vinyl halide oxidatively adds to Ni(I)X to produce a Ni(III) intermediate, $Ni^{III}X_2(CHCH_2)$, which then undergoes comproportionation reactions with Ni(I). Though the assorted outcome in the reaction of **1** and vinyl bromide hints at radical processes, we cannot exclude the intermediacy of Ni(III) species.

Catalysis with (^{iPr}DPDBFphos)Ni^{I}Cl

Encouraged by the clean reactivity between **1** and vinyl chloride, we decided to investigate the catalytic potential of Ni(I) **1** in the original Kumada coupling reaction of vinyl chloride and phenyl Grignard reagent.[30] Using a loading of 5 mol% catalyst with excess vinyl chloride, both Ni(I) **1** and Ni(II) **6** generated styrene as the product in good

yields (~65 to 85%, Table 6.3, entries 1 and 2), with **1** slightly outperforming **6**. The control reaction (Table 6.3, entry 3) showed that no significant amount of styrene is formed under the same conditions in the absence of a catalyst.

Table 6.3. Kumada cross-coupling reactions of vinyl chloride and PhMgBr.[a]

Entry	**Ni Source** (5 mol %)	**Avg. Yield** (%)[b]	**# of runs**
1	[(^{iPr}DPDBFphos)Ni^{I}Cl] **1**	85.9 ± 7.8	4
2	[(^{iPr}DPDBFphos)Ni^{II}Cl$_2$] **6**	66.4 ± 9.8	5
3	no nickel, no ligand	8.7 ± 7.7	4

[a] See Experimental Procedure Section for reaction conditions.

[b] The yield of styrene is determined by GC-MS analysis.

Monovalent nickel species had long been proposed by Tsou and Kochi as intermediates in the nickel-catalyzed biaryl synthesis from aryl halides.[31] Indeed, mechanistic proposals for Ni-catalyzed cross-couplings commonly feature Ni(0), Ni(I), Ni(II), and Ni(III) species, which undergo one- and/or two-electron redox steps in the catalytic cycle.[32-34] Isolated monovalent nickel compounds have been found to be catalytically competent in various cross-coupling schemes.[16-17, 35-36] In one case, the "nickel(I)-terpyridine" catalyst was reformulated as a nickel(II) center bound to a reduced ligand radical based on EPR and DFT studies.[37] The other Ni(I) cross-coupling catalysts mostly have *N*-heterocyclic carbenes (NHC's) as ligands[16-17] and are considered to be *bona fide* Ni(I) species because metal-NHC complexes are not known to undergo ligand-based reductions (although NHC's can partake in π-backbonding).[38] To our knowledge, this report is the first comparative study between an isolated Ni(I)-phosphine complex and its Ni(II) analogue in a cross-coupling reaction.

6.4 Conclusions

Using a wide bite-angle diphosphine ligand, a nickel(I) complex participated in metathesis reactions, small molecule activation and C-X bond cleavage. The metathesis reactions did not yield the desired imido nickel(II) complex due to an inability to deprotonate the aniline nitrogen. With regards to small molecules, the nickel(I) complex was found to cleave $H_2(g)$ to form a nickel(II) hydride. A chloro vinyl nickel(II) complex was isolated from the reaction of nickel(I) with vinyl chloride. Inspired by its reactivity, the nickel(I) was used a catalyst for the formation of styrene from vinyl chloride and PhMgBr.

Given the limited evidence for Ni(I) in cross-coupling reactions, our results are intriguing in that a Ni(I) complex reacts constructively with vinyl–X bonds and is catalytically competent for the cross coupling of vinyl chloride and phenyl Grignard reagent. Definitive experimental proof for the direct involvement of monovalent nickel in cross-coupling catalysis is still lacking. The current results warrant further study of this Ni(I) system, especially to evaluate its scope in other cross-coupling schemes as well as to scrutinize the role of Ni(I) through detailed mechanistic investigations.

6.5 Experimental Procedures

Synthetic Considerations. Unless otherwise stated, all manipulations were performed under a dinitrogen atmosphere in a MBraun glovebox or using standard Schlenk techniques. Standard solvents were deoxygenated by sparging with dinitrogen and dried by passing through activated alumina columns of a SG Water solvent purification system. Deuterated solvents were purchased from Cambridge Isotope Laboratories, Inc., dried over CaH_2, distilled, and stored over activated 4 Å molecular sieves. Elemental analyses were performed by Atlantic Microlab. The synthesis of complexes **1** and **6** was reported in the chapter 6. Other reagents were purchased commercially and used without further purification.

Synthesis of [(^{iPr}DPDBFphos)Ni{NH(2,6-(CHMe$_2$)$_2$C$_6$H$_3$)}] (**2**). Lithium 2,6-di-*iso*-propylphenylamide (0.042 g, 0.23 mmol) was dissolved in 5 mL of Et_2O and cooled to -35°C. Once cold, it was added dropwise to a cold toluene solution of (^{iPr}DPDBFphos)NiCl (0.139 g, 0.21 mmol). An immediate color change from yellow to beet red was observed. Solution was stirred at RT for three hours. The reaction solution was filtered, and the filtrate was evaporated to dryness under reduced pressure. The resulting crude was dissolved in toluene, filtered, and the filtrate was evaporated to dryness under reduced pressure, to give a purple red solid (0.162 g, 96%). X-ray quality crystals were grown from layering a concentrated toluene solution of **2** with Et_2O at -35°C. ^{1}H NMR (300 MHz, C_6D_6): δ 13.40, 8.27, 8.13, 7.48, 7.42, 7.07, 7.05, 7.00, 6.90, 4.06, 3.19, 1.37, 1.06, 0.92, 0.30.

Synthesis of [(^{iPr}DPDBFphos)Ni{NH(2,6-$(CHMe_2)_2C_6H_3$)}][PF_6] (**3**). A suspension of tropylium hexafluorophosphate (0.012 g, 0.05 mmol) in 3 mL of THF was cooled to -35°C. The cold suspension was added dropwise to a cold THF solution of **2** (0.037 g, 0.05 mmol). An immediate color change from purple red to purple blue was observed. After stirring for an hour at RT, the solution was filtered and the filtrate was evaporated to dryness under reduced pressure. The residual solids were washed with cold toluene and Et_2O. ^{31}P NMR (121 MHz, d_8-THF): δ 32.3, -141.8.

Synthesis of [(^{iPr}DPDBFphos)Ni(H)Cl] (**4**). A d_8-THF solution of **1** (0.013 g, 0.02 mmol) was added to a sealable NMR tube. The tube was frozen, evacuated and refilled with excess hydrogen gas. The NMR tube was placed in an oil bath at 60°C for three weeks. Integration of a Ni(I) resonance against the hydride peak gives an approximate 69% conversion. ^{1}H NMR (300 MHz, d_8-THF): δ 8.92, 8.10, 7.69, 7.58. 7.52, 7.30, 2.78, 1.32, 1.08, -23.21 (1H, t, J_{HP} = 75.0 Hz, Ni-H). ^{31}P NMR (121 MHz, d_8-THF): δ 38.0.

Synthesis of [(^{iPr}DPDBFphos)Ni($CH=CH_2$)Cl] (5). A d_8-THF solution of **1** (0.017 g, 0.03 mmol) was added to a sealable NMR tube. The tube was frozen, evacuated and refilled with excess vinyl chloride. An immediate color change was observed from yellow to orange red upon warming to room temperature. After 4 days at room temperature, the NMR spectra showed no starting material and two different products; complexes **5** and **6**, present in a 1:1 ratio. Complex **5** was synthesized independently through the reaction of vinyl chloride and a nickel(0) complex. Single crystals suitable for X-ray diffraction analysis were grown from a THF/Pentane (1:2) solution. UV (THF)

λ_{max}, nm (ε, L mol^{-1} cm^{-1}): 285 (32,000), 308 sh (19,000), 318 sh (15,000), 430 (700). ^{1}H NMR (500 MHz, d_8-THF): δ 8.50 (2H, m, CH), 8.12 (2H, dd, *J* = 1.5 & 8.0 Hz, CH), 7.62 (2H, d, *J* = 8.0 Hz, CH), 7.58 (2H, dd, *J* = 1.5 & 8.0 Hz, CH), 7.50 (2H, t, *J* = 8.0 Hz, CH), 7.49 (2H, t, *J* = 8.0 Hz, CH), 7.36 (2H, m, CH), 5.91 (1H, ddt, J_{HH} = 10.2 & 17.5 Hz, J_{HP} = 5.5 Hz, NiC*H*= CHH′), 4.42 (1H, dt, J_{HH} = 17.5 Hz, J_{HP} = 3.0 Hz, *cis*-NiCH=C*H*H′), 4.14 (1H, dt, J_{HH} = 10.2 Hz, J_{HP} = 4.5 Hz, *trans*-NiCH=CH*H′*), 2.96 (2H, m, PC*H*$(CH_3)_2$), 2.73 (2H, m, PC′*H*$(CH_3)_2$), 1.64 (6H, dd, J_{HH} = 7.0 Hz, J_{HP} = 14.0 Hz, PC′H(C*H*$_3$)(C′H$_3$)), 1.62 (6H, dd, J_{HH} = 7.5 Hz, J_{HP} = 15.0 Hz, PC′H(CH$_3$)(C′*H*$_3$)), 1.36 (6H, dd, J_{HH} = 7.5 Hz, J_{HP} = 15.5 Hz, PCH(C*H*$_3$)(C′H$_3$)), 0.71 (6H, dd, J_{HH} = 6.0 Hz, J_{HP} = 12.0 Hz, PCH(CH$_3$)(C′*H*$_3$)). ^{31}P NMR (121 MHz, d_8-THF): δ 29.1. Anal. Calcd. for $C_{38}H_{45}ClOP_2Ni$: C, 67.73; H, 6.73; N, 0. Found: C, 67.97; H, 6.89; N, 0.0.

General Procedure for Kumada Coupling Reactions. A THF solution of the Ni catalyst (0.003 mmol, 2.14 mL) was added to a sealable reaction flask equipped with a magnetic stir bar, and the solution was frozen with a glovebox LN_2 coldwell bath. Once frozen, a solution of phenylmagnesium bromide (0.06 mmol, 0.02 mL, 3.0 M in Et_2O) diluted with Et_2O (0.84 mL) was added on top and frozen as a separate layer. The reaction flask was then evacuated and charged with excess vinyl chloride. Reactions were allowed to thaw and stir for 22 hours at room temperature. The reaction was quenched by adding 2 mL of Et_2O and 4 mL of 1.0 M HCl to the solution. The organic layer was extracted, dried over $MgSO_4$ and filtered. The filtrate was analyzed on the GC-MS. Yields were calculated using GC-MS peak integrations and a styrene-standard calibration curve.

X-Ray Crystallographic Data Collection and Refinement of the Structures.

A purple block of **2** and a yellow block of **5** were placed onto the tip of a 0.1 mm diameter glass capillary and mounted on a Bruker SMART Platform CCD diffractometer for data collection at 123(2) K. The data collection was carried out using Mo Kα radiation (graphite monochromator). The data intensity was corrected for absorption and decay (SADABS). Final cell constants were obtained from least squares fits of all measured reflections. The structure was solved using SHELXS-97 and refined using SHELXL-97. A direct-methods solution was calculated which provided most non-hydrogen atoms from the E-map. Full-matrix least squares / difference Fourier cycles were performed to locate the remaining non-hydrogen atoms. All non-hydrogen atoms were refined with anisotropic displacement parameters. Hydrogen atoms were placed in ideal positions and refined as riding atoms with relative isotropic displacement parameters.

For **2**, two highly disordered Et_2O molecules could not be modeled accordingly and were removed using the PLATON program, SQUEEZE function.[39] A total of 453 electrons in a volume of 1708 $Å^3$ located at (0, 0, 0) and (0, 0.5, 0.5) in the unit cell were determined. For **5**, a highly disordered THF molecule could not be modeled appropriately and was removed using the PLATON program, SQUEEZE function.[39] A total of 46 electrons in a volume of 353 $Å^3$ located at (0.5, 1, 0) in the unit cell were determined. Crystallographic data for **1** and **5** are summarized in Table 1.

Physical Measurements. ^1H and ^{31}P NMR spectra were acquired on Varian Inova 300 and 500 MHz spectrometers at ambient temperature unless otherwise stated. Chemical

shifts were referenced to residual solvent in ^{1}H NMR spectra, while ^{31}P NMR spectra were referenced to an external reference of 85% H_3PO_4 set to 0 ppm. For **5**, proton assignments were based on a COSY NMR experiment. Electronic spectra of complexes were recorded on a Cary 300 Bio UV-Visible spectrophotometer. Mass spectrometry (MS) data were acquired on a Bruker BioTOF ESI-MS under positive mode.

-Bibliography-

Chapter One References

(1) Squillace, P. J.; Moran, M. J.; Lapham, W. W.; Price, C. V.; Clawges, R. M.; Zogorski, J. S. Volatile Organic Compounds in Untreated Ambient Groundwater of the United States, 1985-1995. *Environ. Sci. Technol.* **1999**, *33*, 4176-4187.

(2) Squillace, P. J.; Moran, M. J. Factors Associated with Sources, Transport, and Fate of Volatile Organic Compounds and Their Mixtures in Aquifers of the United States. *Environ. Sci. Technol.* **2007**, *41*, 2123-2130.

(3) Doherty, R. E. A History of the Production and Use of Carbon Tetrachloride, Tetrachloroethylene, Trichloroethylene and 1,1,1-Trichloroethane in the United States: Part 1 - Historical Background; Carbon Tetrachloride and Tetrachloroethylene. *Environ. Forensics* **2000**, *1*, 69-81.

(4) Doherty, R. E. A History of the Production and Use of Carbon Tetrachloride, Tetrachloroethylene, Trichloroethylene and 1,1,1-Trichloroethane in the United States: Part 2 - Trichloroethylene and 1,1,1-Trichloroethane. *Environ. Forensics* **2000**, *1*, 83-93.

(5) USDHHS, *Report on Carcinogens*; U.S. Department of Health and Human Services: Washington, DC, 2011.

(6) ATSDR, *Toxicological Profile for Tetrachloroethylene*; Agency of Toxic Substances & Disease Registry: Atlanta, GA, 1997.

(7) ATSDR, *Toxicological profile for Trichloroethylene*; Agency of Toxic Subtances & Disease Registry: Atlanta, GA, 2003.

(8) Wartenberg, D.; Reyner, D.; Scott, C. S. Trichloroethylene and Cancer: Epidemiologic Evidence. *Environ. Health Perspect.* **2000**, *108(Suppl. 2)*, 359-363.

(9) Clewell, H. J.; Gentry, P. R.; Gearhart, J. M.; Allen, B. C.; Andersen, M. E. Comparison of Cancer Risk Estimates for Vinyl Chloride using Animal and Human Data with a PBPK Model. *The Science of The Total Environment* **2001**, *274*, 37-66.

(10) Holliger, C.; Schraa, G.; Stupperich, E.; Stams, A. J.; Zehnder, A. J. Evidence for the Involvement of Corrinoids and Factor F_{430} in the Reductive Dechlorination of 1,2-Dichloroethane by Methanosarcina Barkeri. *J. Bacteriol.* **1992**, *174*, 4427-34.

(11) Krone, U. E.; Thauer, R. K.; Hogenkamp, H. P. C. Reductive Dehalogenation of Chlorinated C1-Hydrocarbons Mediated by Corrinoids. *Biochemistry* **1989**, *28*, 4908-4914.

(12) Gantzer, C. J.; Wackett, L. P. Reductive Dechlorination Catalyzed by Bacterial Transition-Metal Coenzymes. *Environ. Sci. Technol.* **1991**, *25*, 715-22.

(13) Smidt, H.; de Vos, W. M. Anaerobic Microbial Dehalogenation. *Annu. Rev. Microbiol.* **2004**, *58*, 43-73.

(14) Burris, D. R.; Delcomyn, C. A.; Deng, B.; Buck, L. E.; Hatfield, K. Kinetics of Tetrachloroethylene-Reductive Dechlorination Catalyzed by Vitamin B_{12}. *Environ. Toxicol. Chem.* **1998**, *17*, 1681-1688.

(15) Burris, D. R.; Delcomyn, C. A.; Smith, M. H.; Roberts, A. L. Reductive Dechlorination of Tetrachloroethylene and Trichloroethylene Catalyzed by Vitamin B_{12} in Homogeneous and Heterogeneous Systems. *Environ. Sci. Technol.* **1996**, *30*, 3047-3052.

(16) Glod, G.; Angst, W.; Holliger, C.; Schwarzenbach, R. P. Corrinoid-Mediated Reduction of Tetrachloroethene, Trichloroethene, and Trichlorofluoroethene in Homogeneous Aqueous Solution: Reaction Kinetics and Reaction Mechanisms. *Environ. Sci. Technol.* **1997**, *31*, 253-260.

(17) Glod, G.; Brodmann, U.; Angst, W.; Holliger, C.; Schwarzenbach, R. P. Cobalamin-Mediated Reduction of cis- and trans-Dichloroethene, 1,1-Dichloroethene, and Vinyl Chloride in Homogeneous Aqueous Solution: Reaction Kinetics and Mechanistic Considerations. *Environ. Sci. Technol.* **1997**, *31*, 3154-3160.

(18) Kliegman, S.; McNeill, K. Dechlorination of Chloroethylenes by Cob(I)alamin and Cobalamin Model Complexes. *Dalton Trans.* **2008**, 4191-4201.

(19) Lesage, S.; Brown, S.; Millar, K. A Different Mechanism for the Reductive Dechlorination of Chlorinated Ethenes: Kinetic and Spectroscopic Evidence. *Environ. Sci. Technol.* **1998**, *32*, 2264-2272.

(20) Semadeni, M.; Chiu, P.-C.; Reinhard, M. Reductive Transformation of Trichloroethene by Cobalamin: Reactivities of the Intermediates Acetylene, Chloroacetylene, and the DCE Isomers. *Environ. Sci. Technol.* **1998**, *32*, 1207-1213.

(21) Follett, A. D.; McNabb, K. A.; Peterson, A. A.; Scanlon, J. D.; Cramer, C. J.; McNeill, K. Characterization of Co-C Bonding in Dichlorovinylcobaloxime Complexes. *Inorg. Chem.* **2007**, *46*, 1645-1654.

(22) Follett, A. D.; McNeill, K. Reduction of Trichloroethylene by Outer-Sphere Electron-Transfer Agents. *J. Am. Chem. Soc.* **2005**, *127*, 844-845.

(23) Follett, A. D.; McNeill, K. Evidence for the Formation of a cis-Dichlorovinyl Anion upon Reduction of cis-1,2-Dichlorovinyl(pyridine)cobaloxime. *Inorg. Chem.* **2006**, *45*, 2727-2732.

(24) McCauley, K. M.; Pratt, D. A.; Wilson, S. R.; Shey, J.; Burkey, T. J.; van der Donk, W. A. Properties and Reactivity of Chlorovinylcobalamin and Vinylcobalamin and Their Implications for Vitamin B_{12}-Catalyzed Reductive Dechlorination of Chlorinated Alkenes. *J. Am. Chem. Soc.* **2005**, *127*, 1126-1136.

(25) McCauley, K. M.; Wilson, S. R.; van der Donk, W. A. Dichloroacetylene Is Not the Precursor to Dichlorinated Vinylcobaloxime and Vinylcobalamin in Cobalt Catalyzed Dechlorination of Perchloro- and Trichloroethylene. *Inorg. Chem.* **2002**, *41*, 5844-5848.

(26) McCauley, K. M.; Wilson, S. R.; van der Donk, W. A. Synthesis and Characterization of Chlorinated Alkenylcobaloximes To Probe the Mechanism of Vitamin B_{12}-Catalyzed Dechlorination of Priority Pollutants. *Inorg. Chem.* **2002**, *41*, 393-404.

(27) McCauley, K. M.; Wilson, S. R.; Van Der Donk, W. A. Characterization of Chlorovinylcobalamin, A Putative Intermediate in Reductive Degradation of Chlorinated Ethylenes. *J. Am. Chem. Soc.* **2003**, *125*, 4410-4411.

(28) Nonnenberg, C.; van der Donk, W. A.; Zipse, H. Reductive Dechlorination of Trichloroethylene: A Computational Study. *J. Phys. Chem.* **2002**, *106*, 8708-8715.

(29) Pratt, D. A.; Van der Donk, W. A. Theoretical Investigations into the Intermediacy of Chlorinated Vinylcobalamins in the Reductive Dehalogenation of Chlorinated Ethylenes. *J. Am. Chem. Soc.* **2005**, *127*, 384-396.

(30) Pratt, D. A.; Van der Donk, W. A. On the Role of Alkylcobalamins in the Vitamin B_{12}-Catalyzed Reductive Dehalogenation of Perchloroethylene and Trichloroethylene. *Chem. Commun.* **2006**, 558-560.

(31) Rich, A. E.; DeGreeff, A. D.; McNeill, K. Synthesis of (Chlorovinyl)cobaloxime Complexes, Model Complexes of Proposed Intermediates in the B_{12}-Catalyzed Dehalogenation of Chlorinated Ethylenes. *Chem. Commun.* **2002**, 234-235.

(32) Shey, J.; McGinley, C. M.; McCauley, K. M.; Dearth, A. S.; Young, B. T.; van der Donk, W. A. Mechanistic Investigation of a Novel Vitamin B_{12}-Catalyzed Carbon-Carbon Bond Forming Reaction, the Reductive Dimerization of Arylalkenes. *J. Org. Chem.* **2002**, *67*, 837-846.

(33) Shey, J.; van der Donk, W. A. Mechanistic Studies on the Vitamin B_{12}-Catalyzed Dechlorination of Chlorinated Alkenes. *J. Am. Chem. Soc.* **2000**, *122*, 12403-12404.

(34) Kliegman, S.; McNeill, K. Reconciling Disparate Models of the Involvement of Vinyl Radicals in Cobalamin-Mediated Dechlorination Reactions. *Environ. Sci. Technol.* **2009**, *43*, 8961-8967.

(35) Rusling, J. F.; Connors, T. F.; Owlia, A. Electrocatalytic Reduction of Ethylene Dibromide by Vitamin B_{12} in a Surfactant-Stabilized Emulsion. *Anal. Chem.* **1987**, *59*, 2123-2127.

(36) Connelly, N. G.; Geiger, W. E. Chemical Redox Agents for Organometallic Chemistry. *Chem. Rev.* **1996**, *96*, 877-910.

(37) Lexa, D.; Saveant, J. M. The Electrochemistry of Vitamin B_{12}. *Acc. Chem. Res.* **1983**, *16*, 235-43.

(38) Schrauzer, G. N. Organocobalt Chemistry of Vitamin B_{12} Model Compounds (Cobaloximes). *Acc. Chem. Res.* **1968**, *1*, 97-103.

(39) Liptak, M. D.; Brunold, T. C. Spectroscopic and Computational Studies of Co^{1+}Cobalamin: Spectral and Electronic Properties of the "Superreduced" B_{12} Cofactor. *J. Am. Chem. Soc.* **2006**, *128*, 9144-9156.

(40) Totten, L. A.; Roberts, A. L. Calculated One- and Two-Electron Reduction Potentials and Related Molecular Descriptors for Reduction of Alkyl and Vinyl Halides in Water. *Crit. Rev. Environ. Sci. Technol.* **2001**, *31*, 175-221.

(41) Schrauzer, G. N.; Deutsch, E. Reactions of Cobalt(I) Supernucleophiles. The Alkylation of Vitamin B_{12s}, Cobaloximes(I), and Related Compounds. *J. Am. Chem. Soc.* **1969**, *91*, 3341-50.

(42) Schrauzer, G. N.; Deutsch, E.; Windgassen, R. J. The Nucleophilicity of Vitamin B_{12s}. *J. Am. Chem. Soc.* **1968**, *90*, 2441-2.

(43) Pearson, R. G.; Sobel, H. R.; Songstad, J. Nucleophilic Reactivity Constants Toward Methyl Iodide and Trans-Dichlorodi(pyridine)platinum(II). *J. Am. Chem. Soc.* **1968**, *90*, 319-26.

(44) Dror, I.; Schlautman, M. A. Role of Metalloporphyrin Core Metals in the Mediated Reductive Dechlorination of Tetrachloroethylene. *Environ. Toxicol. Chem.* **2003**, *22*, 525-533.

(45) Fritsch, J. M.; McNeill, K. Aqueous Reductive Dechlorination of Chlorinated Ethylenes with Tetrakis(4-carboxyphenyl)porphyrin Cobalt. *Inorg. Chem.* **2005**, *44*, 4852-4861.

(46) Fritsch, J. M.; Retka, N. D.; McNeill, K. Synthesis, Structure, and Unusual Reactivity of beta -Halovinyl Cobalt Porphyrin Complexes. *Inorg. Chem.* **2006**, *45*, 2288-2295.

(47) Jones, P. G.; Yang, L.; Steinborn, D. (Cis-1,2-Dichlorovinyl)bis(dimethylglyoximato-N,N')(pyridine-N)cobalt(III) Chloroform Solvate, $[Co(dmgH)_2(py)(CCl=CHCl)].CHCl_3$. *Acta Crystallogr., Sect. C: Cryst. Struct. Commun.* **1996**, *C52*, 2399-2402.

(48) Thoreson, K. A. Probing Reduced Metal Center-Mediated Dechlorination Mechanisms Throught the Use of Model Complexes and Isotope Ratio Mass Spectrometry. Ph.D. Thesis, University of Minnesota, Minneapolis, MN, June 2010.

(49) Lewis, T. A.; Morra, M. J.; Brown, P. D. Comparative Product Analysis of Carbon Tetrachloride Dehalogenation Catalyzed by Cobalt Corrins in the Presence of Thiol or Titanium(III) Reducing Agents. *Environ. Sci. Technol.* **1996**, *30*, 292-300.

(50) Dror, I.; Schlautman, M. A. Metalloporphyrin Solubility: A Trigger for Catalyzing Reductive Dechlorination of Tetrachloroethylene. *Environ. Toxicol. Chem.* **2004**, *23*, 252-257.

Chapter Two References

(1) Bourget-Merle, L.; Lappert, M. F.; Severn, J. R. The Chemistry of β -Diketiminatometal Complexes. *Chem. Rev.* **2002**, *102*, 3031-3066.

(2) Dove, A. P.; Gibson, V. C.; Marshall, E. L.; White, A. J. P.; Williams, D. J. Magnesium and Zinc Complexes of a Potentially Tridentate β-Diketiminate Ligand. *Dalton Trans.* **2004**, 570-578.

(3) Wu, J.; Yu, T.-L.; Chen, C.-T.; Lin, C.-C. Recent Developments in Main Group Metal Complexes Catalyzed/Initiated Polymerization of Lactides and Related Cyclic Esters. *Coord. Chem. Rev.* **2006**, *250*, 602-626.

(4) Xin Xu, X. X., Yaofeng Chen, and Jie Sun Dialkyllanthanide Complexes Containing New Tridentate Monoanionic Ligands with Nitrogen Donors. *Organometallics* **2008**, *27*, 758-763.

(5) Zatka, V.; Holzbecher, J.; Ryan, D. E. Heterocyclic N,N'-disubstituted 1-amino-3-iminopropenes as Analytical Reagents. *Anal. Chim. Acta* **1971**, *55*, 273-8.

(6) Neculai, D.; Roesky, H. W.; Neculai, A. M.; Magull, J.; Schmidt, H.-G.; Noltemeyer, M. Synthesis and Structure of Monomeric and Solvent-Free $LPrX_2$ Compounds Supported by a New β-Diketiminato Ligand [$L=Et_2NCH_2CH_2NC(Me)CHC(Me)NCH_2CH_2NEt_2$, X=Cl, Br, BH_4]. *J. Organomet. Chem.* **2002**, *643-644*, 47-52.

(7) Neculai, D.; Mirela Neculai, A.; Roesky, H. W.; Herbst-Irmer, R.; Walfort, B.; Stalke, D. Vanadium Complexes Incorporating the β-Diketiminato Ligand L. Syntheses and Structures of $LV(OSO_2CF_3)_2$ and $LVPPh_2$. *Dalton Trans.* **2003**, 2831-2834.

(8) Neculai, A. M.; Roesky, H. W.; Neculai, D.; Magull, J. Synthesis of New β-Diketiminato Complexes of Scandium(III): Unprecedented Formation of a Multicyclic Aggregate. *Organometallics* **2001**, *20*, 5501-5503.

(9) Neculai, D.; Roesky, H. W.; Neculai, A. M.; Magull, J.; Herbst-Irmer, R.; Walfort, B.; Stalke, D. The First β-Diketiminato Complex of Terbium Containing Two Alkyl Groups: A Model Compound for $LLnR_2$ (Ln = Lanthanide, R = Alkyl) Systems†. *Organometallics* **2003**, *22*, 2279-2283.

(10) Fritsch, J. M.; Thoreson, K. A.; McNeill, K. Synthesis and Structures of Acyclic Monoanionic Tetradentate Aza β-Diketiminate Complexes of Magnesium, Zinc, and Cadmium. *Dalton Trans.* **2006**, 4814-4820.

(11) Stang, P. J.; Huang, Y. H.; Arif, A. M. Synthesis, Characterization, and Reaction Chemistry of New Trifluoromethanesulfonato Complexes of Rhodium and Iridium: Formation of Cationic Rhodium-Platinum and Iridium-Platinum Heterobinuclear Complexes with Bridging Chloride Ligands. *Organometallics* **1992**, *11*, 231-237.

(12) Lawrance, G. A. Coordinated trifluoromethanesulfonate and fluorosulfate. *Chem. Rev.* **1986**, *86*, 17-33.

(13) Addison, A. W.; Rao, T. N.; Reedijk, J.; van Rijn, J.; Verschoor, G. C. Synthesis, Structure, and Spectroscopic Properties of Copper(II) Compounds Containing Nitrogen-sulphur Donor Ligands; the Crystal and Molecular Structure of Aqua[1,7-bis(N-methylbenzimidazol-2[prime or minute]-yl)-2,6-dithiaheptane]copper(II) Perchlorate. *J. Chem. Soc., Dalton Trans.* **1984**, 1349-1356.

(14) Arjunan, V.; Mohan, S.; Balamourougane, P. S.; Ravindran, P. Quantum Chemical and spectroscopic Investigations of 5-Aminoquinoline. *Spectrochim. Acta, Part A* **2009**, *74*, 1215-1223.

(15) Paira, M. K.; Dinda, J.; Lu, T. H.; Paital, A. R.; Sinha, C. Zn(II), Cd(II) and Hg(II) complexes of 8-aminoquinoline.: Structure, spectra and photoluminescence property. *Polyhedron* **2007**, *26*, 4131-4140.

(16) Jiang, P.; Chen, L.; Lin, J.; Liu, Q.; Ding, J.; Gao, X.; Guo, Z. Novel Zinc Fluorescent Probe Bearing Dansyl and Aminoquinoline Groups. *Chem. Commun.* **2002**, 1424-1425.

(17) Nolan, E. M.; Jaworski, J.; Okamoto, K.-I.; Hayashi, Y.; Sheng, M.; Lippard, S. J. QZ1 and QZ2: Rapid, Reversible Quinoline-Derivatized Fluoresceins for Sensing Biological Zn(II). *J. Am. Chem. Soc.* **2005**, *127*, 16812-16823.

(18) Rurack, K. Flipping the light switch 'ON' - the design of sensor molecules that show cation-induced fluorescence enhancement with heavy and transition metal ions. *Spectrochim. Acta, Part A* **2001**, *57*, 2161-2195.

(19) Vallee, B. L.; Falchuk, K. H. The Biochemical Basis of Zinc Physiology. *Physiol. Rev.* **1993**, *73*, 79(40).

(20) Williams, R. J. P.; Fraústo da Silva, J. J. R. The Distribution of Elements in Cells. *Coord. Chem. Rev.* **2000**, *200-202*, 247-348.

(21) Berg, J. M.; Shi, Y. The Galvanization of Biology: A Growing Appreciation for the Roles of Zinc. *Science* **1996**, *271*, 1081-1085.

(22) Soroka, K.; Vithanage, R. S.; Phillips, D. A.; Walker, B.; Dasgupta, P. K. Fluorescence Properties of Metal Complexes of 8-Hydroxyquinoline-5-Sulfonic Acid and Chromatographic Spplications. *Anal. Chem.* **1987**, *59*, 629-636.

(23) Jiang, P.; Guo, Z. Fluorescent Detection of zinc in Biological Systems: Recent Development on the Design of Chemosensors and Biosensors. *Coord. Chem. Rev.* **2004**, *248*, 205-229.

(24) Xu, Z.; Yoon, J.; Spring, D. R. Fluorescent Chemosensors for Zn^{2+}. *Chem. Soc. Rev.* **2010**, *39*, 1996-2006.

(25) Zhou, X.; Yu, B.; Guo, Y.; Tang, X.; Zhang, H.; Liu, W. Both Visual and Fluorescent Sensor for Zn^{2+} Based on Quinoline Platform. *Inorg. Chem.* **2010**, *49*, 4002-4007.

(26) Magde, D.; Wong, R.; Seybold, P. G. Fluorescence Quantum Yields and Their Relation to Lifetimes of Rhodamine 6G and Fluorescein in Nine Solvents: Improved Absolute Standards for Quantum Yields. *Photochem. Photobiol.* **2002**, *75*, 327-334.

(27) Shannon, R. Revised Effective Ionic Radii and Systematic Studies of Interatomic Distances in Halides and Chalcogenides. *Acta Crystallogr., Sect. A: Found. Crystallogr.* **1976**, *32*, 751-767.

(28) Cramer, C. J.; Truhlar, D. G. Density Functional Theory for Transition Metals and Transition Metal Chemistry. *Phys. Chem. Chem. Phys.* **2009**, *11*, 10757-10816.

(29) Zhao, Y.; Truhlar, D. G. A New Local Density Functional for Main-Group Thermochemistry, Transition Metal Bonding, Thermochemical Kinetics, and Noncovalent Interactions. *J. Chem. Phys.* **2006**, *125*, 194101/1-194101/18.

(30) Hadjisoteriou, M. S.; James, R. A. Water-Soluble Hexacoordinated Metal Complexes of Monoazo Dyes for Water-Thinned Jet-Printing Inks. GB 2372750, January 15, 2002.

(31) SHELXTL *SHELXTL*, V6.14; Bruker AXS: Madison, WI, 2000.

(32) Sheldrick, G. M. *CELL NOW*, 2; Bruker AXS: Madison, WI, 2008.

(33) Frisch, M. J.; Trucks, G. W.; Schlegel, H. B.; Scuseria, G. E.; Robb, M. A.; Cheeseman, J. R.; Montgomery, J. A.; Vreven, T.; Kudin, K. N.; Burant, J. C.; Millam, J. M.; Iyengar, S. S.; Tomasi, J.; Barone, V.; Mennucci, B.; Cossi, M.; Scalmani, G.; Rega, N.; Petersson, G. A.; Nakatsuji, H.; Hada, M.; Ehara, M.; Toyota, K.; Fukuda, R.; Hasegawa, J.; Ishida, M.; Nakajima, T.; Honda, Y.; Kitao, O.; Nakai, H.; Klene, M.; Li, X.; Knox, J. E.; Hratchian, H. P.; Cross, J. B.; Adamo, C.; Jaramillo, J.; Gomperts, R.; Stratmann, R. E.; Yazyev, O.; Austin, A. J.; Cammi, R.; Pomelli, C.; Ochterski, J. W.; Ayala, P. Y.; Morokuma, K.; Voth, G. A.; Salvador, P.; Dannenberg, J. J.; Zakrzewski, V. G.; Dapprich, S.; Daniels, A. D.; Strain, M. C.; Farkas, O.; Malick, D. K.; Rabuck, A. D.; Raghavachari, K.; Foresman, J. B.; Ortiz, J. V.; Cui, Q.; Baboul, A. G.; Clifford, S.; Cioslowski, J.; Stefanov, B. B.; Liu, G.; Liashenko, A.; Piskorz, P.; Komaromi, I.; Martin, R. L.; Fox, D. J.; Keith, T.; Al-Laham, M. A.; Peng, C. Y.; Nanayakkara, A.; Challacombe, M.; Gill, P. M. W.; Johnson, B.; Chen, W.; Wong, M. W.; Gonzalez, C.; Pople, J. A. *Gaussian 03*, D.01; Gaussian, Inc.: Wallingford, CT, 2004.

(34) Zhao, Y.; Truhlar, D. G. *MN-GFM* 4.1; University of Minnesota: Minneapolis, MN, 2008.

(35) Dunlap, B. I.; Connolly, J. W. D.; Sabin, J. R. On First-Row Diatomic Molecules and Local Density Models. *J. Chem. Phys.* **1979**, *71*, 4993.

(36) Vahtras, O.; Almlöf, J.; Feyereisen, M. W. Integral Approximations for LCAO-SCF Calculations. *Chem. Phys. Lett.* **1993**, *213*, 514.

(37) Sierka, M.; Hogekamp, A.; Ahlrichs, R. Fast Evaluation of the Coulomb Potential for Electron Densities using Multipole Accelerated Resolution of Identity Approximation. *J. Chem. Phys.* **2003**, *118*, 9136.

(38) Dolg, M.; Wedig, U.; Stoll, H.; Preuss, H. Energy-Adjusted Ab Initio Pseudopotentials for the First Row Transition Elements. *J. Chem. Phys.* **1987**, *86*, 866-872.

(39) Hehre, W. J.; Radom, L.; Schleyer, P. V. R.; J. A. Pople, *Ab Initio Molecular Orbital Theory*. Wiley: New York, 1986.

Chapter Three References

(1) Burris, D. R.; Delcomyn, C. A.; Deng, B.; Buck, L. E.; Hatfield, K. Kinetics of Tetrachloroethylene-Reductive Dechlorination Catalyzed by Vitamin B_{12}. *Environ. Toxicol. Chem.* **1998**, *17*, 1681-1688.

(2) Burris, D. R.; Delcomyn, C. A.; Smith, M. H.; Roberts, A. L. Reductive Dechlorination of Tetrachloroethylene and Trichloroethylene Catalyzed by Vitamin B_{12} in Homogeneous and Heterogeneous Systems. *Environ. Sci. Technol.* **1996**, *30*, 3047-3052.

(3) Gantzer, C. J.; Wackett, L. P. Reductive Dechlorination Catalyzed by Bacterial Transition-Metal Coenzymes. *Environ. Sci. Technol.* **1991**, *25*, 715-22.

(4) Kliegman, S.; McNeill, K. Dechlorination of Chloroethylenes by Cob(I)alamin and Cobalamin Model Complexes. *Dalton Trans.* **2008**, 4191-4201.

(5) Follett, A. D.; McNabb, K. A.; Peterson, A. A.; Scanlon, J. D.; Cramer, C. J.; McNeill, K. Characterization of Co-C Bonding in Dichlorovinylcobaloxime Complexes. *Inorg. Chem.* **2007**, *46*, 1645-1654.

(6) Follett, A. D.; McNeill, K. Reduction of Trichloroethylene by Outer-Sphere Electron-Transfer Agents. *J. Am. Chem. Soc.* **2005**, *127*, 844-845.

(7) Follett, A. D.; McNeill, K. Evidence for the Formation of a cis-Dichlorovinyl Anion upon Reduction of cis-1,2-Dichlorovinyl(pyridine)cobaloxime. *Inorg. Chem.* **2006**, *45*, 2727-2732.

(8) Fritsch, J. M.; McNeill, K. Aqueous Reductive Dechlorination of Chlorinated Ethylenes with Tetrakis(4-carboxyphenyl)porphyrin Cobalt. *Inorg. Chem.* **2005**, *44*, 4852-4861.

(9) Fritsch, J. M.; Retka, N. D.; McNeill, K. Synthesis, Structure, and Unusual Reactivity of beta -Halovinyl Cobalt Porphyrin Complexes. *Inorg. Chem.* **2006**, *45*, 2288-2295.

(10) McCauley, K. M.; Wilson, S. R.; van der Donk, W. A. Dichloroacetylene Is Not the Precursor to Dichlorinated Vinylcobaloxime and Vinylcobalamin in Cobalt Catalyzed Dechlorination of Perchloro- and Trichloroethylene. *Inorg. Chem.* **2002**, *41*, 5844-5848.

(11) McCauley, K. M.; Wilson, S. R.; van der Donk, W. A. Synthesis and Characterization of Chlorinated Alkenylcobaloximes To Probe the Mechanism of Vitamin B_{12}-Catalyzed Dechlorination of Priority Pollutants. *Inorg. Chem.* **2002**, *41*, 393-404.

(12) Rich, A. E.; DeGreeff, A. D.; McNeill, K. Synthesis of (Chlorovinyl)cobaloxime Complexes, Model Complexes of Proposed Intermediates in the B_{12}-Catalyzed Dehalogenation of Chlorinated Ethylenes. *Chem. Commun.* **2002**, 234-235.

(13) Dror, I.; Schlautman, M. A. Role of Metalloporphyrin Core Metals in the Mediated Reductive Dechlorination of Tetrachloroethylene. *Environ. Toxicol. Chem.* **2003**, *22*, 525-533.

(14) Ciurli, S.; Gambarotta, S.; Floriani, C.; Chiesi-Villa, A.; Guastini, C. Reduced Cobalt-meso-Tetraphenylporphyrin Complexes: Synthesis and Structure of $[Na(thf)_3]_2[Co(TPP)]$. *Angew. Chem. Int. Ed.* **1986**, *25*, 553-554.

(15) Doppelt, P.; Fischer, J.; Weiss, R. Synthesis and Structure of a Cobalt(I) Meso-tetraphenylporphyrin Complex, $[Co^{I}(TPP)][K.cntnd.222]_4Cl_3.H_2O$. *Inorg. Chem.* **1984**, *23*, 2958-2962.

(16) Shi, S.; Daniels, L. M.; Espenson, J. H. Molecular Structure of a Cobalt(I) Complex Lacking a Carbonyl Ligand. A Unique Example of Cobalt-Nitrogen Bond Shortening. *Inorg. Chem.* **1991**, *30*, 3407-3410.

(17) Bowman, A. C.; Milsmann, C.; Atienza, C. C. H.; Lobkovsky, E.; Wieghardt, K.; Chirik, P. J. Synthesis and Molecular and Electronic Structures of Reduced Bis(imino)pyridine Cobalt Dinitrogen Complexes: Ligand versus Metal Reduction. *J. Am. Chem. Soc.* **2010**, *132*, 1676-1684.

(18) Chomitz, W. A.; Arnold, J. Reactivity of a Co(I) $[N_2P_2]$ Complex with Azides: Evidence for a Transient Co(III) Imido Species. *Chem. Commun.* **2008**, 3648-3650.

(19) Ding, K.; Pierpont, A. W.; Brennessel, W. W.; Lukat-Rodgers, G.; Rodgers, K. R.; Cundari, T. R.; Bill, E.; Holland, P. L. Cobalt−Dinitrogen Complexes with Weakened N−N Bonds. *J. Am. Chem. Soc.* **2009**, *131*, 9471-9472.

(20) Knijnenburg, Q.; Hetterscheid, D.; Kooistra, T. M.; Budzelaar, Peter H. M. The Electronic Structure of (Diiminopyridine)cobalt(I) Complexes. *Eur. J. Inorg. Chem.* **2004**, *2004*, 1204-1211.

(21) Dugan, T. R.; Sun, X.; Rybak-Akimova, E. V.; Olatunji-Ojo, O.; Cundari, T. R.; Holland, P. L. A Masked Two-Coordinate Cobalt(I) Complex That Activates C–F Bonds. *J. Am. Chem. Soc.* **2011**, *133*, 12418–12421.

(22) Neculai, A. M.; Roesky, H. W.; Neculai, D.; Magull, J. Synthesis of New β-Diketiminato Complexes of Scandium(III): Unprecedented Formation of a Multicyclic Aggregate. *Organometallics* **2001**, *20*, 5501-5503.

(23) Neculai, D.; Mirela Neculai, A.; Roesky, H. W.; Herbst-Irmer, R.; Walfort, B.; Stalke, D. Vanadium Complexes Incorporating the β-Diketiminato Ligand L. Syntheses and Structures of $LV(OSO_2CF_3)_2$ and $LVPPh_2$. *Dalton Trans.* **2003**, 2831-2834.

(24) Neculai, D.; Roesky, H. W.; Neculai, A. M.; Magull, J.; Herbst-Irmer, R.; Walfort, B.; Stalke, D. The First β-Diketiminato Complex of Terbium Containing Two Alkyl Groups: A Model Compound for $LLnR_2$ (Ln = Lanthanide, R = Alkyl) Systems†. *Organometallics* **2003**, *22*, 2279-2283.

(25) Neculai, D.; Roesky, H. W.; Neculai, A. M.; Magull, J.; Schmidt, H.-G.; Noltemeyer, M. Synthesis and Structure of Monomeric and Solvent-Free $LPrX_2$ Compounds Supported by a New β-Diketiminato Ligand [$L=Et_2NCH_2CH_2NC(Me)CHC(Me)NCH_2CH_2NEt_2$, X=Cl, Br, BH_4]. *J. Organomet. Chem.* **2002**, *643-644*, 47-52.

(26) Zatka, V.; Holzbecher, J.; Ryan, D. E. Heterocyclic N,N'-disubstituted 1-amino-3-iminopropenes as Analytical Reagents. *Anal. Chim. Acta* **1971**, *55*, 273-8.

(27) Klappa, J. J.; Rich, A. E.; McNeill, K. One-Step Synthesis of 3,5-Disubstituted-2-pyridylpyrroles from the Condensation of 1,3-Diones and 2-(Aminomethyl)pyridine. *Org. Lett.* **2002**, *4*, 435-437.

(28) Fritsch, J. M.; Thoreson, K. A.; McNeill, K. Synthesis and Structures of Acyclic Monoanionic Tetradentate Aza β-Diketiminate Complexes of Magnesium, Zinc, and Cadmium. *Dalton Trans.* **2006**, 4814-4820.

(29) Marlier, E. E.; Sadowsky, D.; Cramer, C. J.; McNeill, K. Metal Ion Size and Coordination Mode in Complexes of a β-Diketiminate Ligand with Pendant Quinoline Arms. *Inorg. Chim. Acta* **2011**, *369*, 173-179.

(30) Hadzovic, A.; Song, D.; MacLaughlin, C. M.; Morris, R. H. A Mechanism Displaying Autocatalysis: The Hydrogenation of Acetophenone Catalyzed by RuH(S-binap)(app) Where app Is the Amido Ligand Derived from 2-Amino-2-(2-pyridyl)propane. *Organometallics* **2007**, *26*, 5987-5999.

(31) Song, D.; Morris, R. H. Cyclometalated Tridentate C-N-N Ligands with an Amine or Amido Donor in Platinum(II) and Palladium(II) Complexes and a Novel Potassium Alkoxide Aggregate. *Organometallics* **2004**, *23*, 4406-4413.

(32) Addison, A. W.; Rao, T. N.; Reedijk, J.; van Rijn, J.; Verschoor, G. C. Synthesis, Structure, and Spectroscopic Properties of Copper(II) Compounds Containing Nitrogen-sulphur Donor Ligands; the Crystal and Molecular Structure of Aqua[1,7-bis(N-methylbenzimidazol-2[prime or minute]-yl)-2,6-dithiaheptane]copper(II) Perchlorate. *J. Chem. Soc., Dalton Trans.* **1984**, 1349-1356.

(33) Mishra, V.; Mishra, H.; Mukherjee, R. Generation and Properties of CoI/NiI Species Stabilized by a Tetradentate Pyridylpyrazole Ligand: Crystal Structures of Dialkyl-CoIII Complexes. *Eur. J. Inorg. Chem.* **2009**, *2009*, 2973-2980.

(34) Rusling, J. F.; Connors, T. F.; Owlia, A. Electrocatalytic Reduction of Ethylene Dibromide by Vitamin B_{12} in a Surfactant-Stabilized Emulsion. *Anal. Chem.* **1987**, *59*, 2123-2127.

(35) Connelly, N. G.; Geiger, W. E. Chemical Redox Agents for Organometallic Chemistry. *Chem. Rev.* **1996**, *96*, 877-910.

(36) Lexa, D.; Saveant, J. M. The Electrochemistry of Vitamin B_{12}. *Acc. Chem. Res.* **1983**, *16*, 235-43.

(37) Schrauzer, G. N. Organocobalt Chemistry of Vitamin B_{12} Model Compounds (Cobaloximes). *Acc. Chem. Res.* **1968**, *1*, 97-103.

(38) Schrauzer, G. N.; Deutsch, E. Reactions of Cobalt(I) Supernucleophiles. The Alkylation of Vitamin B_{12s}, Cobaloximes(I), and Related Compounds. *J. Am. Chem. Soc.* **1969**, *91*, 3341-50.

(39) Schrauzer, G. N.; Deutsch, E.; Windgassen, R. J. The Nucleophilicity of Vitamin B_{12s}. *J. Am. Chem. Soc.* **1968**, *90*, 2441-2.

(40) Anderson, R. J.; Dixon, R. M.; Golding, B. T. Alkylcobalamins: Formation by enantioselective alkylation of cob(I)alamin, ^{1}H NMR spectra, and conformational analysis of the alkyl group. *J. Organomet. Chem.* **1992**, *437*, 227-237.

(41) Siega, P.; Randaccio, L.; Marzilli, P. A.; Marzilli, L. G. Metal Coordination by Sterically Hindered Heterocyclic Ligands, Including 2-Vinylpyridine, Assessed by Investigation of Cobaloximes. *Inorg. Chem.* **2006**, *45*, 3359-3368.

(42) Bianchini, C.; Peruzzini, M.; Vacca, A.; Zanobini, F. Metal-Hydride Alkynyl → Metal-Vinylidene Rearrangements Occurring in both Solid State and Solution. Role of the 1-Alkyne Substituent in Determining the Relative Stability of π-Alkyne, Hydride Alkynyl, and Vinylidene Forms at Cobalt *Organometallics* **1991**, *10*, 3697-3707.

(43) Armarego, W. L. F.; Perrin, D. D., *Purification of Laboratory Chemicals*. 4th ed.; Butterworth Heinemann: Oxford, 1996.

(44) SHELXTL *SHELXTL*, V6.14; Bruker AXS: Madison, WI, 2000.

Chapter Four References

(1) Issleib, K.; Muller, D. W. Alkali-Phosphorus Compounds and their Reactivity. III. Preparation of Ditertiary Phosphines $R_2P(CH_2)_nPR_2$. *Chem. Ber.* **1959**, *92*, 3175-82.

(2) Birkholz, M.-N.; Freixa, Z.; van Leeuwen, P. W. N. M. Bite Angle Effects of Diphosphines in C–C and C–X Bond Forming Cross Coupling Reactions. *Chem. Soc. Rev.* **2009**, *38*, 1099.

(3) Dierkes, P.; van Leeuwen, P. W. N. M. The Bite Angle Makes the Difference: a Practical Ligand Parameter for Diphosphine Ligands. *J. Chem. Soc., Dalton Trans.* **1999**, 1519-1530.

(4) Freixa, Z.; Vanleeuwen, P. Trans-Chelating Diphosphines, the Elusive Ligands! *Coord. Chem. Rev.* **2008**, *252*, 1755-1786.

(5) Kramer, P. C. J.; van Leeuwen, P. W. N. M.; Reek, J. N. H. Wide Bite Angle Diphosphines: Xantphos Ligands in Transition Metal Complexes and Catalysis. *Acc. Chem. Res.* **2001**, *34*, 895-904.

(6) Casey, C. P.; Whiteker, G. T.; Melville, M. G.; Petrovich, L. M.; Gavney, J. A.; Powell, D. R. Diphosphines with Natural Bite Angles near 120° Increase Selectivity for *n*-Aldehyde Formation in Rhodium-Catalyzed Hydroformylation. *J. Am. Chem. Soc.* **1992**, *114*, 5535-5543.

(7) Kranenburg, M.; Kamer, P. C. J.; van Leeuwen, P. W. N. M.; Vogt, D.; Keim, W. Effect of the Bite Angle of Diphosphine Ligands on Activity and Selectivity in the Nickel-catalysed Hydrocyanation of Styrene. *J. Chem. Soc., Chem. Comm.* **1995**, 2177-2178.

(8) Boron-Rettore, P.; Grove, D. M.; Venazi, L. M. Transition Metal Complexes with Bidentate Ligands Spanning *Trans*-Positions. Part XIV. Some Complexes of 2,11-bis(diphenylphosphinomethyl)benzo[*c*]phenanthrene with Platinum (0) and their Reactivities. *Helv. Chim. Acta* **1984**, *67*, 65-72.

(9) Bracher, G.; Grove, D. M.; Venanzi, L. M.; Bachechi, F.; Mura, P.; Zambonelli, L. Transition Metal Complexes with Bidentate Ligand 2, 11-Bis (diphenylphosphinomethyl)benzo[*c*]phenanthrene (**1**). X. Preparation and Spectroscopic Properties of *cis*-[$PtCl_2$ (**1**)] *trans*- and *cis*-[PtH (PPh_3) (**1**)] [BF_4] and Crystal and Molecular Structure of *cis*-[$PtCl_2$ (**1**)] · $CHCl_3$. *Helv. Chim. Acta* **1980**, *63*, 2519-2530.

(10) Allen, F. The Cambridge Structural Database: a quarter of a million crystal structures and rising. *Acta Cryst., Sect. B* **2002**, *58*, 380-388.

(11) Orpen, A. G. Applications of the Cambridge Structural Database to Molecular Inorganic Chemistry. *Acta Cryst., Sect. B* **2002**, *58*, 398-406.

(12) van Leeuwen, P. W. N. M.; Kamer, P. C. J.; Reek, J. N. H.; Dierkes, P. Ligand Bite Angle Effects in Metal-catalyzed C−C Bond Formation. *Chem. Rev.* **2000**, *100*, 2741-2770.

(13) Goertz, W.; C. J. Kamer, P.; W. N. M. van Leeuwen, P.; Vogt, D. Application of Chelating Diphosphine Ligands in the Nickel-Catalysed Hydrocyanation of Alk-l-enes and ω-unsaturated Fatty Acid Esters. *Chem. Commun.* **1997**, 1521-1522.

(14) Brown, J. M.; Guiry, P. J. Bite Angle Dependence of the Rate of Reductive Elimination from Diphosphine Palladium Complexes. *Inorg. Chim. Acta* **1994**, *220*, 249-259.

(15) Marcone, J. E.; Moloy, K. G. Kinetic Study of Reductive Elimination from the Complexes (Diphosphine)Pd(R)(CN). *J. Am. Chem. Soc.* **1998**, *120*, 8527-8528.

(16) Zuideveld, M. A.; Swennenhuis, B. H. G.; Boele, M. D. K.; Guari, Y.; van Strijdonck, G. P. F.; Reek, J. N. H.; Kramer, P. C. J.; Goubitz, K.; Fraanje, J.; Lutz, M.; Spek, A. L.; van Leeuwen, P. W. N. M. The Coordination Behaviour of Large Natural Bite Angle Diphosphine Ligands Towards Methyl and 4-Cyanophenylpalladium(II) Complexes. *J. Chem. Soc., Dalton Trans.* **2002**, 2308-2317.

(17) Gillie, A.; Stille, J. K. Mechanisms of 1,l -Reductive Elimination from Palladium. *J. Am. Chem. Soc.* **1980**, *102*, 4933-4941.

(18) Smith, R. C.; Bodner, C. R.; Earl, M. J.; Sears, N. C.; Hill, N. E.; Bishop, L. M.; Sizemore, N.; Hehemann, D. T.; Bohn, J. J.; Protasiewicz, J. D. Suzuki and Heck coupling reactions mediated by palladium complexes bearing trans-spanning diphosphines. *J. Organomet. Chem.* **2005**, *690*, 477-481.

(19) Crocker, C.; Errington, R. J.; Markham, R.; Moulton, C. J.; Odell, K. J.; Shaw, B. L. Large-Ring and Cyclometalated Rhodium Complexes from Some Medium-Chain α,ω-Diphosphines. *J. Am. Chem. Soc.* **1980**, *102*, 4373-4379.

(20) Destefano, N. J.; Johnson, D. K.; Venanzi, L. M. Transition-Metal Complexes with Bidentate Ligands Spanning *trans*-Positions. II. Preparation and Properties of Complexes *trans*-[MX_2(1)] (M = Ni, Pd and Pt; X = Cl, Br and I; 1 = 2, 11-Bis(diphenylphosphinomethyl)benzo[*c*]phenanthrene). *Helv. Chim. Acta* **1976**, *59*, 2683-2690.

(21) Freixa, Z.; Beentjes, M. S.; Batema, G. D.; Dieleman, C. B.; van Strijdonck, G. P. F.; Reek, J. N. H.; Kamer, P. C. J.; Fraanje, J.; Goubitz, K.; van Leeuwen, P. W. N. M. SPANphos: A C_2-Symmetric *Trans*-Coordinating Diphosphane Ligand. *Angew. Chem. Int. Ed.* **2003**, *42*, 1284-1287.

(22) Ding, K.; Miller, D. L.; Young, V. G.; Lu, C. C. Study of the Conformationally Flexible, Wide Bite-Angle Diphosphine 4,6-Bis(3-diisopropylphosphinophenyl)dibenzofuran in Rhodium(I) and Palladium(II) Coordination Complexes. *Inorg. Chem.* **2011**, *50*, 2545-2552.

(23) Kaganovsky, L.; Cho, K.-B.; Gelman, D. New Trans-Chelating Ligands and Their Complexes and Catalytic Properties in the Mizoroki−Heck Arylation of Cyclohexene. *Organometallics* **2008**, *27*, 5139-5145.

(24) Saito, S.; Oh-tani, S.; Miyaura, N. Synthesis of Biaryls via a Nickel(0)-Catalyzed Cross-Coupling Reaction of Chloroarenes with Arylboronic Acids. *J. Org. Chem.* **1997**, *62*, 8024-8030.

(25) Tamao, K.; Sumitani, K.; Kumada, M. Selective Carbon-Carbon Bond Formation by Cross-Coupling of Grignard Reagents with Organic Halides. Catalysis by Nickel-Phosphine Complexes. *J. Am. Chem. Soc.* **1972**, *94*, 4374-4376.

(26) Zhang, K.; Conda-Sheridan, M.; R. Cooke, S.; Louie, J. N-Heterocyclic Carbene Bound Nickel(I) Complexes and Their Roles in Catalysis. *Organometallics* **2011**, *30*, 2546-2552.

(27) Amatore, C.; Jutand, A. Rates and Mechanism of Biphenyl Synthesis Catalyzed by Electrogenerated Coordinatively Unsaturated Nickel Complexes. *Organometallics* **1988**, *7*, 2203-2214.

(28) Miyazaki, S.; Koga, Y.; Matsumoto, T.; Matsubara, K. A New Aspect of Nickel-Catalyzed Grignard Cross-Coupling Reactions: Selective Synthesis, Structure, and Catalytic Behavior of a T-shape Three-Coordinate Nickel(I) Chloride Bearing a Bulky NHC Ligand. *Chem. Commun.* **2010**, *46*, 1932-1934.

Chapter Five References

(1) Ding, K.; Miller, D. L.; Young, V. G.; Lu, C. C. Study of the Conformationally Flexible, Wide Bite-Angle Diphosphine 4,6-Bis(3-diisopropylphosphinophenyl)dibenzofuran in Rhodium(I) and Palladium(II) Coordination Complexes. *Inorg. Chem.* **2011**, *50*, 2545-2552.

(2) Haenel, M. W.; Jakubik, D.; Rothenberger, E.; Schroth, G. Bidentate Phosphines of Heteroarenes: 4,6-Bis(diphenylphosphino)dibenzofuran and 4,6-Bis(diphenylphosphino)dibenzothiophene. *Chem. Ber*. **1991**, *124*, 1705-1710.

(3) Kranenburg, M.; van der Burgt, Y. E. M.; Kamer, P. C. J.; van Leeuwen, P. W. N. M.; Goubitz, K.; Fraanje, J. New Diphosphine Ligands Based on Heterocyclic Aromatics Inducing Very High Regioselectivity in Rhodium-Catalyzed Hydroformylation: Effect of the Bite Angle. *Organometallics* **1995**, *14*, 3081-3089.

(4) Jimenez-Rodriguez, C.; Roca, F. X.; Bo, C.; Benet-Buchholz, J.; Escudero-Adan, E. C.; Freixa, Z.; van Leeuwen, P. W. N. M. SPANphos: Trans-Spanning Diphosphines as *cis* Chelating Ligands! *Dalton Trans.* **2006**, 268-278.

(5) Fairlamb, I. J. S.; Tommasi, S.; Moulton, B. E.; Zheng, W.; Lin, Z.; Whitwood, A. C. Conformational Flexibility in a Carbobicyclic Diphosphinite Ligand. *Eur. J. Inorg. Chem.* **2007**, *2007*, 3173-3178.

(6) Allen, F. The Cambridge Structural Database: a quarter of a million crystal structures and rising. *Acta Cryst., Sect. B* **2002**, *58*, 380-388.

(7) Orpen, A. G. Applications of the Cambridge Structural Database to Molecular Inorganic Chemistry. *Acta Cryst., Sect. B* **2002**, *58*, 398-406.

(8) Kulkarni, A. A.; Daugulis, O. Direct Conversion of Carbon-Hydrogen into Carbon-Carbon Bonds by First-Row Transition-Metal Catalysis. *Synthesis* **2009**, *24*, 4087-4109.

(9) Bullock, R. M., *Catalysis Without Precious Metals*. Wiley-VCH: Weinheim, Germany, 2010.

(10) Fürstner, A.; Leitner, A.; Méndez, M.; Krause, H. Iron-Catalyzed Cross-Coupling Reactions. *J. Am. Chem. Soc.* **2002**, *124*, 13856-13863.

(11) Traylor, T. G.; Hill, K. W.; Fann, W. P.; Tsuchiya, S.; Dunlap, B. E. Aliphatic Hydroxylation Catalyzed by Iron(III) Porphyrins. *J. Am. Chem. Soc.* **1992**, *114*, 1308-1312.

(12) Costas, M.; Que, L. Ligand Topology Tuning of Iron-Catalyzed Hydrocarbon Oxidations. *Angew. Chem. Int. Ed.* **2002**, *41*, 2179-2181.

(13) Britovsek, G. J. P.; England, J.; White, A. J. P. Iron(II), Manganese(II) and Cobalt(II) Complexes containing Tetradentate Biphenyl-Bridged Ligands and their Application in Alkane Oxidation Catalysis. *Dalton Trans.* **2006**, 1399-1408.

(14) Chen, M. S.; White, M. C. A Predictably Selective Aliphatic C–H Oxidation Reaction for Complex Molecule Synthesis. *Science* **2007**, *318*, 783-787.

(15) Bianchini, C.; Meli, A.; Peruzzini, M.; Frediani, P.; Bohanna, C.; Esteruelas, M. A.; Oro, L. A. Selective Hydrogenation of 1-Alkynes to Alkenes Catalyzed by an Iron(II) *cis*-Hydride η^2-Dihydrogen Complex. A Case of Intramolecular Reaction between η^2-H_2 and σ-Vinyl Ligands. *Organometallics* **1992**, *11*, 138-145.

(16) Bart, S. C.; Lobkovsky, E.; Chirik, P. J. Preparation and Molecular and Electronic Structures of Iron(0) Dinitrogen and Silane Complexes and their Application to Catalytic Hydrogenation and Hydrosilation. *J. Am. Chem. Soc.* **2004**, *126*, 13794-13807.

(17) Daida, E. J.; Peters, J. C. Considering $Fe^{II/IV}$ Redox Processes as Mechanistically Relevant to the Catalytic Hydrogenation of Olefins by [PhBPiPr_3]Fe−H_x Species. *Inorg. Chem.* **2004**, *43*, 7474-7485.

(18) Morris, R. H. Asymmetric Hydrogenation, Transfer Hydrogenation and Hydrosilylation of Ketones Catalyzed by Iron Complexes. *Chem. Soc. Rev.* **2009**, *38*, 2282-2291.

(19) Bullock, R. M. An Iron Catalyst for Ketone Hydrogenations Under Mild Conditions. *Angew. Chem. Int. Ed.* **2007**, *46*, 7360-7363.

(20) Hebrard, F.; Kalck, P. Cobalt-Catalyzed Hydroformylation of Alkenes: Generation and Recycling of the Carbonyl Species, and Catalytic Cycle. *Chem. Rev.* **2009**, *109*, 4272-4282.

(21) Gosmini, C.; Moncomble, A. Cobalt-Catalyzed Cross-Coupling Reactions of Aryl Halides. *Isr. J. Chem.* **2010**, *50*, 568-576.

(22) Keim, W. Nickel: An Element with Wide Application in Industrial Homogeneous Catalysis. *Angew. Chem. Int. Ed. Engl.* **1990**, *29*, 235-244.

(23) Younkin, T. R.; Connor, E. F.; Henderson, J. I.; Friedrich, S. K.; Grubbs, R. H.; Bansleben, D. A. Neutral, Single-Component Nickel (II) Polyolefin Catalysts That Tolerate Heteroatoms. *Science* **2000**, *287*, 460-462.

(24) Ittel, S. D.; Johnson, L. K.; Brookhart, M. Late-Metal Catalysts for Ethylene Homo- and Copolymerization. *Chem. Rev.* **2000**, *100*, 1169-1204.

(25) Rosen, B. M.; Quasdorf, K. W.; Wilson, D. A.; Zhang, N.; Resmerita, A.-M.; Garg, N. K.; Percec, V. Nickel-Catalyzed Cross-Couplings Involving Carbon−Oxygen Bonds. *Chem. Rev.* **2010**, *111*, 1346-1416.

(26) Negishi, E.-i. Transition Metal-Catalyzed Organometallic Reactions that Have Revolutionized Organic Synthesis. *Bull. Chem. Soc. Jpn.* **2007**, *80*, 233-257.

(27) Montgomery, J. Nickel-Catalyzed Reductive Cyclizations and Couplings. *Angew. Chem. Int. Ed.* **2004**, *43*, 3890-3908.

(28) Castro, P. M.; Lankinen, M. P.; Leskelä, M.; Repo, T. Polymerisation of Acrylates Catalysed by Methylaluminoxane Activated Ditertiary Phosphine Complexes of Iron and Cobalt Dichlorides. *Macromol. Chem. Phys.* **2005**, *206*, 1090-1097.

(29) Kim, H. S.; Bae, J. Y.; Lee, J. S.; Kwon, O. S.; Jelliarko, P.; Lee, S. D.; Lee, S.-H. Phosphine-Bound Zinc Halide Complexes for the Coupling Reaction of Ethylene Oxide and Carbon Dioxide. *J. Catal.* **2005**, *232*, 80-84.

(30) Chadwell, S. J.; Coles, S. J.; Edwards, P. G.; Hursthouse, M. B.; Imran, A. Synthesis and Characterization of Group 10 Metal Complexes with a New Trifunctional Ether Phosphine. The X-ray Crystal Structures of bis[bis(2-ethoxyethyl)benzylphosphine]dichloronickel(II) and bis[bis(2-ethoxyethyl)benzylphosphine]chlorophenylnickel(II). *Polyhedron* **1995**, *14*, 1057-1065.

(31) Ding, K.; Pierpont, A. W.; Brennessel, W. W.; Lukat-Rodgers, G.; Rodgers, K. R.; Cundari, T. R.; Bill, E.; Holland, P. L. Cobalt−Dinitrogen Complexes with Weakened N−N Bonds. *J. Am. Chem. Soc.* **2009**, *131*, 9471-9472.

(32) Keiter, R. L.; Keiter, E. A.; Hecker, K. H.; Boecker, C. A. A facile, high-yield synthesis of trans-Fe(CO)3(PR3)2 from Fe(CO)5, Fe(CO)4CHO-, HFe(CO)4-, or HFe(CO)3PR3. *Organometallics* **1988**, *7*, 2466-2469.

(33) Rowland, R. S.; Taylor, R. Intermolecular Nonbonded Contact Distances in Organic Crystal Structures: Comparison with Distances Expected from van der Waals Radii. *J. Phys. Chem.* **1996**, *100*, 7384-7391.

(34) Ciurli, S.; Gambarotta, S.; Floriani, C.; Chiesi-Villa, A.; Guastini, C. Reduced Cobalt-meso-Tetraphenylporphyrin Complexes: Synthesis and Structure of $[Na(thf)_3]_2[Co(TPP)]$. *Angew. Chem. Int. Ed.* **1986**, *25*, 553-554.

(35) Norman, N. C.; Orpen, A. G.; Quayle, M. J.; Whittell, G. R. Chlorobis(triphenylphosphine)nickel(I). *Acta Cryst., Sect. C* **2002**, *58*, m160-m161.

(36) Langer, J.; Fischer, R.; Görls, H.; Theyssen, N.; Walther, D. Nickel(I)-Komplexe mit 1,1′-Bis(phosphino)ferrocenen als Liganden. *Z. Anorg. Allg. Chem.* **2007**, *633*, 557-562.

(37) Bai, G.; Wei, P.; Stephan, D. W. A β-Diketiminato−Nickel(II) Synthon for Nickel(I) Complexes. *Organometallics* **2005**, *24*, 5901-5908.

(38) Eckert, N. A.; Dinescu, A.; Cundari, T. R.; Holland, P. L. A T-Shaped Three-Coordinate Nickel(I) Carbonyl Complex and the Geometric Preferences of Three-Coordinate d9 Complexes. *Inorg. Chem.* **2005**, *44*, 7702-7704.

(39) Saraev, V. V.; Kraikivskii, P. B.; Svoboda, I.; Kuzakov, A. S.; Jordan, R. F. Synthesis, Molecular Structure, and EPR Analysis of the Three-Coordinate Ni(I) Complex $[Ni(PPh_3)_3][BF_4]$. *J. Phys. Chem. A* **2008**, *112*, 12449-12455.

(40) Kogut, E.; Wiencko, H. L.; Zhang, L.; Cordeau, D. E.; Warren, T. H. A Terminal Ni(III)−Imide with Diverse Reactivity Pathways. *J. Am. Chem. Soc.* **2005**, *127*, 11248-11249.

(41) Nilges, M. J.; Barefield, E. K.; Belford, R. L.; Davis, P. H. Electronic Structure of Three-Coordinate Nickel(I): Electron Paramagnetic Resonance of Nickel-doped Halobis(triphenylphosphine)copper(I). *J. Am. Chem. Soc.* **1977**, *99*, 755-760.

(42) Kahn, O.; Prins, R.; Reedijk, J.; Thompson, J. S. Orbital Symmetries and Magnetic Interaction between Copper(II) Ions and the O-semiquinone Radical. Magnetic Studies of (di-2-pyridylamine)(3,5-di-tert-butyl-o-semiquinonato)copper(II) perchlorate and bis(bis(3,5-di-tert-butyl-o-semiquinonato)copper(II)). *Inorg. Chem.* **1987**, *26*, 3557-3561.

(43) Schubert, E. M. Utilizing the Evans Method with a Superconducting NMR Spectrometer in the Undergraduate Laboratory. *J. Chem. Educ.* **1992**, *69*, 62.

(44) Evans, D. F.; Fazakerley, G. V.; Phillips, R. F. Organometallic Compounds of Bivalent Europium, Ytterbium, and Samarium. *J. Chem. Soc. A* **1971**, 1931-1934.

(45) Bain, G. A.; Berry, J. F. Diamagnetic Corrections and Pascal's Constants. *Journal of Chemical Education* **2008**, *85*, 532-null.

(46) Becke, A. D. Density-Functional Exchange-Energy Approximation with Correct Asymptotic Behavior. *Phys. Rev. A* **1988**, *38*, 3098.

(47) Perdew, J. P. Density-Functional Approximation for the Correlation Energy of the Inhomogeneous Electron Gas. *Physical Review B* **1986**, *33*, 8822.

(48) Zhao, Y.; Truhlar, D. G. Density Functionals with Broad Applicability in Chemistry. *Acc. Chem. Res.* **2008**, *41*, 157-167.

(49) Zhao, Y.; Truhlar, D. G. A New Local Density Functional for Main-Group Thermochemistry, Transition Metal Bonding, Thermochemical Kinetics, and Noncovalent Interactions. *J. Chem. Phys.* **2006**, *125*, 194101-18.

(50) Frisch, M. J.; Trucks, G. W.; Schlegel, H. B.; Scuseria, G. E.; Robb, M. A.; Cheeseman, J. R.; Scalmani, G.; Barone, V.; Mennucci, B.; Petersson, G. A.; Nakatsuji, H.; Caricato, M.; Li, X.; Hratchian, H. P.; Izmaylov, A. F.; Bloino, J.; Zheng, G.; Sonnenberg, J. L.; Hada, M.; Ehara, M.; Toyota, K.; Fukuda, R.; Hasegawa, J.; Ishida, M.; Nakajima, T.; Honda, Y.; Kitao, O.; Nakai, H.; Vreven, T.; J. A. Montgomery, J.; Peralta, J. E.; Ogliaro, F.; Bearpark, M.; Heyd, J. J.; Brothers, E.; Kudin, K. N.; N.Staroverov, V.; Kobayashi, R.; Normand, J.; Raghavachari, K.; Rendell, A.; Burant, J. C.; Iyengar, S. S.; Tomasi, J.; Cossi, M.; Rega, N.; Millam, J. M.; Klene, M.; Knox, J. E.; Cross, J. B.; Bakken, V.; Adamo, C.; Jaramillo, J.; Gomperts, R.; Stratmann, R. E.; Yazyev, O.; Austin, A. J.; Cammi, R.; Pomelli, C.; Ochterski, J. W.; Martin, R. L.; Morokuma, K.; Zakrzewski, V. G.; Voth, G. A.; Salvador, P.; Dannenberg, J. J.; Dapprich, S.; Daniels, A. D.; Farkas, O.; Foresman, J. B.; Ortiz, J. V.; Cioslowski, J.; Fox, D. J. *Gaussian 09, Revision A.02*, Gaussian, Inc.: Wallingford, CT, 2009.

(51) Weigend, F.; Ahlrichs, R. Balanced Basis Sets of Split Valence, Triple Zeta Valence and Quadruple Zeta Valence Quality for H to Rn: Design and Assessment of Accuracy. *Phys. Chem. Chem. Phys.* **2005**, *7*, 3297-3305.

Chapter Six References

(1) Jolly, P. W.; Jonas, K.; Krüger, C.; Tsay, Y. H. The Preparation, Reactions and Structure of bis[bis(tricyclohexylphosphine)nickel] dinitrogen, $\{[(C_6H_{11})_3P]_2Ni\}_2N_2$. *J. Organomet. Chem.* **1971**, *33*, 109-122.

(2) Aresta, M.; Nobile, C. F.; Albano, V. G.; Forni, E.; Manassero, M. New Nickel-Carbon Dioxide Complex: Synthesis, Properties, and Crystallographic Characterization of (carbon dioxide)-bis(tricyclohexylphosphine)nickel. *J. Chem. Soc., Chem. Commun.* **1975**, 636-637.

(3) Mindiola, D. J.; Hillhouse, G. L. Synthesis, Structure, and Reactions of a Three-Coordinate Nickel-Carbene Complex, {1,2-Bis(di-tert-butylphosphino)ethane}$NiCPh_2$. *J. Am. Chem. Soc.* **2002**, *124*, 9976-9977.

(4) Mindiola, D. J.; Hillhouse, G. L. Terminal Amido and Imido Complexes of Three-Coordinate Nickel. *J. Am. Chem. Soc.* **2001**, *123*, 4623-4624.

(5) Melenkivitz, R.; Mindiola, D. J.; Hillhouse, G. L. Monomeric Phosphido and Phosphinidene Complexes of Nickel. *J. Am. Chem. Soc.* **2002**, *124*, 3846-3847.

(6) Ingleson, M. J.; Fullmer, B. C.; Buschhorn, D. T.; Fan, H.; Pink, M.; Huffman, J. C.; Caulton, K. G. Influence of the d-Electron Count on CO Binding by Three-Coordinate $[(^tBu_2PCH_2SiMe_2)_2N]$Fe, -Co, and -Ni. *Inorg. Chem.* **2007**, *47*, 407-409.

(7) Bai, G.; Wei, P.; Stephan, D. W. A β-Diketiminato−Nickel(II) Synthon for Nickel(I) Complexes. *Organometallics* **2005**, *24*, 5901-5908.

(8) Holland, P. L.; Cundari, T. R.; Perez, L. L.; Eckert, N. A.; Lachicotte, R. J. Electronically Unsaturated Three-Coordinate Chloride and Methyl Complexes of Iron, Cobalt, and Nickel. *J. Am. Chem. Soc.* **2002**, *124*, 14416-14424.

(9) Puiu, S. C.; Warren, T. H. Three-Coordinate β-Diketiminato Nickel Nitrosyl Complexes from Nickel(I)−Lutidine and Nickel(II)−Alkyl Precursors. *Organometallics* **2003**, *22*, 3974-3976.

(10) Hu, X.; Castro-Rodriguez, I.; Meyer, K. Synthesis and Characterization of Electron-Rich Nickel Tris-Carbene Complexes. *Chem. Commun.* **2004**, 2164-2165.

(11) Schaub, T.; Backes, M.; Radius, U. Nickel(0) Complexes of N-Alkyl-Substituted N-Heterocyclic Carbenes and Their Use in the Catalytic Carbon−Carbon Bond Activation of Biphenylene. *Organometallics* **2006**, *25*, 4196-4206.

(12) Schmedake, T. A.; Haaf, M.; Paradise, B. J.; Powell, D.; West, R. Two Trigonal Ni(silylene)$_3$ Complexes. *Organometallics* **2000**, *19*, 3263-3265.

(13) Kogut, E.; Wiencko, H. L.; Zhang, L.; Cordeau, D. E.; Warren, T. H. A Terminal Ni(III)−Imide with Diverse Reactivity Pathways. *J. Am. Chem. Soc.* **2005**, *127*, 11248-11249.

(14) Bai, G.; Stephan, D. W. Formation of C-C and C-N Bonds in Ni^{II} Ketimide Complexes via Transient Ni^{III} Aryl Imides. *Angew. Chem. Int. Ed.* **2007**, *46*, 1856-1859.

(15) Iluc, V. M.; Miller, A. J. M.; Anderson, J. S.; Monreal, M. J.; Mehn, M. P.; Hillhouse, G. L. Synthesis and Characterization of Three-Coordinate Ni(III)-Imide Complexes. *J. Am. Chem. Soc.* **2011**, *133*, 13055–13063.

(16) Miyazaki, S.; Koga, Y.; Matsumoto, T.; Matsubara, K. A New Aspect of Nickel-Catalyzed Grignard Cross-Coupling Reactions: Selective Synthesis, Structure, and Catalytic Behavior of a T-shape Three-Coordinate Nickel(I) Chloride Bearing a Bulky NHC Ligand. *Chem. Commun.* **2010**, *46*, 1932-1934.

(17) Zhang, K.; Conda-Sheridan, M.; R. Cooke, S.; Louie, J. N-Heterocyclic Carbene Bound Nickel(I) Complexes and Their Roles in Catalysis. *Organometallics* **2011**, *30*, 2546-2552.

(18) Mindiola, D. J.; Waterman, R.; Jenkins, D. M.; Hillhouse, G. L. Synthesis of 1,2-bis(di-tert-butylphosphino)ethane (dtbpe) Complexes of Nickel: Radical Coupling and Reduction Reactions Promoted by the Nickel(I) Dimer [(dtbpe)NiCl]$_2$. *Inorg. Chim. Acta* **2003**, *345*, 299-308.

(19) Hoskin, A. J.; Stephan, D. W. Early Transition Metal Hydride Complexes: Synthesis and Reactivity. *Coord. Chem. Rev.* **2002**, *233-234*, 107-129.

(20) Kubas, G. J. Fundamentals of H_2 Binding and Reactivity on Transition Metals Underlying Hydrogenase Function and H_2 Production and Storage. *Chem. Rev.* **2007**, *107*, 4152-4205.

(21) He, T.; Tsvetkov, N. P.; Andino, J. G.; Gao, X.; Fullmer, B. C.; Caulton, K. G. Mechanism of Heterolysis of H_2 by an Unsaturated d^8 Nickel Center: via Tetravalent Nickel? *J. Am. Chem. Soc.* **2010**, *132*, 910-911.

(22) Curtis, C. J.; Miedaner, A.; Ciancanelli, R.; Ellis, W. W.; Noll, B. C.; DuBois, M. R.; DuBois, D. L. $[Ni(Et_2PCH_2NMeCH_2PEt_2)_2]^{2+}$ as a Functional Model for Hydrogenases. *Inorg. Chem.* **2003**, *42*, 216-227.

(23) Wilson, A. D.; Newell, R. H.; McNevin, M. J.; Muckerman, J. T.; DuBois, M. R.; DuBois, D. L. Hydrogen Oxidation and Production Using Nickel-Based Molecular Catalysts with Positioned Proton Relays. *J. Am. Chem. Soc.* **2006**, *128*, 358-366.

(24) Darensbourg, M. Y.; Ludwig, M.; Riordan, C. G. Spectroscopic and Chemical Studies of Nickel(II) Hydrides. *Inorg. Chem.* **1989**, *28*, 1630-1634.

(25) Green, M. L. H.; Saito, T. A stable nickel hydride complex: trans-hydridochlorobis(tricyclohexylphosphine)nickel. *Journal of the Chemical Society D: Chemical Communications* **1969**, 208b.

(26) Jones, G. D. J.; Vicic, D. A. A 1-Norbornene Adduct of a Transition Metal and an Electrochemical Study of the Bridgehead Olefin Complex. *Organometallics* **2005**, *24*, 3821-3823.

(27) Chow, Y. L.; Li, H. Light-Promoted Catalysis of Nickel Hydride Complexes in the Isomerization and Hydrogenation of *cis*, *cis*-1,5-cyclooctadiene: Mechanistic Studies. *Can. J. Chem.* **1986**, *64*, 2229-2231.

(28) Chow, Y. L.; Li, H.; Yang, M. Light-Promoted Catalytic Hydrogenation of Olefins with Nickel Complexes: the Formation of Nickel Hydrides from the Reaction of Ni(1) Complexes with Hydrogen. *Can. J. Chem.* **1988**, *66*, 2920-2927.

(29) Lee, C. H.; Cook, T. R.; Nocera, D. G. HX Addition and Photochemical H_2 Elimination by Ni NHC Complexes. *Inorg. Chem.* **2011**, *50*, 714-716.

(30) Tamao, K.; Sumitani, K.; Kumada, M. Selective Carbon-Carbon Bond Formation by Cross-Coupling of Grignard Reagents with Organic Halides. Catalysis by Nickel-Phosphine Complexes. *J. Am. Chem. Soc.* **1972**, *94*, 4374-4376.

(31) Tsou, T. T.; Kochi, J. K. Mechanism of Biaryl Synthesis with Nickel Complexes. *J. Am. Chem. Soc.* **1979**, *101*, 7547-7560.

(32) Rosen, B. M.; Quasdorf, K. W.; Wilson, D. A.; Zhang, N.; Resmerita, A.-M.; Garg, N. K.; Percec, V. Nickel-Catalyzed Cross-Couplings Involving Carbon−Oxygen Bonds. *Chem. Rev.* **2010**, *111*, 1346-1416.

(33) Gómez-Benítez, V.; Baldovino-Pantaleón, O.; Herrera-Álvarez, C.; Toscano, R. A.; Morales-Morales, D. High Yield Thiolation of Iodobenzene Catalyzed by the Phosphinite Nickel PCP Pincer Complex: [NiCl{C_6H_3-2,6-($OPPh_2$)$_2$}]. *Tetrahedron Lett.* **2006**, *47*, 5059-5062.

(34) Amatore, C.; Jutand, A. Rates and Mechanism of Biphenyl Synthesis Catalyzed by Electrogenerated Coordinatively Unsaturated Nickel Complexes. *Organometallics* **1988**, *7*, 2203-2214.

(35) Jones, G. D.; McFarland, C.; Anderson, T. J.; Vicic, D. A. Analysis of Key Steps in the Catalytic Cross-Coupling of Alkyl Electrophiles under Negishi-like Conditions. *Chem. Commun.* **2005**, 4211-4213.

(36) Phapale, V. B.; Buñuel, E.; García-Iglesias, M.; Cárdenas, D. J. Ni-Catalyzed Cascade Formation of C(sp3)-C(sp3) Bonds by Cyclization and Cross-Coupling Reactions of Iodoalkanes with Alkyl Zinc Halides. *Angew. Chem. Int. Ed.* **2007**, *46*, 8790-8795.

(37) Jones, G. D.; Martin, J. L.; McFarland, C.; Allen, O. R.; Hall, R. E.; Haley, A. D.; Brandon, R. J.; Konovalova, T.; Desrochers, P. J.; Pulay, P.; Vicic, D. A. Ligand Redox Effects in the Synthesis, Electronic Structure, and Reactivity of an Alkyl−Alkyl Cross-Coupling Catalyst. *J. Am. Chem. Soc.* **2006**, *128*, 13175-13183.

(38) Hu, X.; Castro-Rodriguez, I.; Olsen, K.; Meyer, K. Group 11 Metal Complexes of N-Heterocyclic Carbene Ligands: Nature of the Metal Carbene Bond. *Organometallics* **2004**, *23*, 755-764.

(39) Spek, A. L. *Acta Crystallogr.* **1990**, *A46*, C34.